PALEOCLIMATE AND PALEOENVIRONMENT OF THE PRINCE CREEK AND CANTWELL FORMATIONS, ALASKA: TERRESTRIAL EVIDENCE OF A MIDDLE MAASTRICHTIAN GREENHOUSE EVENT

By

Susana Salazar Jaramillo

RECOMMENDED:

Dr. Tom Trainor

Dr. Patrick Druckenmiller

Dr. Sarah Fowell
Advisory Committee Co-Chair

Dr. Paul McCarthy
Advisory Committee Co-Chair

Dr. Paul McCarthy
Chair, Department of Geology and Geophysics

APPROVED:

Dr. Paul Layer
Dean, College of Natural Science and Mathematics

Dr. John Eichelberger
Dean of the Graduate School

4/24/14
Date

PALEOCLIMATE AND PALEOENVIRONMENT OF THE PRINCE CREEK AND CANTWELL FORMATIONS, ALASKA: TERRESTRIAL EVIDENCE OF MIDDLE MAASTRICHTIAN GREENHOUSE EVENT

A

DISSERTATION

Presented to the Faculty

of the University of Alaska Fairbanks

In Partial Fulfillment of the Requirements

for the Degree of

DOCTOR OF PHILOSOPHY

By

Susana Salazar Jaramillo, B.S., M.S.

Fairbanks, Alaska

May 2014

Abstract

I studied the paleoclimate and paleonvironmental conditions of the Prince Creek Formation, North Slope Alaska, and the lower Cantwell Formation in Denali National Park, Alaska. I used data from pollen analysis, clay mineral analysis and stable isotope analysis of clay minerals and organic matter applied to paleosols of the Prince Creek Formation. In the lower Cantwell Formation, I reconstructed the sedimentary environment, produced a terrestrial carbon stable isotope record and obtained a ~ 69.5 Ma radiometric age for the lower Cantwell Formation.

Clay analysis in the Prince Creek Formation indicates that the genesis of the paleosols was strongly influenced by the properties of the parent material and that an epiclastic bentonitic source contributed to the development of non-allophanic properties which suggests the presence of Andept-like paleosols. Paleosols formed on the floodplains of the Prince Creek Formation reveal features attributed to wet-dry cycles as a result of seasonal flooding, perhaps due to snow melt in the ancestral Brooks Range. Carbon and oxygen isotope analyses, and the geochemistry of paleosol Bw/Bt horizons indicate mean annual precipitation values between 745.56 and 1426.88 ±221.38 mm/yr and mean annual temperatures of 12 ±4.4 °C. The meteoric water $\delta^{18}O$ value calculated from smectite at a 6.3 °C mean annual temperature is ~ -24 ‰. The calculated value is $\delta^{18}O$-depleted as is expected for high latitudes during the Late Cretaceous.

Sedimentary facies analysis suggests that The East Fork measured section of the lower Cantwell Formation was likely deposited in the distal part of an alluvial fan. A new U-Pb age of 69.5 ±0.7 Ma from bentonites and carbon isotope values of bulk sedimentary organic matter and wood fragments indicates that a greenhouse event, known as the mid-Maastrichtian Event (MME), is recorded at the East Fork of the Toklat River Section. A mean annual precipitation value of ~ 517.92 ±134.44 mm/yr was obtained from $\delta^{13}C$ terrestrial organic matter.

The coeval nature of the lower Cantwell Formation (~69.5 Ma) and the Prince Creek Formation (~69.2 Ma) suggests that the MME likely affected the Prince Creek Formation as well. In the Prince Creek Formation, the age, precipitation, temperature and meteoric water composition from bentonite smectites are consistent with increased precipitation due to an intensified paleo-arctic hydrological cycle, which may have been the result of increased latent heat transport during the mid-Maastrichtian greenhouse episode.

Table of Contents

List of Figures

Page

List of Tables

Page

List of Appendices

Page

General Introduction

The discovery of dinosaur remains, the well preserved fossil record and the presence of paleosols in the Prince Creek Formation (Parrish et al., 1987; Brouwers et al., 1987; Clemens and Nelms, 1993; Fiorillo et al., 2010a,b; Flaig et al., 2011, 2013), North Slope, Alaska, and in the Cantwell Formation (Fiorillo et al., 2009; Tomsich et al., 2010; Fiorillo and Adams, 2012), central Alaska Range, allows advances in the reconstruction of Cretaceous paleoclimate. Studying past climate in northern Alaska is important because Alaska occupied a high-latitude position and experienced greenhouse conditions during the Cretaceous (Flaig, 2010). An understanding of the greenhouse Cretaceous climate can be used to identify potential changes from greenhouse effects in the modern climate system. Interpretations of Cretaceous climate in the Prince Creek and Cantwell formations have previously been carried out using palynology, paleosols, and the climate leaf analysis multivariate program (CLAMP) (Parrish and Spicer, 1988; Spicer and Parrish, 1990; Fiorillo et al., 2010b; Tomsich et al., 2010). In this dissertation, I approach paleoclimatic reconstruction of the Cretaceous greenhouse Arctic with different proxies. I reconstruct paleoenvironments of the Prince Creek and Cantwell formations based on qualitative and semi-quantitative paleoclimatic data extracted from pollen analysis, clay mineral analysis and stable isotope analyses of clay minerals and organic matter, and I identify the first evidence for the middle Maastrichtian event (MME), a period of increased global warming, in terrestrial sediments from Alaska. These new data provide a clearer picture of the environments and climate changes in high-latitude Alaska during the Late Cretaceous.

The project objectives are:

1) Determine the origin of clay minerals using mineralogical (X-ray diffraction (XRD) and geochemical data (X-ray flurorescence (XRF), electron microprobe and stable isotope analyses). Pedogenic clays provide information about surface processes during paleosol formation.

2) Estimate the temperature of the water during pedogenic clay formation using stable isotopes in clays. Pedogenic clays achieve isotopic equilibrium with soil water during their formation; hence analyses of pedogenic clays will permit an assessment of paleoprecipitation during paleosol formation.

3) Compare the results obtained from the Prince Creek Formation with results from the Cantwell Formation to determine a paleo-arctic latitudinal temperature and precipitation gradient between interior Alaska and the arctic coast.

4) Use carbon-isotope ratios, derived from fossil wood fragments and bulk organic matter, to identify shifts in the global carbon cycle and paleo-atmospheric CO_2 (Gröcke , 2002) such as the middle Maastrichtian event (MME) (Keller, 2001; Bralower et al., 2002; Nordt et al., 2003; Dworkin et al., 2005; Frank et al., 2005).

5) Determine the depositional environment and the age of bentonites found at the East Fork Toklat River section of the Cantwell Formation using U-Pb geochronology, and compare the age with the palynological record (Ridgway et al., 1997).

These objectives are covered in three chapters:

Chapter 1 "Origin of Clay Minerals in Alluvial Paleosols, Prince Creek Formation, North Slope Alaska: Influence of Volcanic Ash on Pedogenesis in the Late Cretaceous Arctic." I am the primary author of this paper. I performed the lab analyses with samples collected by Peter Flaig. I analyzed all the lab data and made the interpretations presented in the paper.

Chapter 2 "Determining Late Maastrichtian climate of the lower Cantwell Formation, Alaska: terrestrial isotopic evidence of warmer conditions." In this paper I am the primary author. I collected samples from the the field, measured the stratigraphic section, and did the lab analyses. I interpreted the data presented in the paper.

Chapter 3 “Multi-proxy Paleoclimatic Interpretation of the Paleo-arctic Prince Creek Formation, North Slope, Alaska.” I am the primary author of this paper. I performed the lab analyses and interpreted the data presented.

Chapter 1. Origin of Clay Minerals in Alluvial Paleosols, Prince Creek Formation, North Slope Alaska: Influence of Volcanic Ash on Pedogenesis in the Late Cretaceous Arctic[1]

1.1 Abstract

We studied the mineralogical and chemical composition of the clay-size fraction (< 2 μm) of three paleosol profiles and two bentonites from the Late Cretaceous (Maastrichtian) Prince Creek Formation, North Slope, Alaska. Analyses of X-ray diffraction (XRD) patterns and chemical compositions of clays indicate that the main detrital minerals observed in the clay-size fraction are smectite, discrete illite, kaolinite, chlorite, and quartz. The clay mineral assemblage is derived from fluvial detritus associated with pre-existing sediments eroded from the Brooks Range, mixed with reworked volcanic ash fall-derived bentonites. XRD patterns of the total clay and fine clay fractions (< 0.2 μm) indicate that the main mixed-layer clay is illite/smectite. We consider the illite/smectite to be the product of illitization of smectite during weathering and pedogenesis. Diagenetic transformation of smectite to illite is unlikely in the Prince Creek Formation as maximum burial temperatures never exceeded~ 48 °C, less than the temperature required to transform smectite into illite during diagenesis. In the Prince Creek Formation, smectitic parent materials were deposited by epiclastic volcanic ash-rich alluvium that accumulated on imperfectly drained floodplains. The predominance of bentonite-derived smectite (>80%), low bulk density, phosphorous accumulation, Fe and Al mass-balance trends and the presence of Fe-Al-humus complexes in one paleosol profile (KRM) is interpreted as evidence of andic soil properties and, therefore, as an Andept-like alluvial paleosol.

[1] SUSANA SALAZAR JARAMILLO, PAUL J. MCCARTHY, TOM P. TRAINOR, SARAH J. FOWELL. 2014. "Origin of Clay Minerals in Alluvial Paleosols, Prince Creek Formation, North Slope Alaska: Influence of Volcanic Ash on Pedogenesis in the Late Cretaceous Arctic." Journal of Sedimentary Research.

1.2 Introduction

Clay mineral studies from pre-Quaternary paleosols are increasingly common and can provide significant qualitative and quantitative information on paleoclimate and soil environmental properties, surface weathering characteristics, and diagenesis (e.g. Środoń, 1999; Vitali et al., 2002; Huggett and Cuadros, 2005; Sheldon and Tabor, 2009). Clay minerals originate from a variety of different processes but only those clay minerals that are the product of surface weathering give information about pedogenesis and paleoclimate (Singer, 1980; Singer, 1984). Therefore, it is important to differentiate clay minerals found in terrestrial sedimentary deposits based on whether they are the products of pedogenesis (low temperature weathering), diagenesis (burial alteration), transport (detrital clays), or some combination of two or more of these processes (Wilson, 1999).

Studies of clay minerals from high latitude paleosols remain scarce (e.g. Kodama et al., 1976; Foscolos et al., 1977) and the Prince Creek Formation provides an exquisite opportunity to examine clay mineral development in paleosols that formed under paleo-arctic greenhouse climate conditions. A more refined understanding of surface processes under ancient warm-Earth climate states has significant societal implications as Earth undergoes a current phase of global warming (Montañez et al., 2007; Parrish et al., 2012). Paleomagnetic reconstructions indicate that the Prince Creek Formation, North Slope, Alaska, was deposited at a paleolatitude of 83°-85° N during the Late Cretaceous (Ziegler et al., 1983; Lawver et al., 2002), and recent sedimentological, paleopedological, paleobotanical and paleontological studies provide details of this ancient arctic ecosystem (Fiorillo et al., 2010 a,b; Flaig et al., 2011, 2013). High density dinosaur bonebeds in the Prince Creek Formation (Fiorillo et al., 2010a) were deposited on a sedimentologically active, low-lying coastal plain adjacent to the paleo-arctic ocean (Flaig et al., 2011).

The purpose of this paper is to characterize the clay minerals present in three alluvial paleosols from the Late Cretaceous (Maastrichtian) Prince Creek Formation that formed in a much warmer arctic but one with a polar light regime similar to that experienced at high latitudes today (Spicer, 2003; Spicer and Herman, 2010; Tomsich et al., 2010). We

identify the origin of these clays and their parent materials, interpret the pedogenic processes acting on these floodplains, and discuss the paleosol types. Low pH, phosphorous accumulation, Fe and Al-humus complexes, high organic matter, and an abundance of 2:1 clay minerals lead to the hypothesis that the genesis of the paleosols was strongly influenced by the properties of the parent material. Further, the clay minerals from epiclastic sources contributed to the development of non-allophanic properties leading us to suspect the presence of Andept-like paleosols.

1.3 Geologic Setting

1.3.1 Stratigraphy

The Prince Creek Formation is a Late Cretaceous (Maastrichtian) alluvial-deltaic coastal plain succession that was deposited in the Colville Basin, an east-west-trending, asymmetrical foreland basin to the north of the Brooks Range mountain belt (Fig. 1.9.1). The foreland basin-fill was deposited from middle Jurassic through Tertiary (Bird and Molenaar, 1992). The Prince Creek Formation interfingers with, and is overlain by, marine and marginal-marine sediments of the Schrader Bluff Formation (Fig. 2; Mull et al., 2003; Phillips, 2003).

The age of the entire Prince Creek Formation extends from Campanian to Paleocene, (Conrad et al.,1990; Moor et al., 1994; Bice et al., 1996), however, recent biostratigraphic and geochronologic analyses from exposures along the Colville River (Fig. 1.9.1) indicate an early Maastrichtian age for all of the samples included in our data set (Fiorillo et al., 2010a, b; Flaig, 2010; Flaig et al., 2011, 2013). The Prince Creek Formation was buried to depths of ~ 600 to 2000 m (Burns et al., 2005), and vitrinite reflectance values suggest a maximum burial temperature of ~ 48 °C (Barker and Pawlewicz., 1986; Robinson 1989; Johnson and Howell 1996).

1.3.2 Depositional Environments

The Prince Creek Formation consists of interbedded, very fine- to fine-grained sandstone, conglomerate, organic-rich siltstone, and coal with thin bentonites and tuffs, and abundant remains of both vertebrates and plants (Mull et al., 2003). Detailed descriptions of facies and alluvial architecture of the Prince Creek Fm. are presented elsewhere (Fiorillo et al., 2010a, b; Flaig et al. 2011), but a brief summary is provided here. The Prince Creek Formation is interpreted as a large, tidally influenced alluvial/deltaic depositional system consisting of meandering trunk channels, meandering and anastomosing distributary channels, and mud-rich floodplain deposits with paleosols (Phillips, 2003; Fiorillo et al., 2010a, b; Flaig et al., 2011, 2013). The depositional system grades northward into deltaic distributary channels and marginal marine interdistributary bays and tidal flats (Phillips, 2003; Flaig et al., 2011; Fiorillo et al., 2010a).

1.3.2.1 Fluvial Channels.

The Prince Creek Fm. contains three distinct channel-forms. Medium- to fine-grained multi-story sandbodies that lack root traces and are capped with inclined heterolithic stratification (IHS) that are interpreted as large meandering trunk channels. The presence of IHS, composed of rhythmically repeating sand and mud couplets, suggests a tidal influence (Flaig et al. 2011).

Single-story, fine-grained sandbodies, encased in floodplain fines, dominated by IHS and rooted throughout are interpreted as small, meandering distributary channels (Flaig et al. 2011). Other small, very-fine to fine-grained, single-story, current-rippled and ubiquitously rooted sandbodies that are present in tiers at a single stratigraphic level are interpreted as laterally stable ribbon sandbodies (Flaig et al. 2011).

1.3.2.2 Floodplains, Paleosols and Biota.

Alluvial plains in the Prince Creek Formation are dominated by fine-grained sediments reflecting a variety of floodplain sub-environments. Small sheet-like sandstones and siltstones are interpreted as crevasse splays and levees (Flaig et al., 2011). Thin packages of interbedded, ripple cross-laminated, rarely rooted or burrowed siltstone and mudstone are interpreted as small floodplain lakes and ponds (Flaig et al., 2011). Organic-rich mudstone, carbonaceous shale, and coal (typically < 0.5 m thick) record organic deposition in swamps or on poorly drained floodplains. Thin (< 1 m thick) tuffs and bentonites are locally present.

Drab-colored, rooted and mottled siltstones and mudstones are interpreted as paleosols (Brandlen 2008; Fiorillo et al. 2010a, 2010b; Flaig et al., 2013). Field characteristics, micromorphology, geochemistry and palynology have been analyzed in detail for nine pedotypes representing the range of pedogenic development in the Prince Creek Formation (Flaig et al., 2013). The paleosols are all relatively immature and are characterized by blocky structures, gley and redoxymorphic features, abundant carbonaceous organic material, Fe-depletion coatings on soil structural surfaces, and siderite, suggesting that the soils were periodically wet and anoxic. Redoximorphic features, record episodic water-table fluctuations, and form through the reduction, movement, and re-oxidation of Fe- and Mn-oxides and hydroxides after water saturation and desaturation (Vepraskas and Lindbo, 2012; Lindbo et al., 2010). The presence of Fe-rich mottles, ferruginous and manganiferous nodules, void and grain coatings, burrows, and weakly developed illuvial clay coatings, suggests periodically oxidizing conditions and periodic drying out of some of the soils (Fiorillo et al., 2010a, b; Flaig et al., 2013). Specific conditions for Fe and Mn reduction are: saturation with oxygen-depleted water, the presence of sufficient organic matter and micro-organisms, and temperatures above 5 ºC that permit biological activity (Vepraskas, 1996). Formation of concentric nodules occurs over many wet and dry cycles or fluctuations of the water table (D´Amore et al., 2004).

Abundant and diverse biotic remains have been recovered from Prince Creek paleosols. Palynomorphs include: (1) *in-situ* and reworked peridinioid dinocysts and acritarchs; (2) brackish and freshwater algae such as *Botryococcus braunii, Pedisatrum, Sigmapollis psilatus,* and *Pterospermella*; (3) projectate pollen including *Aquilapollenites quadrilobus*, *Aquilapollenites aucellatus*, *Aquilapollenites scabridus*, and *Azonia cribrata*; (4) *Wodehouseia edmontonicola*; (5) pollen from lowland trees, shrubs, and herbs dominated by *Cranwellia*, *Reticulatasporites*, *Perinopollenites*, and *Taxodiaceaepollenites*; (6) Bisaccate pollen; (7) fern and moss spores dominated by *Deltoidospora*, *Laevigatosporites*, *Lycopodiumsporites*, *Osmundacidites*, and *Psilatriletes*; and (8) fungal hyphae (Flaig, 2010).

1.3.2.3 Paleosols for Clay Mineralogical Study.

In this paper we focus on clay minerals from three paleosol profiles, North Kikak-Tegoseak (NKT), Kikiakrorak

River Mouth (KRM) and Liscomb Bonebed (LBB), from a south-to-north transect along the Colville River, Alaska (Fig. 1.9.1). Brief descriptions of the main characteristics and biota associated with these three profiles are given below, and full details can be found in Flaig et al. (2013).

1.3.2.3.1 North Kikak-Tegoseak Paleosol (NKT):

The NKT paleosol forms the upper part of a 4.5 m-thick cumulative paleosol succession (Fig. 1.9.3; Flaig et al., 2013). This paleosol consist of 80 cm of light olive-grey (5Y 5/2) blocky mudstone containing abundant carbonaceous root traces, overlain by 70 cm of dark yellowish-brown (10YR 4/2) blocky mudstone with few, very fine carbonaceous root traces. This is overlain by 80 cm of very dark grey (5Y 3/1) blocky mudstone with siderite nodules up to 2 cm in diameter and rare, very fine root traces. The upper surface is truncated and the paleosol is capped by 20 cm of carbonaceous shale with abundant

plant fragments. This paleosol is interpreted as similar to an *Aquic Inceptisol* (Soil Survey Staff, 1999).

The biota in the NKT paleosol is dominated by bisaccate (conifer) pollen, *Laevigatosporites* (ferns), and *in situ* and reworked peridinioid dinocysts, and the sedimentology indicates soil formation in a point bar setting (Flaig et al., 2011). This suggests that point bars supported fern communities while pollen from hinterland conifers and older, reworked peridinioid dinocysts was incorporated into point bar soils by upland erosion, fluvial transport and deposition during floods (Flaig et al., 2013).

1.3.2.3.2 Kikiakrorak River Mouth Paleosol (KRM):

The KRM paleosol forms the upper part of a 4.0 m-thick compound paleosol (Fig. 1.9.4A; Flaig et al., 2013). The base of this paleosol consists of 70 cm of massive, very fine-grained sandstone which is gradationally overlain by a 160 cm-thick ripple cross-laminated to massive, dark olive grey (5Y 3/2) siltstone. The top of the siltstone contains current-ripples, carbonaceous root-traces, and plant fragments and is overlain by 90 cm of light olive grey (5Y 5/2) blocky mudstone. This paleosol is interpreted as similar to an *Aquic Inceptisol* (Soil Survey Staff, 1999). Palynomorph assemblages in the KRM paleosol are dominated by *Aquilapollenites scabridus* and *Psilatriletes* suggesting soil development at the margin of a freshwater swamp (Flaig et al., 2013).

1.3.2.3.3 Liscomb Bonebed Paleosol (LBB):

The LBB paleosol is a 4.25 m-thick compound paleosol (Fig. 1.9.4B). The lower paleosol is a 75 cm-thick massive to blocky siltstone that contains carbonaceous root traces and plant fragments and is overlain by 80 cm of brown (10YR 4/3) blocky mudstone with very fine carbonaceous root traces. The brown mudstone is overlain by 25 cm of carbonaceous shale with abundant plant fragments. This paleosol is interpreted as similar to an *Aquic Inceptisol* (Soil Survey Staff, 1999). The upper part of this compound paleosol is a 90 cm-thick light olive grey (5Y 5/2) blocky mudstone with carbonaceous

root traces, jarosite halos up to 5 mm-thick and rare euhedral gypsum crystals. This paleosol is interpreted as a potential acid sulphate soil (Fanning and Fanning, 1989).

Palynomorph assemblages of the LBB paleosol are dominated by bisaccate (conifer) pollen, *Laevigatosporites* (ferns), *Sigmapollis psilatus* (algae), *Taxodiaceaepollenites* (lowland trees) and include both *in situ* and reworked peridinioid dinocysts. This suggests pedogenesis in an area of the lower delta plain, adjacent to distributary channels, that repeatedly received overbank alluvium (Flaig et al., 2013).

1.4 Methods

Nineteen samples from the three selected paleosol profiles (NKT, KRM, LBB) and two bentonite samples (KKT, PFDV 17; Fig. 1.9.1) were selected for detailed clay mineralogical and geochemical analyses.

1.4.1 Clay Mineral Identification

The <2 μm clay fraction was separated by sedimentation using the pipette method (Burt, 2004). Preferred-orientation clay mineral slides were prepared with the filter transfer method (Moore and Reynolds, 1997). The <0.2 μm fraction was isolated from the total clay by centrifugation using the time and speed calculated with Centriset (Poppe and Eliason, 2009). Appendix.1.12.1 shows a summary of the lab methods.

The clay mineralogy of coarse (<2 μm) and selected fine (<0.2 μm) clay-size fractions was determined by X-ray diffraction (XRD) using a Panalytical X'PERT PRO Materials Research Diffractometer (MRD), at the University of Alaska Fairbanks *Advanced Instrumentation Laboratory* (AIL). The instrument utilized a Cu k-α source (45kV and 40mA), a Ni filter, 0.02 radian Soller slits, a ½ degree divergence slit, and an Xcellerator strip detector. Three scans, 2 to 60° 2θ, were performed for each sample using a 0.0125° step size and a count time of 20 s/step. Each sample was interpolated to a mean step value of 0.02°.

Seven XRD runs were performed for each < 2 μm sample; these include an air dried sub-sample, Ca-, Mg- and K-saturated sub-samples, an ethylene-glycol (EG) solvated sub-sample (24 hours), and sub-samples heated at 300 ºC and 550 ºC for four hours. Random powder mounts of the air-dried <2 μm clay fraction were prepared in 0.7 mm glass capillary tubes to determine illite polytypes and distinguish between dioctahedral and trioctahedral clay minerals. Two XRD runs were performed on selected < 0.2 μm samples following Mg-saturation and EG solvation.

Clay mineral identification was carried out according to Moore and Reynolds (1997). Illite-smectite (I/S) mixed-layered clays were identified following Środoń (1984, 1999). The I/S interstratification analysis (random, partially ordered, and ordered) was determined qualitatively by comparison with calculated diffraction profiles and tables that show the relationship between clay composition and peak position (Moore and Reynolds, 1997; Reynolds, 1980). We used R=0 (random ordered) taken from the "Reichweite" (R) notation (Reynolds, 1980). Polytypes were identified by diagnostic peaks (Moore and Reynolds, 1997) and quantified using the intensity ratio of peaks at 2.80 Å /2.58 Å (Maxwell and Hower, 1967). Semi-quantitative analyses of the diffraction data were carried out using Mineral Intensity Factors (MIF´s) taken from the literature (Biscaye, 1965; Laves and Jähn, 1972; Tributh 1991; Kahle et al., 2002) and also calculated using NEWMOD (Reynolds, 1985). The amount of each clay mineral can be calculated based on the MIF (Mineral Intensity Factors) using the so-called 100% approach. This method gives the relative proportions of the clay minerals normalized to 100% (Moore and Reynolds, 1997; Kahle et al., 2002). The MIF can be obtained through the application of a relationship between diffracted X-ray intensity and instrumental, geometric, and crystallographic parameters (see for more details Moore and Reynolds, 1997), or in the lab by preparing mixtures with known amounts of the mineral of interest and the chosen internal standard (Środoń et al., 2001). Some authors (e.g. Bronger, 2003) adopt the MIF values reported in the literature (examples of MIF values are in Laves and Jähn, 1972; Biscaye, 1965; Weir et al., 1975). Semi-quantitative methods (like the MIF

approach) are analyses expressed in terms of quality but for which the uncertainty is not known or unreasonably large (Hillier, 2003).

We assumed that smectite (montmorillonite), illite, kaolinite, chlorite, quartz and I/S mixed-layers constituted 100 % of the mineralogy in the total clay fraction. The area of the peaks in the Mg-glycolated samples used were: 17 Å peak for smectite (montmorillonite), 10 Å peak for illite, 7.2 Å peak for kaolinite, 7.1 Å peak for chlorite, and 4.26 Å peak for quartz. The illite/smectite (I/S) 002/003 reflection was used to estimate weight percent. The MIF taken from literature are in Appendix 1.12.2.

1.4.2 Geochemistry

The weight percent of clay minerals, determined from semi-quantitative analyses of the XRD data, was verified with geochemical data obtained using a Cameca SX-50 electron microprobe at the University of Alaska Fairbanks *Advanced Instrumentation Laboratory* (AIL). Compositional analyses of the <2 μm clay fraction were acquired on the microprobe operated with a 40º takeoff angle, a beam energy of 15 keV, a beam current of 10 nA, and a beam diameter of 10 μm. Elemental analyses were acquired using the analyzer crystals LIF for Mn ka, Fe ka, PET for K ka, Ca ka, and TAP for Al ka, Mg ka, Na ka, Si ka and the EDS for Ti ka. Calibrations were performed relative to both mineral and synthetic standards from CAMECA and SPI Inc., with detection limits in the 0.01 wt. % range. The counting time was 10 seconds for Mg ka, Si ka, Al ka, Ca ka, K ka, Mn ka, Fe ka, and Na ka, and 60 seconds for Ti ka. Oxygen was calculated by cation stoichiometry and included in the matrix correction. H_2O was calculated by difference from 100%.

Abundances (in wt. %) of the light major oxides SiO_2, Al_2O_3, Fe_2O_3, Na_2O, MgO, P_2O_5, K_2O, CaO, MnO and TiO_2 were measured from bulk samples using a PANalytical Axios wavelength-dispersive X-ray fluorescence spectrometer (WD-XRF) at the University of Alaska Fairbanks *Advanced Instrumentation Laboratory*. Each analyte was calibrated against certified standard reference materials available from the United States Geological

Survey and the United States National Institute of Standards and Technology. The accuracy of calibrations relative to reference materials is generally within 10%, whereas the precision (1σ) of replicate analyses (3x) of a representative sample is better than 0.01 wt.%. Samples were prepared by powdering using hardened steel vials from SPEX CertiPrep Group, and pressed into 35 mm diameter pellets using a polyvinyl alcohol binder. Major oxide concentrations were used for geochemical mass-balance calculations (Brimhall and Dietrich, 1987; Brimhall 1991a, b) after bulk density measurements were determined by the clod method (Blake and Hartge, 1986).

1.4.3 Extractable Fe, Al and Si

Paleosol samples were processed at the University of Alaska *Matanuska Experimental Farm Soils Laboratory.* Acid ammonium oxalate and sodium pyrophosphate extraction procedures (Parfitt and Childs, 1988; McKeague,1978) were used to identify amorphous forms of Fe and Al. Acid ammonium oxalate extracts Al and Fe from allophane, imogolite and Al/Fe-humus complexes (Al_o and Fe_o) (McKeague, 1978; Wada, 1989), as well as Si from allophane and imogolite (Si_o) and Fe from ferrihydrite (Parfitt and Childs, 1988). Sodium pyrophosphate extracts amorphous inorganic forms of Al and Fe (Al_p and Fe_p) only slightly but it does extract Fe from ferrihydrite and goethite. Sodium pyrophosphate extractable Fe is, therefore, not a reliable indicator of Fe in Fe-humus complexes. In contrast, pyrophosphate-extractable Al corresponds to Al in Al-humus complexes (Parfitt and Childs, 1988; van Breemen and Buurman, 2002).

The acid ammonium oxalate extraction is also used to identify andic soil properties, which is a diagnostic soil characteristic used for Andisol classification (Soil Survey Staff, 1999).

1.5 Results

1.5.1 Paleosol Clay Mineral Identification

XRD patterns from three paleosols (NKT, KRM, LBB) from the Prince Creek Formation are shown in Figs. 1.9.5-1.9.10. In all three paleosols the total clay fraction (<2 μm) contains discrete smectite (S) as indicated by the shift of the 13.74 Å and 12.08 Å peaks in the Ca and Mg saturated samples to ~17Å in the Ca and Mg EG saturated samples, respectively (Fig. 1.9.9). Discrete illite (I) is identified by peaks at 10 Å, 5 Å and 3.3 Å in all samples. Kaolinite (Kaol) is identified by peaks at 7.2 Å and 3.58 Å that collapse upon heating to 550ºC (Fig. 1.9.6). Chlorite (Chl) is identified by peaks at 14.15 Å, 7.1 Å, 4.72 Å and 3.54 Å. Heating to 550 ºC results in the collapse of the smectite and kaolinite peaks and an increase in the intensity of the illite peak (10 Å) in the K-saturated samples (Fig. 1.9.6). In contrast, the 14.15 Å chlorite peak persists, even after glycolation of Mg-saturated samples and heating to 550 ºC (Fig. 1.9.6). Mixed-layered illite-smectite (I/S) is identified from EG-solvated samples by peaks near 8.5-8.9 Å and 5.5-5.6 Å. The region near 10º and 16° 2θ shows reflections of the 001/002 (peaks near 8.5-8.9 Å) and 002/003 (peaks near 5.5-5.6 Å) I/S peaks (Fig. 1.9.5, 1.9.7, 1.9.9). The presence of a peak near 8.5-8.7 Å in EG- solvated samples suggests that I/S interstratification is random (R=0) and smectite-rich (Moore and Reynolds, 1997). Interstratified illite/smectite consists of various combinations of illite layers and smectite layers stacked parallel to the c-axis (Reynolds, 1980). R0 ordering occurs when the smectite layers are numerous (>50%) and the stacking sequence is in random order (Parry et al., 2002). R signifies the most distant layer in an interstratified sequence that affects the probability of occurrence of the final layer (Reynolds, 1980). R = 0 means random or no neighboring dependence and, therefore, no preferred sequence in stacking of layers (Środoń, 1999). Quartz is identified in the clay-size fraction by peaks at 4.26 Å and 3.34 Å (Figs. 1.9.5, 1.9.7, 1.9.9).

Paleosol profiles NKT, KRM and LBB all have similar clay fraction diffraction patterns, indicating similiarity in the clay mineralogy regardless of provenance. Variability between the profiles is restricted to relative abundances in the mineral assemblages (Fig. 1.9.12).

1.5.2 Smectite Characterization

Montmorillonite is the only variety of smectite identified in all three paleosols. It was identified by a sharp peak at ~17 Å (001) of glycolated Mg-saturated samples (Fig.1.9.10). The 002 and 003 basal reflections of the smectite EG-solvated samples are weak and occur in the region of the 001/002 and 002/003 basal reflections for I/S. Higher order reflections (e.g. ~2.81Å in EG-solvated samples) are detectable, indicating the presence of discrete smectite (Figs. 1.9.8, 1.9.9). Heating K-saturated samples to 300 ºC and 550 ºC results in collapse of the ~17 Å peak to 10 Å, further suggesting the presence of smectite (Fig. 1.9.6). The 006 reflection in randomly oriented powder mounts shows a montmorillonite peak of 1.49Å in the 62.22° to 61.67º 2θ region (Fig. 1.9.11b).

Microprobe analysis of the clay samples further suggests that montmorillonite is the type of smectite present in the clay mineral assemblages when comparing the geochemical data with the Na-montmorillonite (SWy-2) standard (Table 1.10.1). The excess Fe detected in the microprobe analysis is probably due to amorphous Fe precipitates in pedogenic features such as iron oxide mottles, nodules and coatings (Flaig et al., 2013; Figs. 1.9.3, 1.9.4).

1.5.3 Illite Characterization

Discrete illite basal reflections do not change with any treatment, showing a periodicity in the 00L diffraction patterns. The discrete illite rational series of d(001) compared to the non-regular reflections of the mixed-layered I/S is useful to differentiate discrete illite from I/S mixed-layered clays (Środoń, 1984) (Figs. 1.9.5, 1.9.7, 1.9.9). The 00L (001, 002 and 004) illite peaks do not shift with glycolation (Figs. 1.9.5-1.9.7, 1.9.9) and the

d≈5 Å (Figs. 1.9.5, 1.9.7,1.9.9) and d≈1.99 Å (Fig. 1.9.8) peaks are present in most samples and remain in that position regardless of the treatments.

In randomly oriented samples, the 060 reflections are used to identify illite polytypes (Fig. 1.9.11a; Moore and Reynolds, 1997). All samples show at least three of the $2M_1$ polytype diagnostic reflections at 3.88 Å, 3.49 Å, 3.20 Å, 2.98 Å, 2.86 and 2.79 Å (Fig. 1.9.11a). The $2M_1$ polytype reflections at 3.49 Å, 3.20 Å, 2.98 Å, 2.86 and 2.79 Å are well-defined (Fig. 1.9.11a) while the 1M polytype reflections are weak or absent except for a weak reflection at 3.07 Å that is present in samples LBB 20 and LBB 23, suggesting small amounts of the1M polytype in those samples (Fig. 1.9.11a).

1.5.4 Illite/Smectite (I/S) Characterization

Smectite is the main component of the I/S mixed-layered clays. In the total clay diffraction patterns, two broad peaks (~8.7Å and ~5.6 Å) in the region near 10° 2θ and 16 to 17.7° 2θ show reflections of the I/S 001/002 and 002/003 peaks, respectively (Figs. 1.9.5-1.9.7, 1.9.9-1.9.10). The significant shift in the peak of the EG-solvated sample that occurs as a shoulder of the 001 illite reflection is diagnostic of I/S (Figs. 1.9.6, 1.9.10). In the EG-solvated samples the ordering type of the I/S (Reichweite) is determined by the position of the reflection between 5º and 8.5º 2θ (Moore and Reynolds, 1997). The percent of illite layers in the I/S can be estimated by the difference between the 001/002 and 002/003 reflections (Δ2θ) (Moore and Reynolds, 1997). In all the samples the illite content of the I/S mixed-layered clay varies between 10 and 20% (Fig. 1.9.13). In the <0.2 μm fraction, I/S is the main mixed-layer clay (Fig. 1.9.14).

1.5.5 Kaolinite Characterization

The 001 and 002 kaolinite reflections are nearly superimposed upon the chlorite 00L series. Nevertheless, in the NKT and KRM profiles it is possible to differentiate, kaolinite (3.58Å) and chlorite (3.54Å), as two sharp peaks next to each other at 25° 2θ (Fig. 1.9.6). The presence of the 003 peaks of both chlorite and kaolinite allows the identification of

each mineral since neither of these reflections interferes with the reflection from the other (Figs. 1.9.5, 1.9.6, 1.9.7, 1.9.9). Heating at 550 ºC collapses the kaolinite peaks, confirming its presence in the paleosols (Fig. 1.9.6).

1.5.6 Chlorite Characterization

The 001 and 003 reflections of chlorite, d≈14.15Å and d≈4.72Å respectively, allow differentiation of chlorite from kaolinite (Figs. 1.9.5, 1.9.7, 1.9.9). After heating at 550ºC, the 001 chlorite reflection increases in intensity and the 002, 003 and 004 reflections are weakened indicating the presence of discrete chlorite (Moore and Reynolds, 1997;Fig. 1.9.6). Chlorite is present mainly in the LBB profile (Figs. 1.9.9, 1.9.12).

1.5.7 Clay Mineral of the Bentonites

Montmorillonite is the only clay mineral identified in the PFDV and KKT bentonites. Mg-saturated and glycolated samples expand to ~17 Å. The series of basal reflections, with no splitting associated with glycolation, indicates well-ordered stacking sequences with no interstratification (e.g. Olsson and Karnland, 2011) (Fig. 1.9.15).

1.5.7 Semi-quantitative Cay Mineral Analysis

Fig. 1.9.12 illustrates the representative weight percent distribution for the clay minerals within the NKT, LBB and KRM paleosol profiles determined using the MIF 100% approach (Kahle et al., 2002). There is low variability between the profiles. The clay mineral assemblages of the three profiles consist of discrete smectite, illite, kaolinite, chlorite and mixed-layer I/S. We estimated the MIF values by using MIF values taken from the literature (Weir et al., 1975; Kahle et al., 2002; Biscaye, 1965) and values using the NEWMOD program (Reynolds, 1985). Semi-quantitative analysis shows that smectite is the dominant clay mineral in the three profiles (60%-81%) and almost the only constituent of the bentonites (>95%) (Fig.1.9.15). Discrete illite (4%-21%) and I/S

mixed-layered clays (5%-15%) are present in all paleosol samples, while kaolinite (0%-8%) and chlorite (0%-9%) are a minor component of the clay assemblages. Chlorite is mainly present in the LBB profile (Fig. 1.9.9) and kaolinite is mainly present in the NKT profile (Fig. 1.9.5).

In all three profiles the illite abundance shows an inverse relationship with smectite (Fig. 1.9.12). Further, the proportion of I/S mixed-layered clays increase upward (in the stratigraphic sense) until a maximum value, and then decrease to the top of the paleosols (Fig.1.9.12).

Within the NKT profile the illite abundance decreases up to NKT 42 where the trend reverses and smectite increases from NKT 34 to NKT 42. Kaolinite is present in all NKT horizons except NKT 46. Kaolinite decreases upward until NKT 42. There is no apparent trend in chlorite and it is only present in NKT 34 and NKT 46 (Fig. 1.9.12). I/S mixed-layered clays are R0 illite(0.10)/smectite until NKT 42 where the illite content in the mixed-layered clays increases to R0 illite(0.20)/smectite (Fig. 1.9.13). In the soil profile there is a discontinuity at NKT 42 that is also marked by the Ti/Zr ratio from whole-rock geochemistry (Fig.1.9.3). The amount of illite in the I/S mixed-layered clays increases in the Bg horizon (NKT 42, NKT 44) (Fig.1.9.3).

In the LBB profile there is a change in the wt. % trend of illite and smectite from LBB 20 to LBB 21 (Fig.1.9.12). There is a discontinuity marked by the Ti/Zr ratio from whole-rock geochemistry that separates two paleosols (Fig.1.9.4). One paleosol is formed by LBB 19 and LBB 20, the second paleosol is formed by LBB 21 to LBB 23, as shown by the pedogenic features and geochemistry (Fig.1.9.4). Kaolinite is only present in the upper paleosol (LBB 21 to LBB 23). On the other hand, chlorite is present in all samples and shows a trend that increases upward in the profile (Fig.1.9.12). I/S mixed-layered clays show the same trend in the two paleosols, they decrease from R0 illite(0.20)/smectite at the bottom to R0 illite(0.15)/smectite at the top (Fig.1.9.13).

In the KRM profile there is a change in the proportions of the clay minerals at KRM 23. This change is also marked by an increase in the I/S mixed-layered clay (Fig.1.9.12). The amount of illite in the I/S mixed-layered clays increases from R0 illite(0.10)/smectite to R0 illite(0.25)/smectite in the Bg horizon (KRM 23) (Fig.1.9.13).

1.5.8 Clay Mineral Geochemistry

Using the standard composition of kaolinite (KGa-1), Na-montmorillonite (SWy-2), illite (IMt-1) and Chlorite (CCa-2) (Van Olphen et al., 1979; Table 1.10.2) and weight percent values obtained from XRD (Fig.1.9.12), we calculated the chemical composition of the paleosol clay samples (Table 1.10.3). The calculated chemical compositions are compared with microprobe analyses of the clays as a cross-check on the overall analysis (Fig. 1.9.16; Table 1.10.1 and table 1.10.3). There is a good correlation between the two methods, particularly for the more abundant components (SiO_2, Al_2O_3 and Fe_2O_3) (R^2 = 0.9884). There is a reasonable correlation for the less abundant components (MgO, K_2O, CaO, Na_2O and TiO_2) (R^2 = 0.36), which might be due to analytical error or variability in the composition of soil minerals.

1.5.9 Geochemical Composition of Bentonites

Two bentonite samples (KKT and PFDV-17, Fig. 1.9.1) plot in the rhyolitic to rhyodacitic compositional fields on a Zr/TiO_2–Nb/Y classification diagram (Fig. 1.9.17; Winchester and Floyd, 1977).

In order to test the hypothesis that the clay minerals in the Prince Creek paleosols are derived, at least partly, from bentonite parent materials with a similar chemical composition to KKT and PFDV 17, pure smectite and illite end members were plotted using the Al/K-Si/K diagram (Fig. 1.9.18; De Caritat et al., 1994). The smectite end member values were taken from the electron probe micro-analysis data of our bentonite samples (Table 1.10.1). Illite end member values were taken from the ideal illite stiochiometry (IMt-1) (Van Olphen et al., 1979;Table 1.10.2). When clay mineral

chemical compositions of all NKT, KRM and LBB profiles, obtained from the microprobe, are plotted on the diagram, there is a strong linear compositional relationship (R^2=0.98) between illite, the bentonites and the paleosol clay samples (Fig. 1.9.18).

1.5.10 Geochemical Mass Balance Calculations

Molecular ratios of relatively inert geochemical indicators are commonly used to locate lithologic discontinuities in soils and paleosols (Chittleborough et al., 1984; McCarthy et al., 1997). Ti and Zr are found in minerals that are resistant to alteration and, therefore, tend to accumulate as weathering progresses (Maynard, 1992). In uniform parent materials, ratios of Ti/Zr should change gradually and uniformly with depth, without sharp inflections or reversals in trends (Birkeland, 1999). Depth plots of calculated Ti/Zr ratios indicate large inflections that coincide with discontinuities identified on the basis of grain size and micromorphological features. The NKT profile shows a change in the trend of the Ti/Zr ratio at NKT 42 (Fig. 1.9. 3). In the LBB profile there is a change in this ratio at LBB 20 (Fig. 1.9. 4) and in KRM there is a gradual decrease in the Ti/Zr ratio with depth and a small inflection at KRM 23 (Fig. 1.9.4). These inflections coincide with parent material discontinuities in these paleosols.

Geochemical mass-balance calculations are widely used to identify residual enrichment, volume changes and element translocation that reflect weathering trends in soils and paleosols (Brimhall et al., 1991a, b; Driese et al., 1992; McCarthy and Plint, 2003). Mass balance calculations need to be viewed with caution in alluvial systems since some of the observed geochemical variability may be related to geochemical variability in the original parent materials. Ti was selected as the immobile index element for mass balance calculations because its distribution with depth was generally less variable than that of Zr.

Volume change calculations (strain) using Ti as the immobile strain marker indicate moderate collapse at KRM 23 that coincides with changes in the clay mineralogy and also with the proportion of illite in the I/S mixed-layered clays (Figs. 1.9.4, 1.9.13). Moderate collapse is also identified at LBB 20, that corresponds to a discontinuity

identified on the basis of grain size and the Ti/Zr ratio (Fig.1.9. 4). Moderate dilation occurs at NKT 40 and NKT 42 suggesting additions of new alluvial parent material (Fig. 1.9.3).

To interpret weathering trends in the paleosols, the C horizons were used as an approximation of the parent material of the soil profiles. The mass transport calculations show gains (positive values) or losses (negative values) of each major element in the paleosols compared to the parent materials.

The NKT profile has Fe depletion and minor depletion of Al and Si in the NKT 46, NKT 44 and NKT 42 (Bg and Bw) horizons, and significant accumulation in the NKT 40 (Bt) horizon. There is also a general depletion of Ca, Mg Na and K except at NKT 42 where a positive excursion corresponds with a lithological discontinuity. Phosphorous shows loss except in the NKT 40 horizon where it shows a gain of 30% (Fig.1.9.3).

In the KRM profile, all horizons (except KRM 25, the uppermost one) show Si and Al depletion (maximum loss of 36%) and phosphorous mass-balance values between 0.2 and 2 (20-200%) indicating pronounced P accumulation. Manganese shows significant accumulation of 30-100%, and depletion in the upper horizon (KRM 25) of 90%. Mg, Na and K show similar trends to Al and Si but increases occur in the upper two horizons (KRM 25 and KRM 24) (Fig.1.9.4).

Geochemical variability in the LBB profile is attributed to lithological discontinuities since LBB is a composite paleosol.

1.5.11 Extractable Iron and Aluminum

Al_p/Al_o and Fe_p/Fe_o ratios in Andisols indicate the relative proportions of active Al and Fe in organic complexes (Pinheiro et al., 2004). Al_p/Al_o ratios can be used to separate allophanic Andisols (ratio < 0.5) and non-allophanic Andisols (ratio > 0.5) (Saigusa et al., 1991 in Shoji et al., 1993). The acid ammonium oxalate and pyrophosphate extraction values (Table 1.10.5) show that active Fe and Al are significant components of the NKT

and KRM paleosol profiles. The NKT 42 and KRM 25 horizons have 3.8% and 3.4%, respectively, of Al_o plus 1/2 Fe_o (Table 1.10.5), which meet the required characteristics for andic soil properties. The data in table 1.10.5 show that horizons NKT 42 and KRM 25 also have Al_p/Al_o ratios >0.5.

1.6 Discussion

Here, the various clays identified are interpreted as pedogenic, diagenetic or detrital. From the inherited clays we characterized, we inferred the parent material source and use pedogenic clays to identify pedogenic processes and infer the environmental conditions required for their formation.

1.6.1 Clay Mineral Origin

Clay minerals in soils and paleosols result from three main processes: detrital inheritance, transformation, and neoformation (Wilson, 1999). Authigenic clays are transformed or neoformed clays that originate *in situ* by pedogenesis and/or diagenesis (Vitali et al., 2002). Initial soil parent materials typically contain inherited detrital clay minerals of diverse types and these may alter, depending on the stability of the clays, with surface soil solutions (Birkeland, 1999).

1.6.2 Detrital Smectite

Smectite, particularly montmorillonite, can have either a detrital or pedogenic origin in paleosols. Montomorillonite is formed in pedogenic environments under low temperature (surficial), alkaline conditions (pH > 7.5), with high concentrations of soluble silica and basic cations (Ca^{2+}, Mg^{2+}, Na^{+}) and low concentrations of K^{+} (Essington, 2004; Borchardt, 1989). We suggest that the smectite in our paleosols is inherited from the parent material rather than having formed in a pedogenic environment because: 1) the organic-rich nature of the paleosols suggests an acidic groundwater regime (likely pH <

4.5), 2) there is a significant source of K^+ from micas present in bulk samples, and 3) the relative proportions of smectite within individual profiles do not show a vertical trend with depth as would be expected in soils. Furthermore, some studies suggest there is a distinction between soil smectites and bentonitic smectites. Soil smectites are typically Fe-rich beidellites which are the most stable smectites in pedogenic environments, and they form at the expense of montmorillonite (Righi et al. 1998 in Sucha et al., 2001; Środoń, 1999). Since smectite in Prince Creek paleosols is mainly montmorillonte (Fig.1.9.10, 1.9.11b) we interpret it as bentonitic in origin rather than pedogenic.

The smectite found in the studied paleosols is likely to be the reworked and re-deposited product of weathered volcanic ash. Smectite is the most abundant clay mineral in the three profiles (60%-81%), followed by illite (4%-21%). In order to check if our clay samples are a mixture of detrital illite and detrital smectite, we plotted the geochemical data obtained from microprobe analyses of the NKT, KRM and LBB profiles on a Si/K vs. Al/K diagram (Fig. 1.9.18) with illite and smectite as end members. We used an ideal illite composition and a bentonite composition from a measured section at the Kikak-Tegoseak dinosaur quarry (near the KKT profile; Fiorillo et al., 2010 a, b; Flaig et al., 2011). The diagram (Fig. 1.9.18) shows a compositional relationship between illite, bentonite and the other Prince Creek clay samples. All the clay samples plot between the two end-members suggesting that their composition is the result of a mixture of detrital illite (see discussion below) with bentonite-derived smectite.

The smectite-rich bentonites can be considered the potential source for the epiclastic smectite in the NKT, KRM and LBB profiles. This is consistent with the fact that smectites are common in sediments and sedimentary rocks after periods of above average volcanism, such as that which occurred during the Cretaceous (Borchard, 1989).

1.6.3 Detrital Discrete Illite

Illite, illite polytypes and I/S mixed-layered clays identified in this study do not show evidence of a progressive illitization associated with burial diagenesis. During diagenesis,

smectite can alter to illite through a transformation sequence of smectite to I/S of different compositions, and finally to illite (Cuadros and Altaner., 1998; Meunier, 2005). The appearance of 2M1 illite polytypes coincides with the beginning of the lowest-temperature metamorphic zone during burial diagenesis (Moore & Reynolds, 1997). The 2M1 illite polytype is the most abundant polytype in our samples (Fig. 1.9.11a). For example, applying the intensity ratio at 2.80 Å /2.58 Å (Maxwell and Hower, 1967) we estimated the percentage of the 2M1 polytype of the LBB 23 sample where the peak area of the 2.80 Å is 0.3 counts, the peak area of the 2.58 Å is 1.62 counts and the 2.80Å/2.58Å ratio is 0.19, which gives a % 2M1 of 75%.

If 2M1 is the most abundant polytype, then the illite is probably derived from erosion of once deeply buried Cretaceous sediments in the Brooks Range. Burial diagenesis to metamorphic grade is unlikely in the Prince Creek Formation since maximum burial temperatures, based on vitrinite-reflectance values, never exceeded 48° C (Robinson 1989, Johnson and Howell, 1996) which is not sufficient to trigger the mineral reactions required to transform smectite into illite during diagenesis (Meunier, 2005). This is true even for Cretaceous sediments subjected to temperatures as low as 50ºC (Meunier, 2005). As a result, we interpret discrete illite as detrital, likely sourced from very low- to low-grade metamorphic rocks in the Brooks Range. We also consider detrital illite the potential source of K^+ for the smectite illitization process. In bulk samples, the K_2O plot of XRF data vs. microprobe data (of the clay fraction) shows a good correlation (Fig.1.9.19) suggesting that illite is the major source of K^+.

1.6.4 Detrital Chlorite

Primary chlorite in soils is typically of detrital origin (Barnhisel and Bertsch, 1989). Chlorite occurrence in the NKT and KRM profiles is minimal and it does not follow a vertical trend (Fig. 1.9.12). In the LBB profile, chlorite is a detectable component of the clay fraction (up to 8%) and it shows an increase vertically within the profile. The chlorites found in our samples exhibit the characteristic 00L reflections (7Å) of

trioctahedral chlorites, which are considered inherited from the parent material (as opposed to pedogenic hydroxy-interlayered vermiculite (HIV) or pedogenic chlorite) (Allen and Hajek, 1989). The lack of intermediate species, such as chlorite-vermiculite, vermiculite or chlorite-smectite, in our samples and the weak paleosol development suggests that a detrital origin for the chlorites is the most reasonable interpretation. Chlorite is a common clay mineral in recent sediments from the Beaufort Sea and Artic Ocean where it is derived from sedimentary and metasedimentay rocks from the Brooks Range and the North Slope of Alaska (Naidu et al., 1971).

1.6.5 Detrital Kaolinite

Relative proportions of kaolinite (0-8%) show no apparent trends with depth in the LBB, NKT and KRM profiles (Fig. 1.9.12), suggesting it may have a detrital origin. Kaolinite formation *in situ* is not common in weakly developed soils (Wilson, 1999). In the three Prince Creek paleosols kaolinite is interpreted as detrital instead of authigenic since kaolinite formation under surface weathering conditions is typical of highly developed soils in the tropics (e.g Aristizabal et al., 2005). Generally it occurs in freely drained, acid- and base-depleted tropical environments, where an abundant supply of water ensures the availability of the required silica and alumina cations (Wilson, 1999). Detrital kaolinite is a common clay mineral in recent sediments of the Beaufort Sea and Arctic Ocean where it is derived from sedimentary and metasedimentary rocks from the Brooks Range and the North Slope (Naidu et al., 1971). We invoke a similar detrital origin for kaolinite in clays of the Prince Creek Formation.

1.6.6 Pedogenic I/S Mixed Layered Clays

I/S is the only mixed-layered clay identified in our paleosol samples (Fig.1.9.5-1.9.7, 1.9.9). I/S comprises 5%-15% of the total clay fraction in all samples (Fig.1.9.12). In the three profiles, I/S shows an increasing upward trend, reaching a maximum in the subsurface horizons and decreasing again toward the surface horizons (Fig. 1.9.12). The

random stacking order found in NKT, KRM and LBB samples is consistent with supergene, rather than diagenetic, illitization (e.g. Huggett and Cuadros, 2005). In the <0.2 μm fraction, I/S is the main clay mineral (Fig. 1.9.14) and this fine clay fraction (<0.2 μm) is more representative of pedogenic clays since no quartz (a common mineral in the detrital fraction) is present. The presence of similar amounts of I/S in all samples may be the result of I/S being transformed *in situ* and, subsequently,it is more likely to be pedogenic than detrital.

Huggett and Cuadros, (2005) suggest that the transition of smectite to illite at low temperature occurs through Fe reduction in octahedral sites leading to increased layer charge, coupled with K fixation by smectite. The Fe reduction seems to be the result of wetting (reducing) and drying (oxidizing) cycles in gleyed soils, in which re-oxidation of reduced Fe is never complete (Huggett and Cuadros, 2005).

Similar drainage conditions are present in the gley horizons (Bg) of the NKT and KRM paleosols (Fig.s 3 and 4) which suggests that the illitization of smectite could be the result of wetting (reducing) and drying (oxidizing) cycles. Wetting and drying conditions are documented from coastal plain sub-environments of the Prince Creek Formation as the result of flooding due to periods of intense seasonal runoff related to melting snow, ice, and permafrost in the ancestral Brooks Range (Flaig, 2010). In the NKT (NKT42, NKT 44) and KRM (KRM 21, KRM 22, KRM 23) profiles the illite (pedogenic illite) of the I/S increases in the Bg horizon suggesting a relationship between illite (pedogenic illite) formation and gley horizons (Figs. 1.9.3, 1.9.4, 1.9.13). In the LBB profile the percent of illite (pedogenic illite) in the I/S increases in the Bw horizon (Fig.1.9.4, 1.9.13). This correlation is probably also due to the reducing environment of gley soils that favors illitization by Fe reduction as suggested by Huggett and Cuadros (2005). Therefore, I/S likely formed from transformation of smectite rather than from primary (detrital) illite.

It is unlikely that smectite in the I/S formed from transformation of primary illite. The formation of smectite requires a soil pH greater than >7.5, high silica concentrations and low aluminum concentrations (Borchardt et al., 1989). None of these conditions are

consistent with the organic-rich nature of the paleosols which suggest an acidic groundwater regime. Therefore we conclude that illitization of primary smectite is the probable mechanism for generating I/S mixed-layered clays in the Prince Creek Formation. Illitization of smectite is a common feature of burial diagenesis but it also occurs in soil environments (e.g. Huggett and Cuadros, 2005). There are several arguments that favor a pedogenic origin for the I/S rather than a diagenetic one:

1) Vitrinite reflectance data from the Prince Creek Formation indicates a maximum burial temperature of 48° C which is not sufficient to trigger the mineral reactions required to transform smectite into illite during diagenesis (Pollastro, 1993; Meunier, 2005).

2) In the first stages of diagenetic transformation, illite forms randomly ordered mixed-layered minerals with smectite. As the reaction progresses, the stacking sequence becomes ordered and the illite content rises (Meunier, 2005). Illite in our I/S mixed-layered clays is R=0 and illite content varies between 10-25% in all the NKT, KRM and LBB samples. There is no progression in the stacking order or in the amount of illite in the mixed-layered clays.

3) The bentonite layers that we interpret as the smectite source for the paleosol clays do not contain any I/S mixed-layered clays. As a consequence the process of illitization, resulting in I/S in the PCF appears to be exclusively of pedogenic origin.

In summary, smectite is the most abundant clay mineral in the three profiles (60%-81%) followed by illite (4%-21%), I/S (5%-15%), chlorite (0%-9%) and kaolinite (0%-5%) (Fig. 1.9.12). Discrete illite, smectite, chlorite and kaolinite are interpreted as detrital in origin. In contrast, I/S is interpreted as pedogenic in origin. For NKT, KRM and LBB paleosol profiles, the parent material is interpreted, for the most part, as a mixture of detrital smectite (from a bentonitic source) and detrital illite from Cretaceous rock units in the Brooks Range (Naidu et al., 1971) probably mixed with reworked sediments. Reworked material derived from sedimentary and metasedimentay rocks from the Brooks Range and the North Slope of Alaska is a likely explanation for the presence of kaolinite

and chlorite (e.g. Naidu et al., 1971). The fine clay fraction (<0.2µm) is considered to be purely pedogenic because I/S is the main component and no detrital material, such as quartz, is present (Fig. 1.9.14). I/S clays are not considered to be diagenetic since the maximum burial temperature of these paleosols is not sufficient to trigger the mineral reactions required to transform smectite into illite during diagenesis (Meunier, 2005). For example, the rate of reaction in smectite is a function of geothermal gradient, with most changes occurring at 100 °C, a depth of about 1.5km (Velde et al., 1986 in Borchardt et al., 1989). These values are higher than the burial temperature estimated for the Prince Creek Formation (Robinson, 1989; Johnson and Howell, 1996).

1.6.7 Geochemical Composition of the Bentonites

The monomineralic character (pure montmorillonite) of the KKT and PFDV beds is shown in Fig. 1.9. 15. A plot of standard montmorillonite against the geochemical data of bentonites (clay fraction) and bulk sample geochemistry shows a very good 1:1 correlation (Fig. 1.9. 20, Table 1.10.4). These results indicate that the chemical composition of these bentonites is similar to the composition of a standard montmorillonite.

Bentonites are monomineralic rocks composed of smectite (montmorillonite) (Meunier, 2005). Bentonite samples (KKT, PFDV) plotted on the Zr/TiO_2–Nb/Y classification diagram (Winchester and Floyd, 1977) show an original rhyolitic to rhyodacitic composition (Fig. 1.9.17).

1.6.8 Mass-balance, Bulk Density, and Acid Ammonium Oxalate and Pyrophosphate Extraction

The geochemical trends in the NKT and KRM profiles show characteristics that can be interpreted as the result of redox processes and the presence of andic soil properties (Figs. 1.9. 3, 1.9.4). For example, the depletion of Fe and Al in NKT 46 and NKT 44 and the Fe and Al gain in NKT 40 can be attributed to a possible lithologic discontinuity and/or

accumulation in the B horizon of Fe and Al complexes translocated from the upper horizons. Acid ammonium oxalate and pyrophosphate extractable Fe and Al values (Table 1.10.5) indicate that hydrous oxides of Fe and Al are significant components of the NKT and KRM paleosols and are have formed complexes with humus.

When no volcanic glass is present, as is the case for the Prince Creek paleosols, the required characteristics for a soil to be recognized as having andic properties are that it must contain less than 25 weight percent organic carbon and meet the following additional criteria (Soil Survey Staff, 1999):

- Al plus 1/2 Fe extractable % (by ammonium oxalate) totals 2% or more; and
- A bulk density, measured at 33 kPa water, of 0.9 g/cm^3 or less; and
- Phosphate retention of 85% or more.

The NKT 42 horizon has a value of 3.8% of Al plus 1/2 Fe, however, the bulk density (table 1.10.7) and phosphate retention, based on mass-balance calculations, do not meet the requirements for andic soil properties. This may be, at least partially, because the mass-balance geochemical calculations are based on the lowest horizon as the parent material. Extractable Fe and Al values are > 2% indicating that even though phosphate retention and bulk densities are not high enough to meet criteria for andic soil properties, NKT still shows that the pedogenic processes were operating. In addition, NKT may be more weakly developed than KRM.

The KRM profile exhibits trends of Al and Si depletion and significant phosphorous gain (60-200%) (Fig. 1.9.4). Phosphorous accumulation, Al and Si depletion and low bulk density values are interpreted as evidence of andic trends (Bestland et al., 2002). The organic-rich nature of the paleosol favors the interpretation of low pH and possible migration of Fe/Al-humus complexes. This interpretation is consistent with an anti-allophanic trend (see Shoji et al., 1993). According to the acid ammonium oxalate extraction, the KRM 25 horizon has 3.4% of Al_o plus 1/2 Fe_o, low bulk density and a

phosphorous gain >100%, all of which we interpret as evidence for andic soil properties. The Mn accumulation, shown in the mass-balance calculation of the KRM profile (Fig. 1.9. 4), is consistent with the significant presence of manganese nodules (Flaig et al., 2013). In the KRM paleosol profile, the morphological features and the presence of amorphous Fe^{3+} precipitates (see microprobe data) suggest that there is a balance in the reducing and oxidizing tendencies that is diagnostic for redoximorphic soils (Essington, 2004).

1.6.9 Influence of Volcanic Ash and Paleosol Formation

Andisols are volcanic ash soils with properties inherited from or associated with properties of tephra (Shoji et al.,1993). Andisols include amorphous materials commonly formed during weathering of tephra and other materials and typically have a significant content of volcanic glass, low bulk density, and a high organic matter content (Birkeland, 1999; Soil Survey Staff, 1999). Andisols are also formed from non-tephric materials such as sedimentary rocks and mixed materials of tephra and loess (Shoji et al., 1993).

Paleosols can be classified as paleo-andisols if they have andic soil properties in sub-horizons that total 30 cm or more within 50 cm of the paleosol surface; or have >5% volcanic glass, a NaF soil pH of 9.3 and lack carbonate; or if lithified, have 5% volcanic glass in the 0.02–2.0 mm fraction in an isotropic matrix as observed in thin section (Nettleton et al., 2000). Nevertheless, key features like volcanic glass and andic soil properties typically do not persist in paleosols. Amorphous forms of silicon and aluminium, like volcanic glass and allophone, change over time to minerals like clays (Mack et al., 1993). Paleo-Andisols have been identified in Oligocene alluvial successions in the John Day Formation, Oregon, USA, based on geochemical interpretation of trends in phosphorus accumulation, potassium retention, and alumina and iron depletion (Bestland, 2002). The KRM profile shows similar trends of phosphorus accumulation and potassium retention. Additionally, this profile shows evidence of andic soil properties. Despite this evidence for andic soil properties in one

profile, the NKT, KRM and LBB paleosols are weakly developed and similar to modern *Aquic Entisols* or *Aquic Inceptisols* (Flaig et al., 2011).

The main parent material of NKT, KRM and LBB paleosols is smectite (>60%) derived from bentonites. On the Prince Creek coastal plain, the bentonite-derived smectite was incorporated as detrital material (epiclasts) that was subsequently deposited as alluvium on floodplains. The fact that the parent material is mostly of epiclastic origin, bulk densities are low, phosphorous contents are high, and Fe Al-humus complexes are present, led us to suspect the presence of Andept-like paleosols (Soil Survey Staff, 1975). The presence of allophone cannot be demonstrated in these paleosols which suggests an anti-allophanic trend. The 2:1 and 2:1:1 clay minerals and their intergrades are known to form in modern soils derived from volcanic ejecta, and these layer silicates are the dominant clay minerals in non-allophanic Andisols (Shoji et al., 1993). Furthermore, non-allophanic andisols are characterized by acidic pH values, which were probably prevalent in the Prince Creek Formation during pedogenesis.

The NKT, KRM and LBB paleosols are truncated soils where the diagnostic A horizon is absent, presenting another difficulty to the identification of the soil type. Nevertheless, the subsurface horizons of Andisols, typically Bw horizons (Shoji et al., 1993), are present in all three paleosol profiles. The mass balance shows some trends in the KRM profile that can be interpreted as phosphorous accumulation and Al and Si depletion. These trends and features, such as high organic matter and abundance of 2:1 clay minerals, indicate that the genesis of the paleosols was strongly influenced by the properties of the parent material and that the clay minerals from epiclastic sources contributed to the development of non-allophanic andic properties.

Studies of volcanic ash soils in different parts of the world illustrate the effect of climate on the soil colloidal fraction (Zehetner et al., 2003; Ugolini and Dahlgren, 2002). Soils characterized by non-allophanic clay mineralogy, an abundance of 2:1 layer silicates, intense formation of Al- and Fe-humus complexes, and a marked accumulation of humus are known to be developed from non-colored glass under mean annual precipitation

values >1000 mm (Shoji et al., 1993). The morphologic features in NKT, KRM and LBB indicate poorly drained paleosols that dried out periodically. Under poor drainage, the organic matter accumulates and its microbial decomposition is retarded by seasonal, reducing conditions, formation of Al-humus complexes, and humification (Shoji et al., 1993).

The final transformation of smectite to illite in the interlayered illlite-smectite clays occured *in situ* in the paleosol profiles NKT, KRM and LBB. The paleosols formed on the floodplains of the Prince Creek Formation reveal features of wet-dry cycles (e.g. Fiorillo et al. 2009; Fiorillo et al. 2010b; Flaig, 2010; Flaig et al., 2011) as a result of seasonal flooding due to variations in temperature and precipitation related to the high paleo-latitude of Alaska (82-85° N) in the Late Cretaceous (Flaig et al., 2011). Under these conditions, hydric soils (*Aquic Entisols* or an *Aquic Inceptisols*) are favored. Mn nodules and the presence of amorphous Fe^{3+} precipitates are indicators of redoximorphic features in hydric soils (Vepraskas and Lindbo, 2012). Since the paleosols were waterlogged, the organic matter accumulated and decomposed slowly. The reduced iron and the gray color in gley horizons are due, in part, to the bacterial decomposition of the organic matter at temperatures above freezing, and pH values close to 5, consistent with the non-allophanic trend discussed above. Chromas of 2 in the paleosols suggest that they were reduced for significant periods of time. In these waterlogged paleosols the process of pedogenic illitization can be explained by repeated wetting and drying cycles. Weathering of volcanic glass under organic matter-rich conditions with a pH < 4.9 results in organic acids being available to form metal-humus complexes. Humus competes for Al, reducing the Al available for co-precipitation with silica to form aluminosilicate minerals (Shoji et al., 1993). This process that inhibits the formation of allophane and imogolite is an anti-allophanic process.

These pedogenic processes are consistent with the paleoclimatic reconstructions of the Late Cretaceous North Slope ecosystem (Flaig et al., 2013). Redox-processes and illitization of smectite are known to occur in soils and paleosols subjected to alternating

phases of wetting and drying which may be the result of fluctuations in water table levels or the results of seasonal saturation, perhaps due to spring flooding from snow melt in the ancestral Brooks Range.

1.7 Conclusions

The clay mineralogy of the NKT, KRM and LBB paleosols of the Prince Creek Formation shows that: 1) smectite (montmorillonite) is the main clay mineral (>60 wt%) in all samples, 2) the KKT and PFDV-17 bentonites are monomineralic rocks composed of smectite, specifically montmorillonite, 3) the smectite-rich bentonites can be considered the probable source for the epiclastic smectite in the three paleosol profiles, 4) discrete illite, kaolinite and chlorite are of detrital origin, 5) I/S is the main mixed-layered clay in all samples, 6) illitization of primary smectite to produce I/S has a pedogenic origin rather than a diagenetic one, and 7) detrital illite is the most likely source of K^+ for transformation of smectite to I/S mixed layered clay.

Geochemical mass-balance, bulk density, acid ammonium oxalate and pyrophosphate extractions show that: 1) hydrous oxides of Fe and Al are significant components of the NKT and KRM paleosols and formed complexes with humus, 2) KRM has low bulk density and phosphorous gain of >100% that we interpret as evidence for andic soil properties, and 3) the NKT paleosol meets only one of the three criteria for andic soil properties (extractable Fe and Al > 2%) indicating that andic pedogenic processes were occurring but that NKT is probably more weakly developed.

Low pH, phosphorous accumulation, Fe- and Al-humus complexes, high organic matter and an abundance of 2:1 clay minerals indicate that the genesis of the paleosols was strongly influenced by volcanic ash in the parent material and that clay minerals from epiclastic sources contributed to the development of non-allophanic properties. Therefore the Prince Creek paleosols are considered Andept-like paleosols.

1.8 Acknowledgments

Financial support for this research was provided by the National Science Foundation (OPP-425636 to McCarthy), Alaska Geological Society (AGS), International Association of Sedimentologists (IAS), University of Alaska Museum of the North and the Advanced Instrumentation Laboratory (AIL) at the University of Alaska Fairbanks. The authors wish to thank Colciencias Colombia for economic support and Melissa Dick at University of Alaska Matanuska Experimental Farm Soils Laboratory for the soil analyses. The authors also wish to thank Peter Flaig for providing paleosol macro- and micromorphological information, and Rainer Newberry, Andrés Ochoa and Ken Severin, for their assistance with data analyses and interpretations.

1.9 Figures

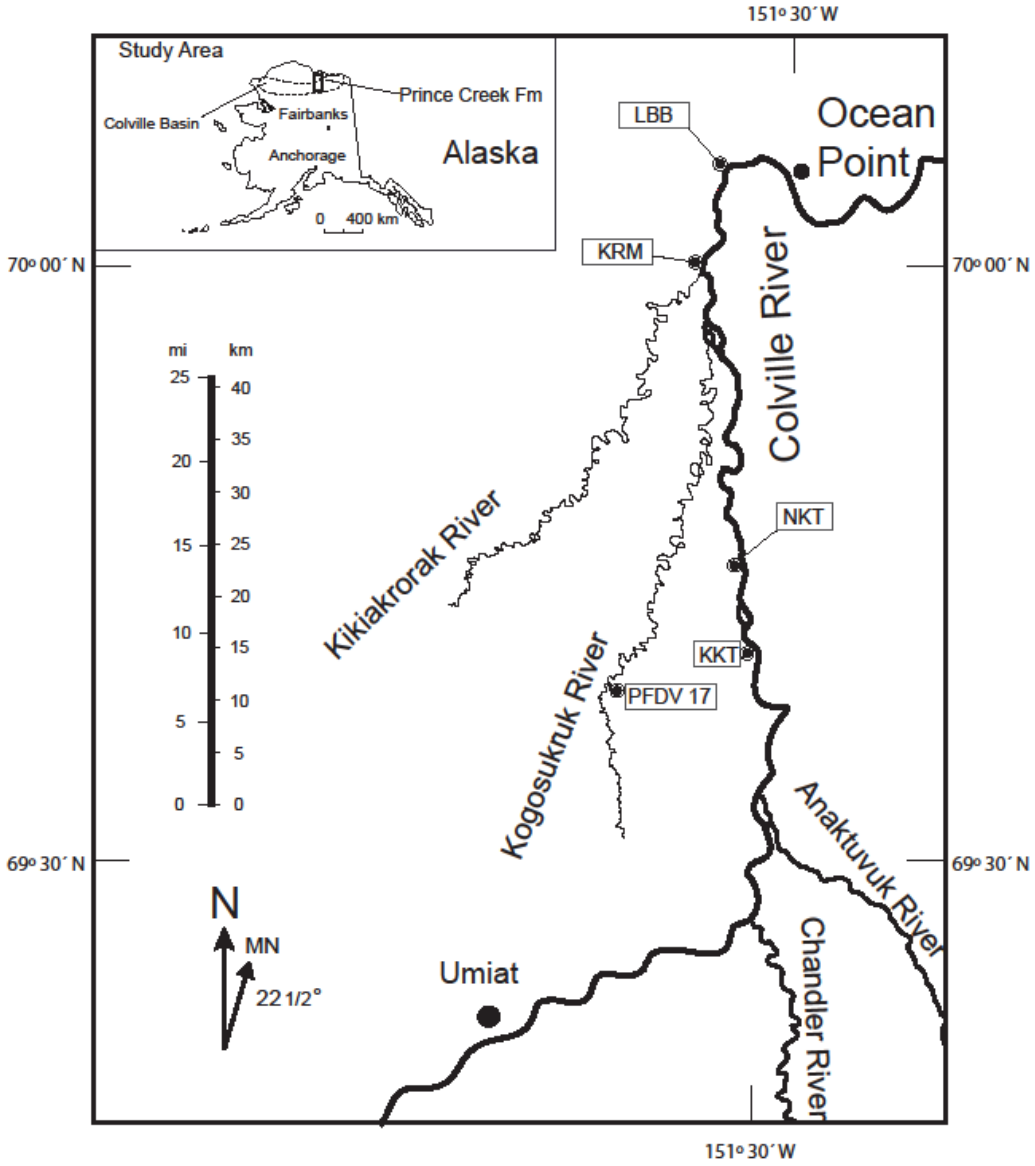

Fig. 1.9.1. Location of study area illustrating the location of the stratigraphic sections and the paleosol profiles of the Prince Creek Formation, Colville River, North Slope, Alaska used here. The labeled squares illustrate the name of the stratigraphic sections, two bentonite layers (KKT and PFDV-17), and the paleosol profiles North Kikak-Tegoseak Paleosol (NKT), Kikiakrorak River Mouth Paleosol (KRM) and Liscomb Bonebed Paleosol (LBB). Inset figure of Alaska at the top left shows the location of the Colville River and Coville Basin.

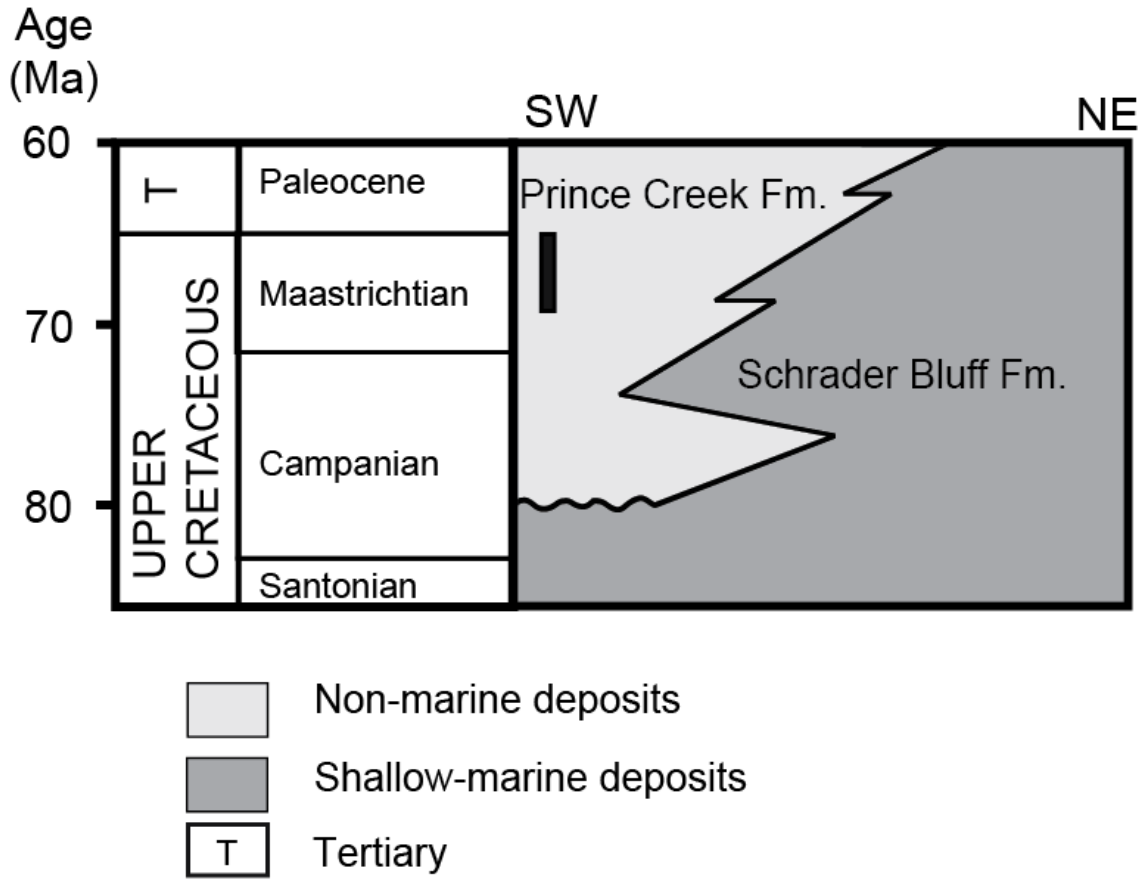

Fig. 1.9.2. Simplified diagram showing the age of the Prince Creek Formation and stratigraphic relationships with the marine and marginal-marine sediments of the Schrader Bluff Formation. The black line indicates the temporal extent of the Prince Creek Formation in our study area.

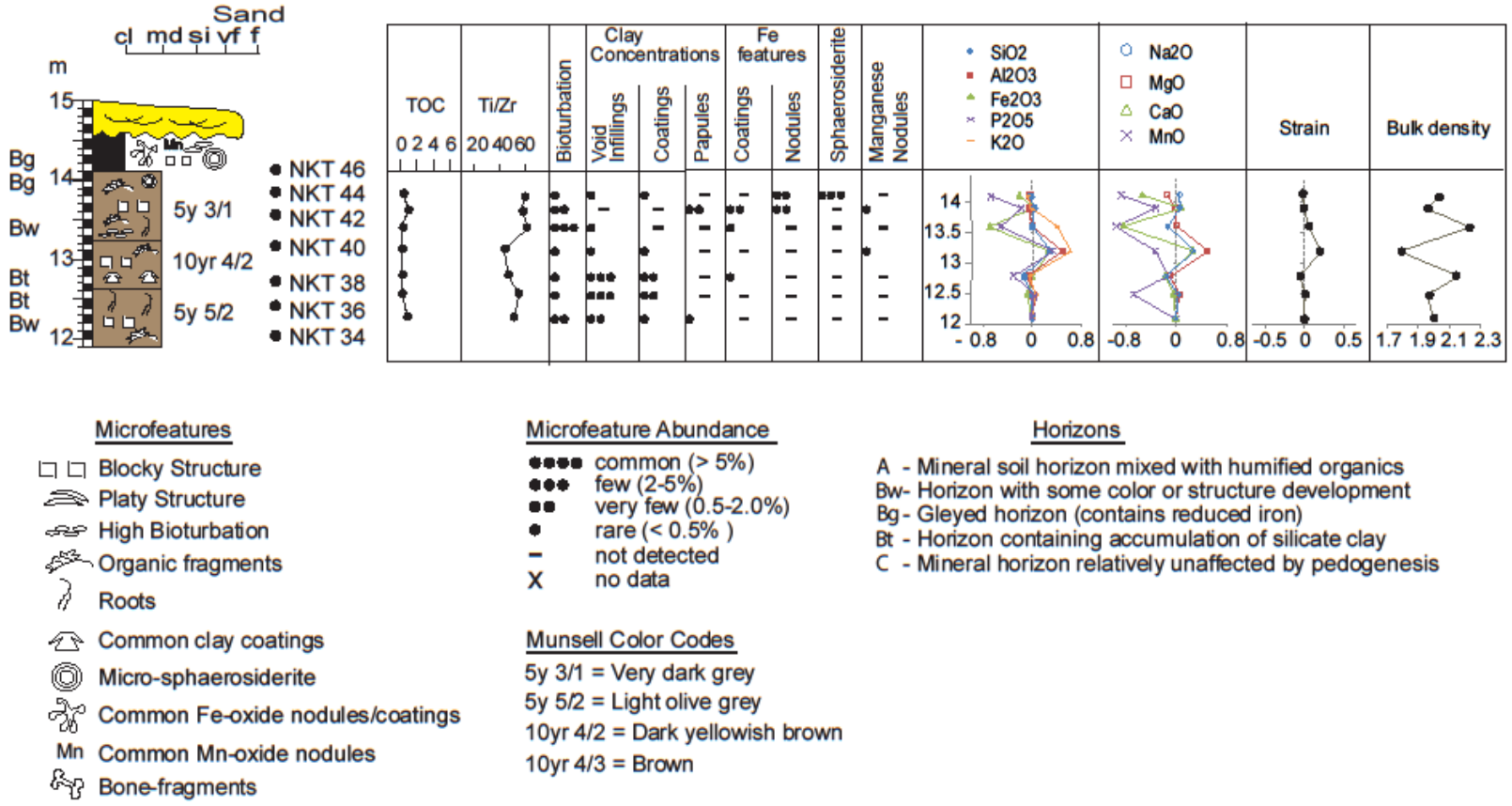

Fig. 1.9.3. Detailed profile log of NKT paleosol including legend for figures 1.9.3 and 1.9.4. The figure includes macro- and microfeatures, bulk density, strain and mass balance calculations. TOC=Total Organic Carbon. A discontinuity at NKT42 is marked by the Ti/Zr ratio. As indicated by volume change calculations (strain), moderate dilation occurs at NKT 40 and NKT 42 suggesting additions of new alluvial parent material. Phosphorous shows loss except in the NKT 40 horizon where it shows a gain of 30%.

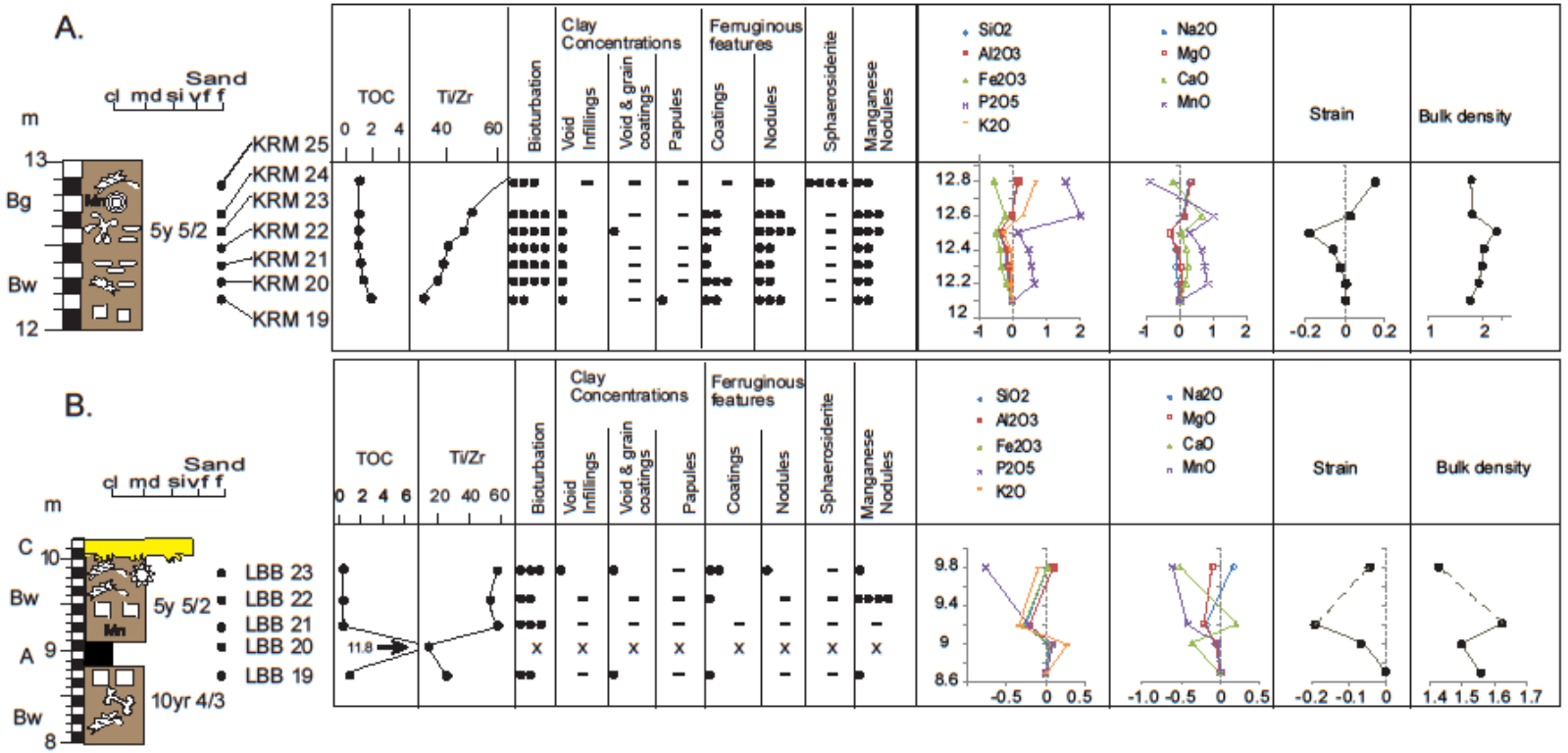

Fig. 1.9.4. Detailed logs of KRM (A) and LBB (B) paleosols showing macro- and microfeatures, bulk density, strain and mass balance calculations. See Figure 1.9.3 for legend. The Ti/Zr ratio shows a discontinuity at LBB 20 that separates two paleosols. One paleosol formed in LBB 19 and LBB 20 and a second paleosol formed in LBB 21 to LBB 23. Moderate collapse at KRM 23 is indicated by volume change calculations (strain). In the KRM profile, all horizons (except KRM 25, the uppermost one) show Si and Al depletion and pronounced P accumulation.

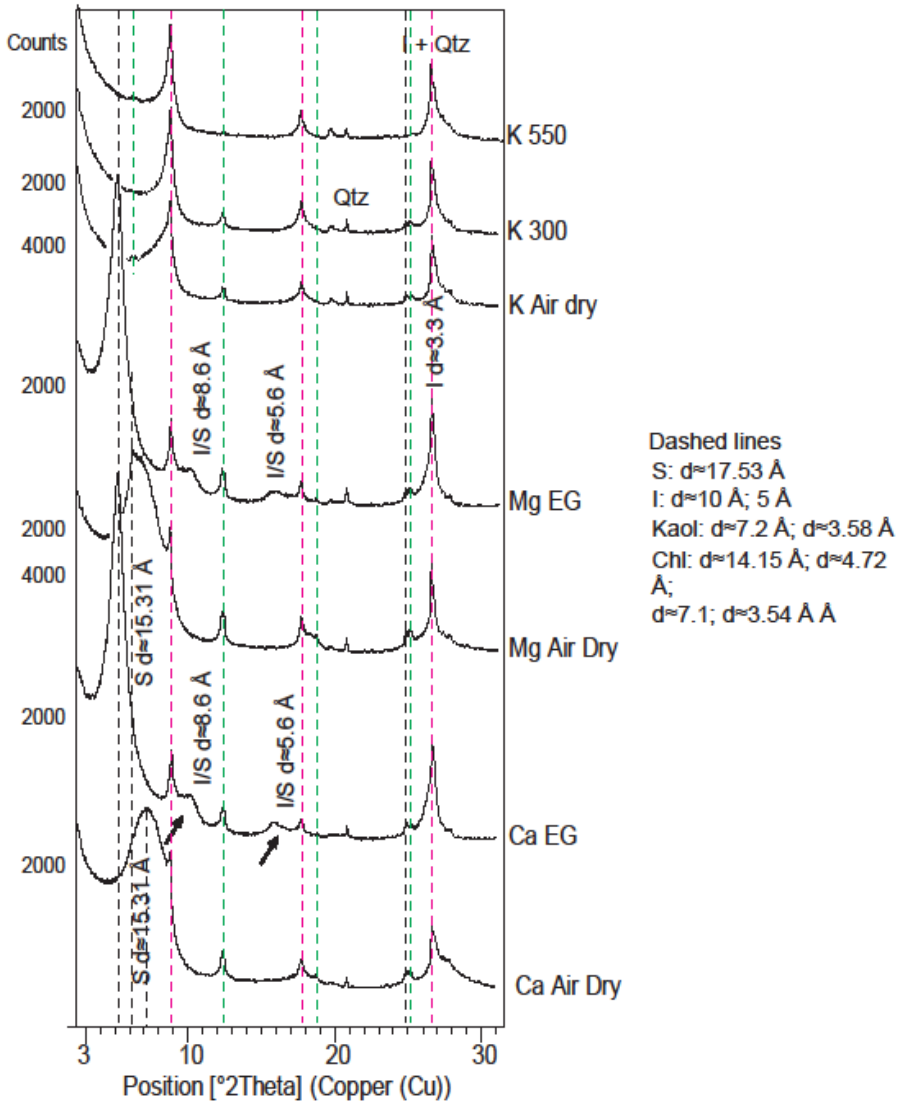

Fig. 1.9.5. X-ray diffraction patterns of oriented aggregate mounts of total clay fraction showing all the treatments for sample NKT 34. The reflections of the 001/002 and 002/003 I/S peaks are in the region near 10º and the region 16 to 17.7° 2θ, and are characterized by two broad peaks (~8.7Å and ~5.6 Å). Quartz is identified in the clay-size fraction by peaks at 4.26 Å and 3.34 Å. In Fig.s 1.9.5,1.9.7 and 1.9.9, Ca Air Dry= air dried, Ca2+ -saturated sample; Ca EG=ethylene glycolated, Ca2+ -saturated sample; Mg Air Dry= air dried, Mg2+-saturated sample; Mg EG= ethylene glycolated, Mg2+ -saturated sample; K Air Dry= air dried, K+ -saturated sample; K 300= K+ -saturated sample after heating at 300ºC for at least 4 hours; and K 500= K+ -saturated sample after heating at 550ºC for at least 4 hours. S=smectite, Chl=chlorite, I=illite, Kaol=kaolinite, I/S=illite/smectite, Qtz=quartz. The d-spacing in Å is shown next to each clay mineral. Green dashed line indicates main chlorite peaks, black dashed line indicates main smectite peaks and pink dashed line indicates main illite peaks.

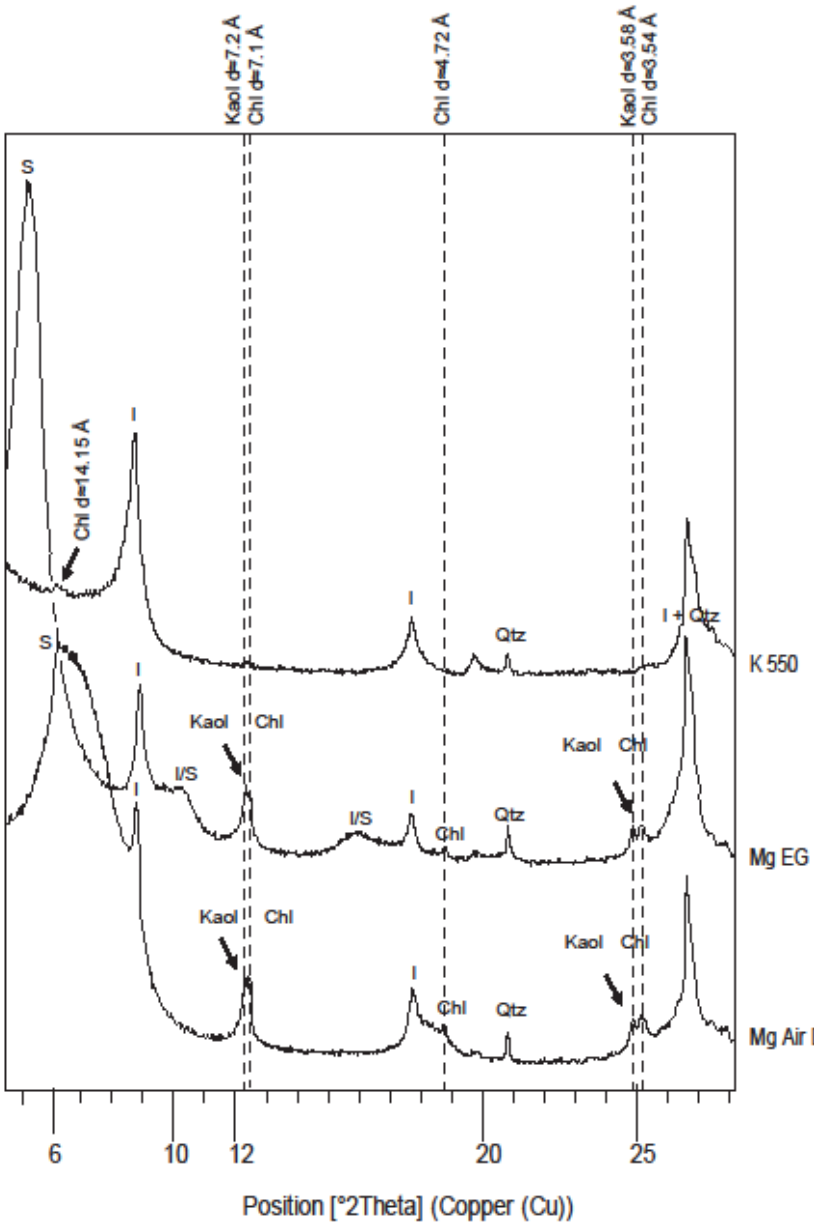

Fig. 1.9.6. Detailed X-ray diffraction pattern of sample NKT 34 showing the d≈14.15Å diagnostic peak of chlorite (which persists even after glycolation of Mg-saturated samples and heating to 550ºC), the kaolinite peaks at 7.2 Å and 3.58 Å that collapse upon heating to 550ºC and an increase in the intensity of the illite peak (10 Å) of the K-saturated samples after heating to 550ºC. The 001 and 002 kaolinite peaks and 002 and 004 chlorite peaks can be differentiated, the I/S peaks and the discrete smectite and discrete illite peaks are shown. Collapse of ~17 Å smectite peak to 10 Å is observed after heating K-saturated samples to 300ºC and 550ºC.

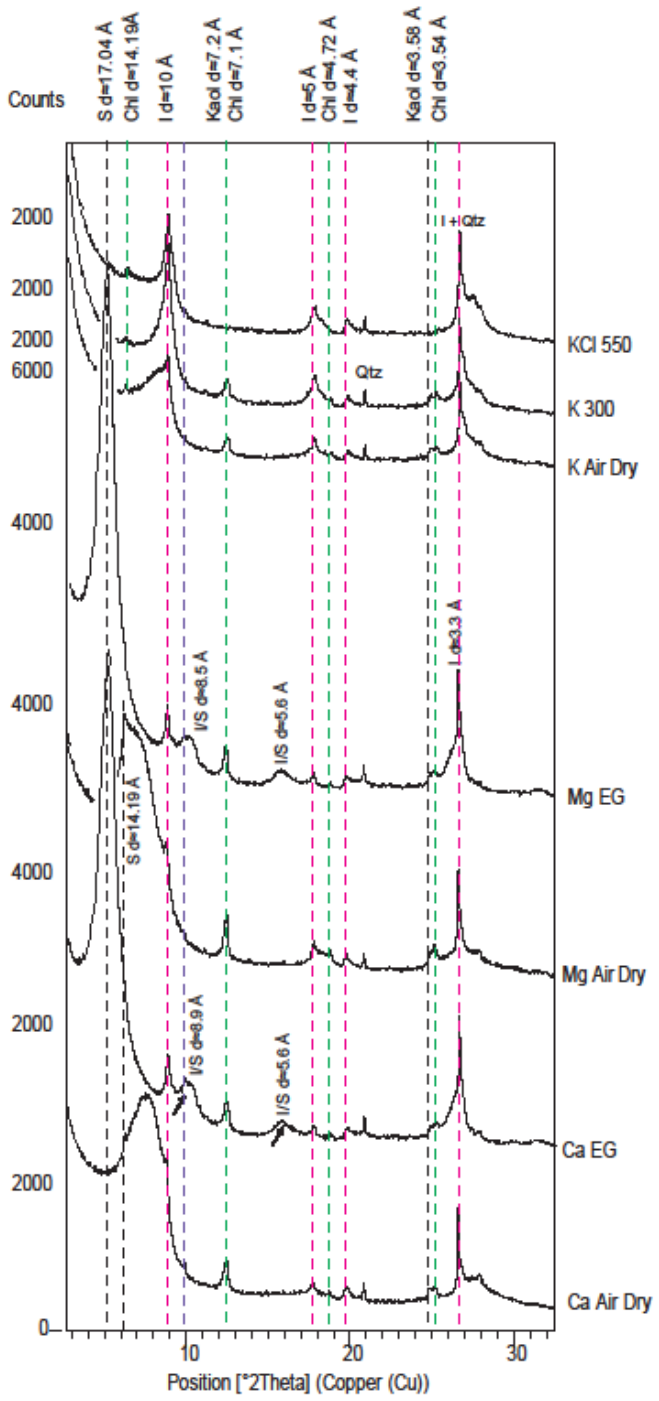

Fig. 1.9.7. X-ray diffraction patterns of oriented aggregate mounts of total clay fraction showing all the treatments for sample KRM 19. See Fig. 1.9.5 for legend. The region near 10º and 16° 2θ shows reflections of the 001/002 and 002/003 I/S peaks. Quartz is identified in the clay-size fraction by peaks at 4.26 Å and 3.34 Å.

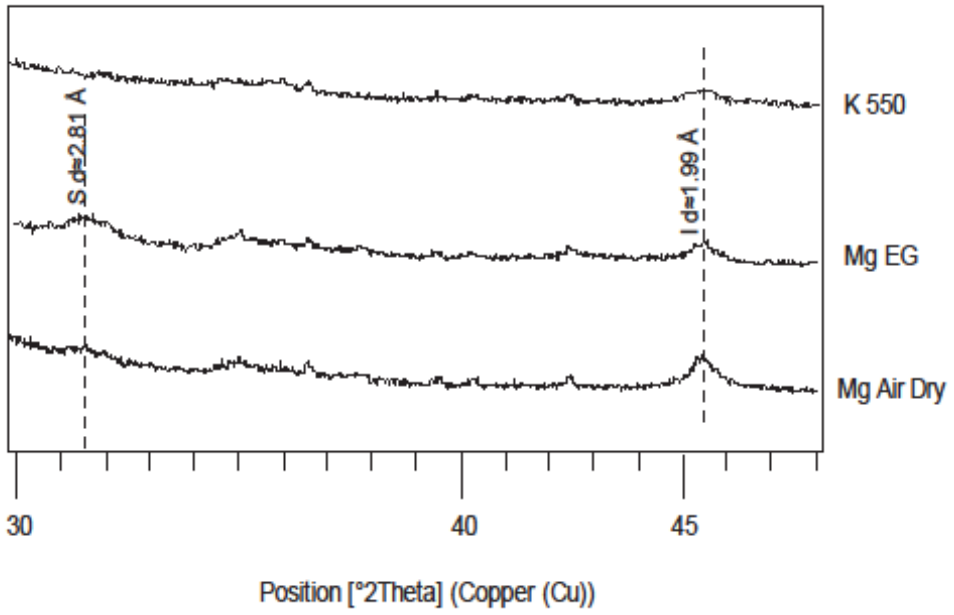

Fig. 1.9.8. Detailed X-ray diffraction pattern of KRM 19 sample showing the d≈2.81Å peak of discrete smectite in the glycolated sample and the d≈1.99 Å peak of discrete illite that is present in all samples despite the treatments. 2.81Å higher order reflection in EG-solvated indicates the presence of discrete smectite.

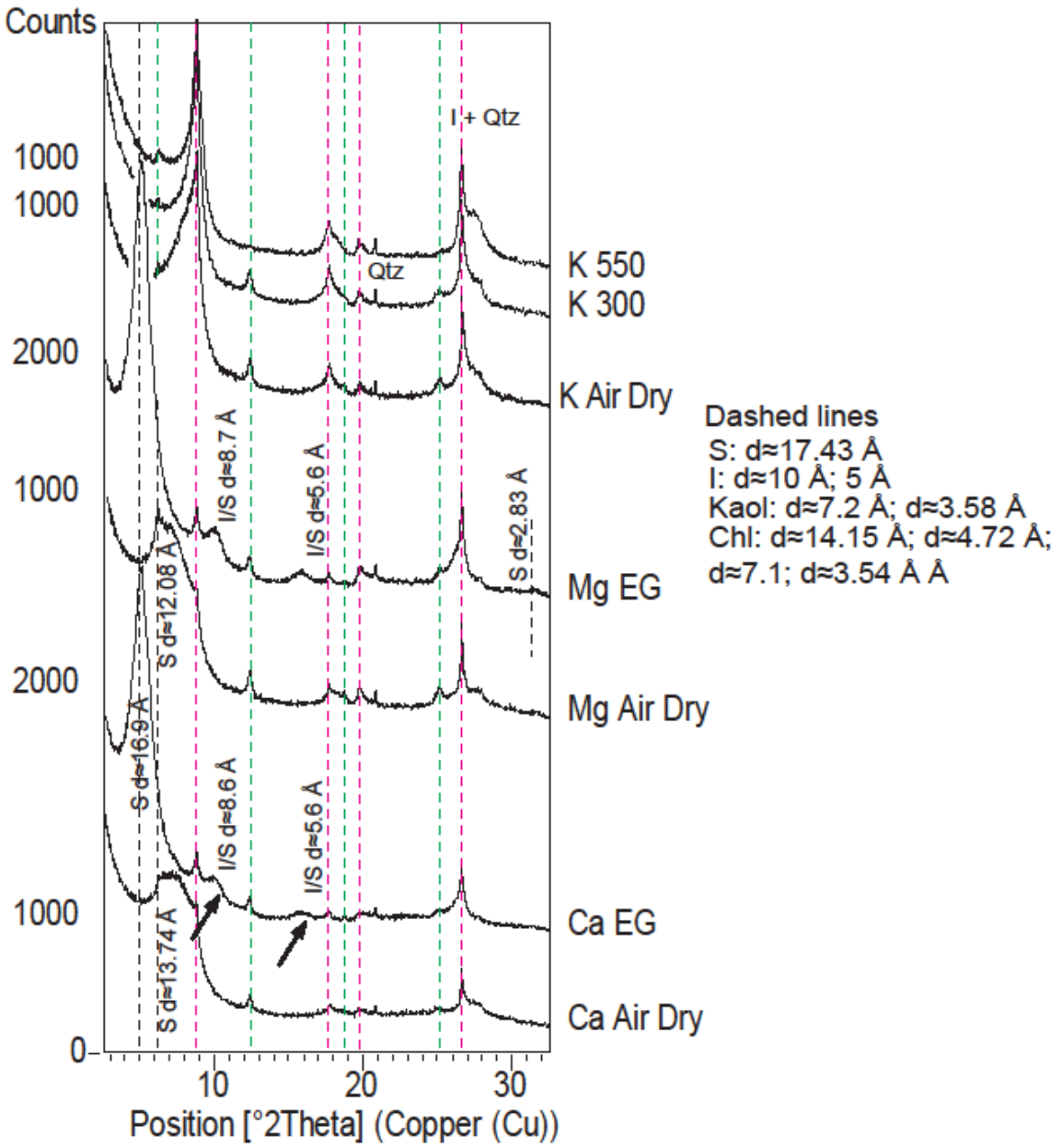

Fig. 1.9.9. X-ray diffraction patterns of oriented aggregate mounts of total clay fraction showing all the treatments for sample LBB 19. See Fig. 1.9.5 for legend. The black dashed lines indicate the main smectite peaks. Discrete smectite (S) is indicated by the shift of the 13.74 Å and 12.08 Å peaks in the Ca- and Mg-saturated samples to ~17Å in the Ca- and Mg EG-saturated samples respectively. The region near 10º and 16° 2θ shows reflections of the 001/002 and 002/003 I/S peaks. Quartz is identified in the clay-size fraction by peaks at 4.26 Å and 3.34 Å. The 2.81Å higher order reflection in the EG-solvated sample indicates the presence of discrete smectite.

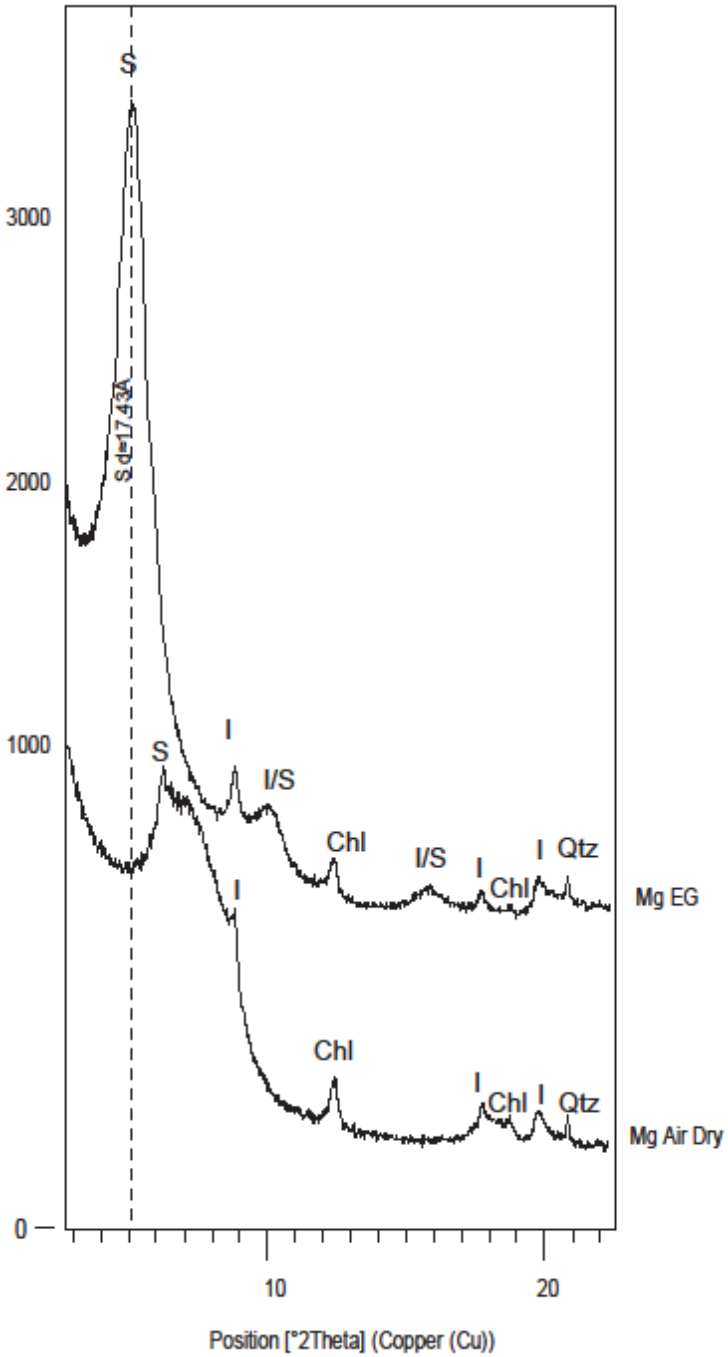

Fig. 1.9.10. Detailed X-ray diffraction pattern of LBB 19 sample showing the I/S peaks and the discrete smectite and discrete illite peaks. Montmorillonite is identified by a sharp peak at ~17 Å (001) of glycolated Mg-saturated sample.

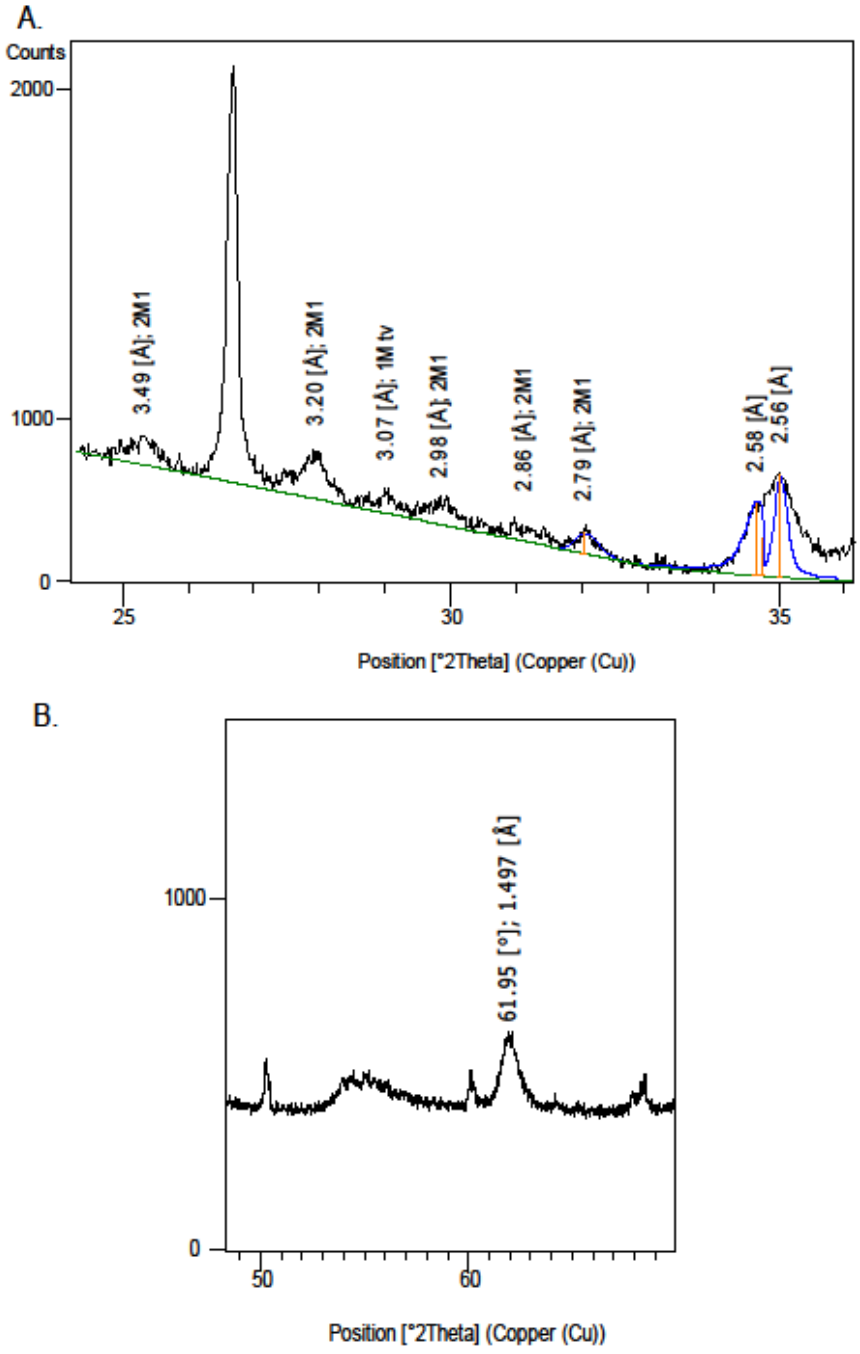

Fig. 1.9.11. A. Representative XRD pattern of random oriented total clay mount of sample LBB 23. The pattern shows a mixture of 1M and 2M1 polytypes. Some diagnostic reflections in the area of the 2.79 Å and 2.58 Å peaks (Maxwell and Hower 1967) are indicated. B. Detailed XRD pattern of random oriented total clay mount showing the 006 reflection in the 62.22° to 61.67º 2θ region of the 1.49Å montmorillonite peak.

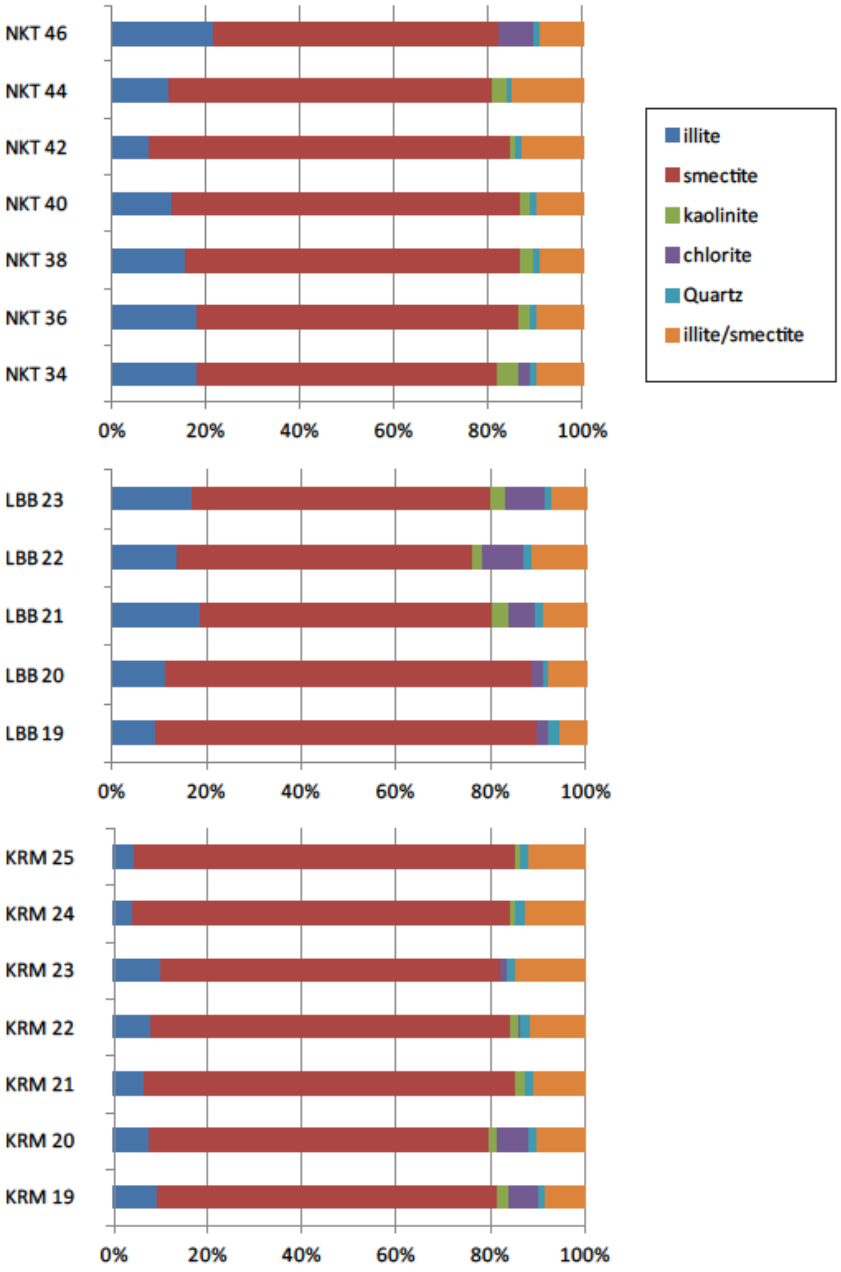

Fig. 1.9.12. Mineralogical composition and wt% of each clay mineral species based on integrated peak intensities in Mg-glycolated and Ca-glycolated sample. Dark blue bar indicates illite wt%, red indicates smectite wt%, green indicates kaolinite wt%, purple indicates chlorite wt%, light blue indicates quartz wt%, and orange indicates I/S wt%. Iillite abundance shows an inverse relationship with smectite abundance. The proportion of I/S mixed-layer clays increase upward until a maximum value and then decrease to the top of the paleosols.

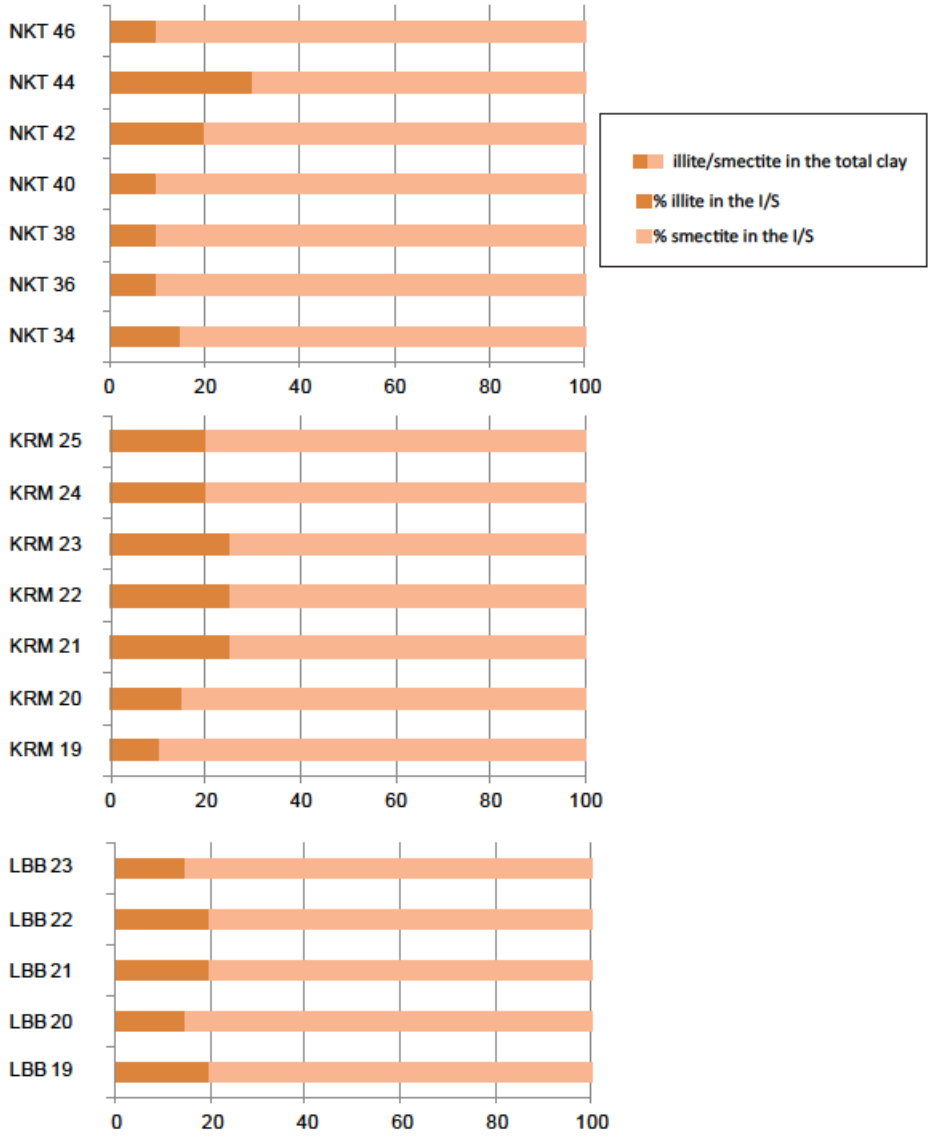

Fig. 1.9.13. Percent of illite in I/S estimated based on 001/002 and 002/003 I/S peaks of Mg-glycolated samples (Moore and Reynolds, 1997). I/S mixed-layered clays are R0 illite(0.10)/smectite until NKT 42 where the illite content in the mixed-layered clays increases to R0 illite(0.20)/smectite. In the LBB profile, I/S mixed-layered clays show the same trend in the two paleosols, decreasing from R0 illite(0.20)/smectite at the bottom to illite(0.15)/smectite at the top. The amount of illite in the I/S mixed-layered clays increases from R0 illite(0.10)/smectite to R0 illite(0.25)/smectite in the Bg horizon of KRM 23.

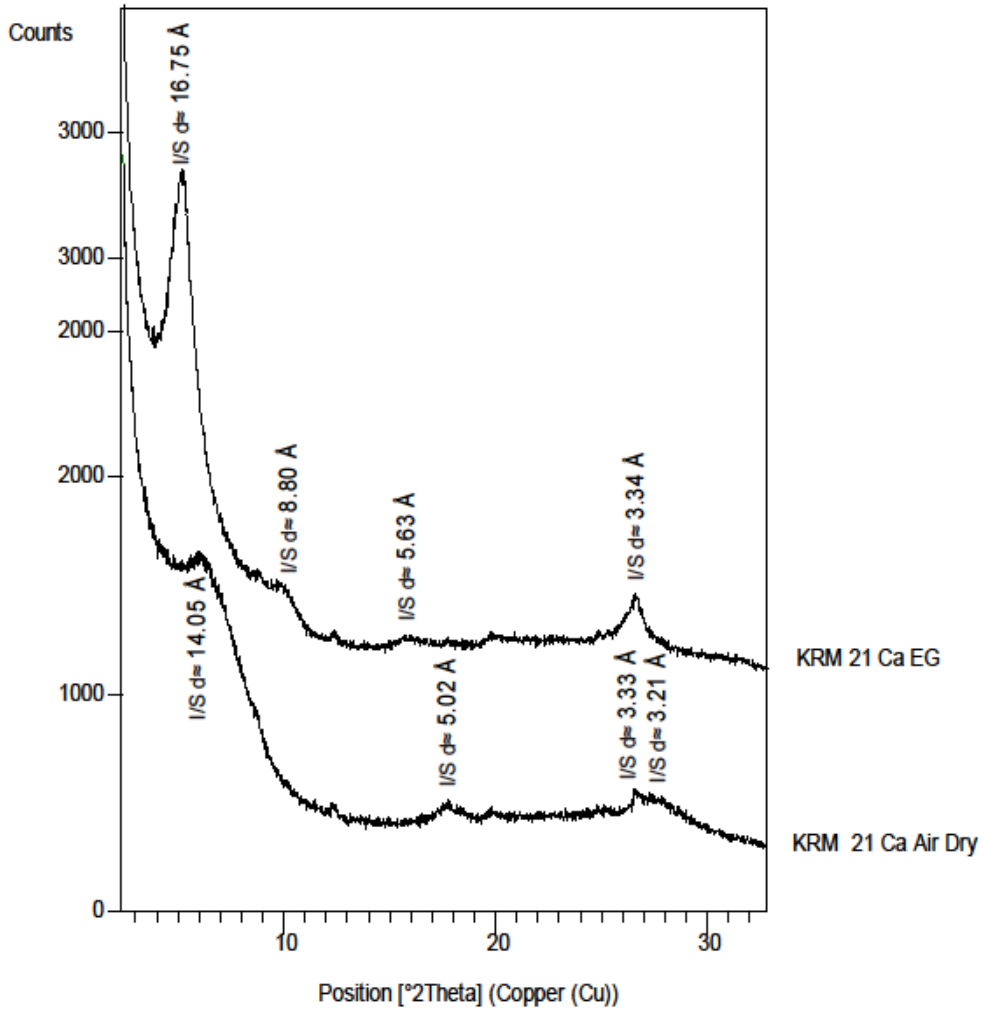

Fig. 1.9.14. XRD pattern from sample KRM 21 showing that I/S is the main clay mineral in the fine clay (<0.2 μm) fraction.

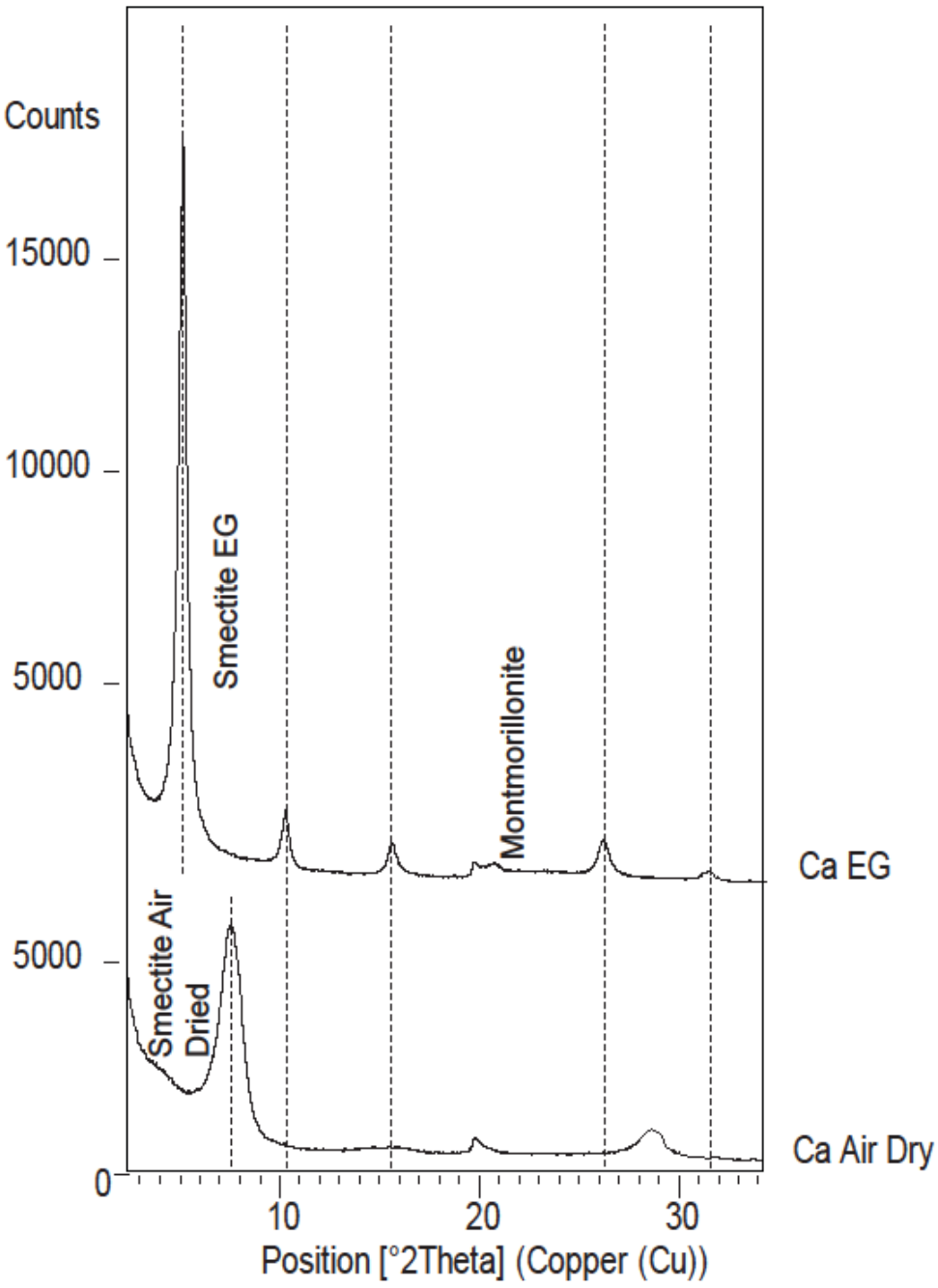

Fig. 1.9.15. Representative XRD pattern of oriented mount of clay-size fraction of KKT bentonite. The spectrum shows a rational series of the diagnostic reflections of smectite, specifically montmorillonite.

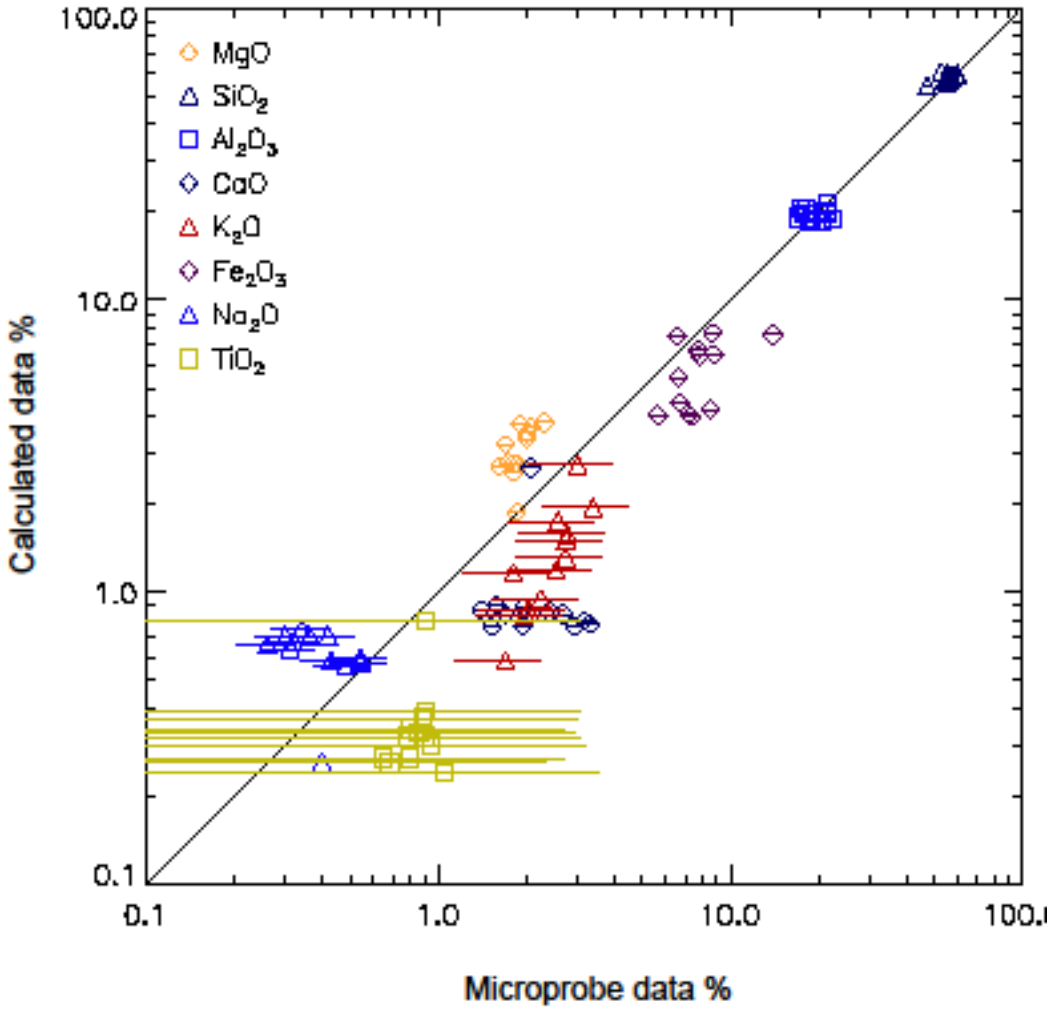

Fig. 1.9.16. Correlation between measured microprobe composition and XRD compositional data. The line of intercept 0 and slope 1 shows there is a good correlation between the two methods, particularly for the more abundant components (SiO2, Al2O3 and Fe2O3).

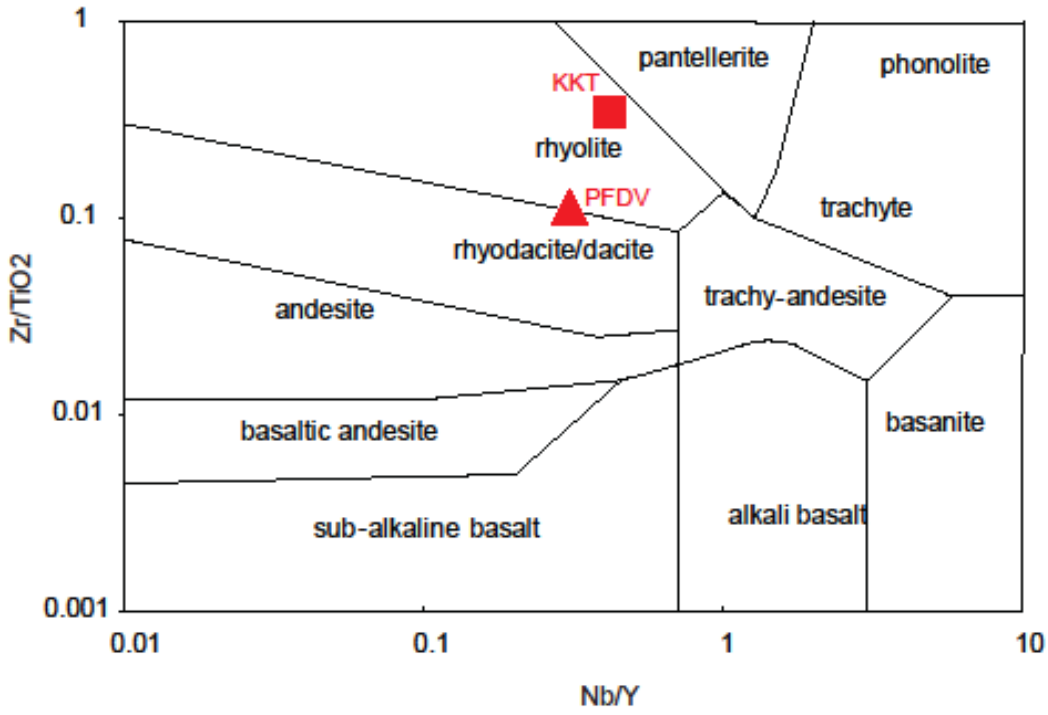

Fig. 1.9.17. Zr/TiO2–Nb/Y classification diagram taken from Winchester and Floyd (1977) showing an original rhyolitic to rhyodacitic composition for the bentonites (KKT and PFDV).

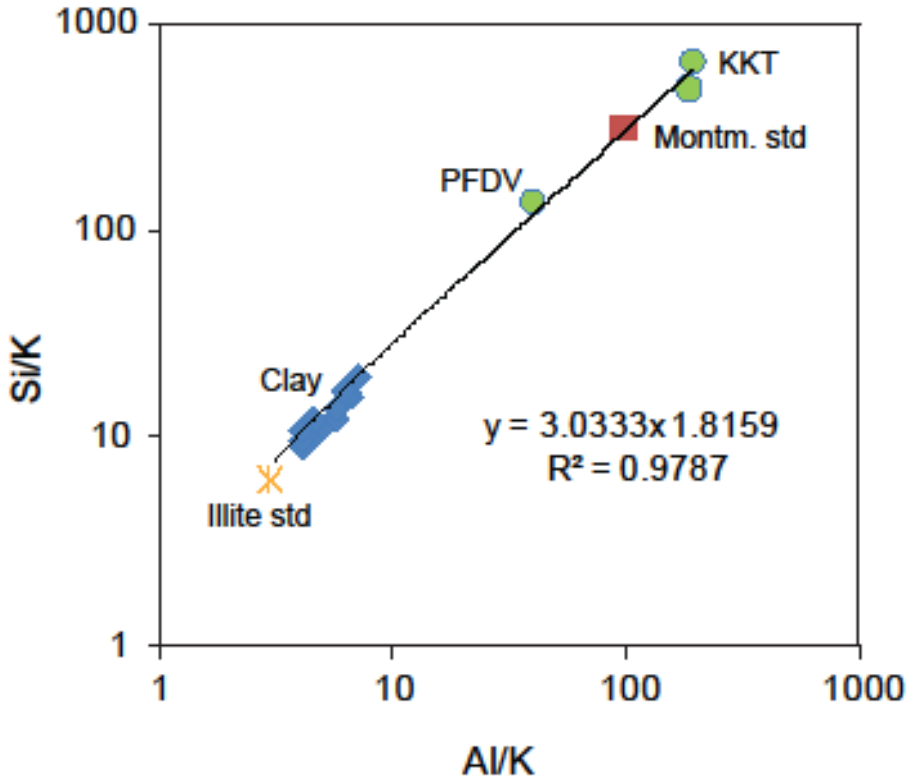

Fig. 1.9.18. Si/K vs. Al/K diagram (De Caritat et al., 1994) using ideal illite IMt-1 (Van Olphen et al., 1979) and KKT bentonite composition as end members. The linear regression has a R^2=0.98 and shows a compositional relationship between illite, bentonite and the paleosol clay samples.

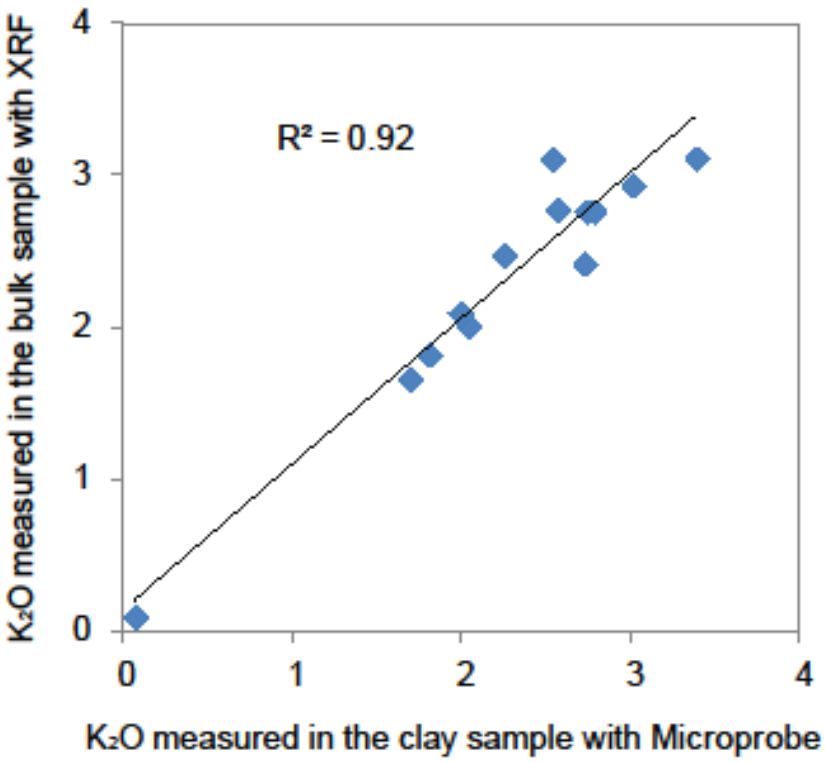

Fig. 1.9.19. Relationship between microprobe K2O from clay separates and the XRF K_2O from the bulk sample.

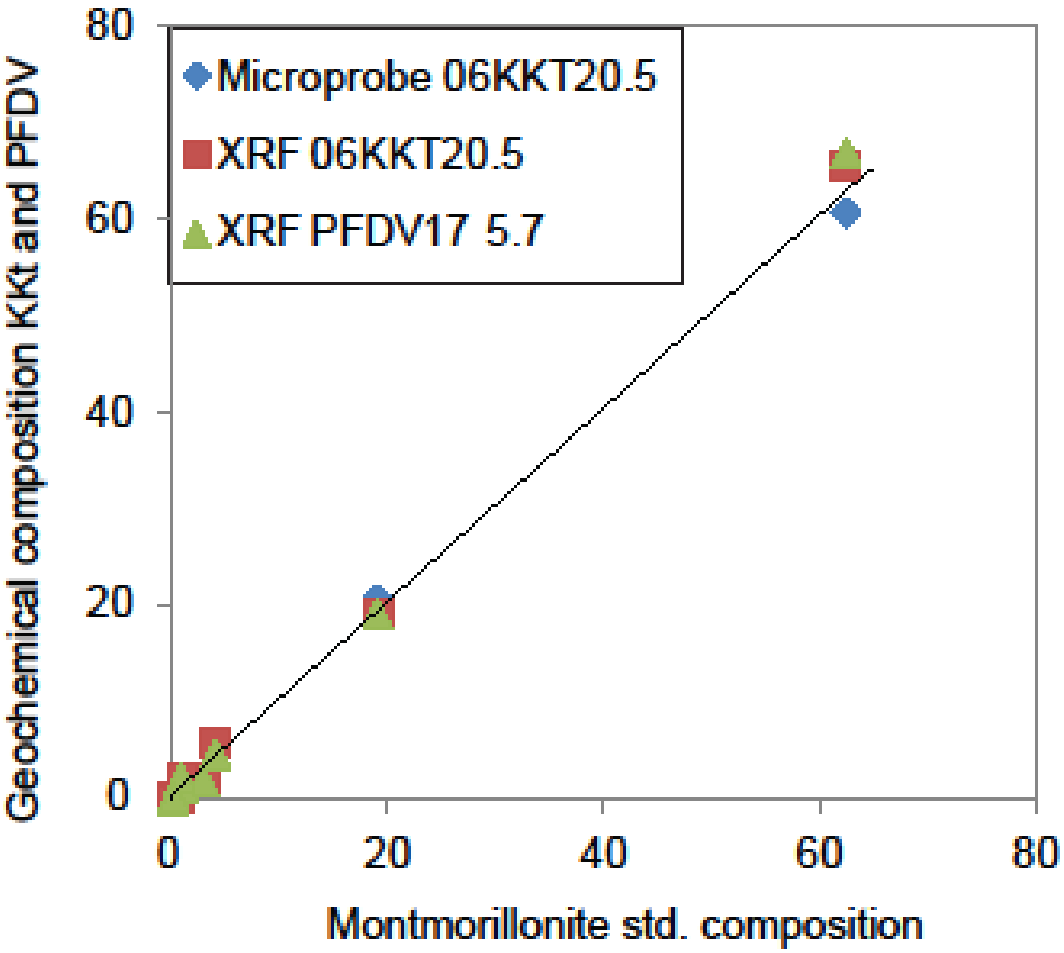

Fig. 1.9.20. 1:1 correlation between a standard montmorillonite (source CMS) with the bentonites from the study area (geochemical data determined by XRF and microprobe analyses).

1.10 Tables

Table 1.10.1. Electron probe microanalysis of total clay fraction in oriented samples for the NKT, KRM and LBB paleosol profiles and the KKT bentonite.

Electron Probe Microanalysis of total clay fraction									
	MgO	**SiO_2**	**Al_2O_3**	**CaO**	**K_2O**	**MnO**	**Fe_2O_3**	**Na_2O**	**TiO_2**
NKT 36	1.85	55.38	21.43	2.07	3.01	0	7.77	0.4	0.9
NKT 38	1.88	55.66	21.26	2.67	2.73	0.01	6.73	0.26	0.8
NKT 42	1.62	57.38	20.74	2.4	2.03	0.02	7.18	0.36	0.8
NKT 44	1.82	55.32	22.4	3.16	2.53	0	5.66	0.31	0.78
NKT 46	2.08	55.07	21.62	1.95	3.38	0.03	6.57	0.48	0.94
LBB 20	1.7	52.79	18.05	1.96	1.8	0.01	6.67	0.3	0.68
LBB 21	2	56.01	18.12	1.52	2.56	0.01	8.8	0.54	0.91
LBB 22	1.91	47.18	17.08	2.91	2.72	0.56	13.99	0.43	0.86
LBB 23	2.3	54.39	17.41	3.31	2.77	0.01	8.67	0.54	0.89
KRM 19	2.02	55.97	19.97	1.69	2.25	0.03	7.8	0.32	0.9
KRM 22	1.73	59.55	18.89	1.4	1.98	0	8.55	0.42	0.65
KRM 25	1.81	59.95	18.63	1.59	1.69	0.02	7.37	0.34	1.05
KKT	1.84	60.78	20.67	1.91	0.07	0.01	6.04	0.19	0.21

Table 1.10.2. Standard chemical composition of kaolinite (KGa-1), Na-montmorillonite (SWy-2), illite (IMt-1) and Chlorite (CCa-2) (Van Olphen et al., 1979).

Major element geochemistry of standard minerals									
	MgO	**SiO_2**	**Al_2O_3**	**CaO**	**K_2O**	**MnO**	**Fe_2O_3**	**Na_2O**	**TiO_2**
Montmorillonite	2.95	62.42	19.05	0.98	0.2	0.03	4.06	0.84	0.21
Kaolinite	0.01	42.9	36.49	0.05	0	0.03	0.2	0.03	2.36
Illite	2.56	49.3	24.25	0.43	7.83	0.03	7.32	0	0.55
Chlorite	17.2	26	20	0.25	0	0.1	47.4	0	0.476
Ferruginous smectite	1.75	43.75	7.95	2.05	0.03	0.03	25.25	0	0.54

Table 1.10.3. Calculated geochemical compositions of clay minerals from XRD (wt%). The calculated values are plotted in Fig. 1.10.12

	MgO	SiO_2	Al_2O_3	CaO	K_2O	MnO	Fe_2O_3	Na_2O	TiO_2
NKT 36	1.88	55.7	21.26	2.67	2.73	0.01	6.73	0.26	0.8
NKT 38	2.75	59.5	20.31	0.84	1.51	0.03	4.45	0.66	0.34
NKT 42	2.71	58.3	18.8	0.86	0.86	0.03	4.07	0.71	0.27
NKT 44	2.57	55.9	19.02	0.8	1.19	0.03	4.05	0.64	0.32
NKT 46	3.7	55.6	19.71	0.77	1.95	0.03	7.52	0.56	0.3
LBB 20	3.21	60.2	19.66	0.89	1.16	0.03	5.44	0.71	0.26
LBB 21	3.35	56.5	20.46	0.76	1.75	0.03	6.55	0.57	0.39
LBB 22	3.76	53.8	19.19	0.76	1.31	0.03	7.62	0.58	0.33
LBB 23	3.81	56.8	20.55	0.78	1.58	0.03	7.73	0.59	0.37
KRM 19	3.51	58.3	19.79	0.84	0.95	0.03	6.45	0.67	0.32
KRM 22	2.78	58.6	18.86	0.87	0.83	0.03	4.23	0.71	0.27
KRM 25	2.76	59.5	18.58	0.9	0.58	0.03	4	0.75	0.24

Table. 1.10.4. Geochemical analyses of bentonites from the Prince Creek Formation and standard montmorillonite.

Method	Sample	MgO	SiO_2	Al_2O_3	CaO	K_2O	MnO	Fe_2O_3	Na_2O	TiO_2
Microprobe	**KKT**	1.84	60.78	20.67	1.91	0.07	0.01	6.04	0.19	0.21
XRF	**KKT**	2.41	65.56	19.3	2.15	0.1	0.01	5.92	0.35	0.2
XRF	**PFDV**	1.82	66.96	19.31	1.37	0.49	0.02	4.71	2.24	0.19
Microprobe	**Montm. Std**	2.95	62.42	19.05	0.98	0.2	0.03	4.06	0.84	0.21

Table. 1.10.5. Acid ammonium oxalate and pyrophosphate extractable Fe, Al and Si from the NKT and KRM paleosol profiles.

	Acid Ammonium Oxalate (g/kg)			Na-Pyrophosphate (g/kg)		Allophane and Imogolite	Ferrhydrite			
	Fe_o	Al_o	Si_o	Fe_p	Al_p	$(Al_o–Al_p)/Si_o$	$(\%Fe_o \times 1.7)$	Al_p/Al_o	Fe_p/Fe_o	$Al_o+1/2\ Fe_o$
KRM-19	0.48	0.21	0.23	0.11	0.1	1.63	0.82	0.48	0.23	0.45
KRM-20	0.18	0.15	0.14	0.09	0.11	0.99	0.31	0.73	0.5	0.24
KRM-21	0.16	0.13	0.17	0.1	0.1	1.21	0.27	0.77	0.63	0.21
KRM-22	0.18	0.13	0.14	0.12	0.13	0.99	0.31	1	0.67	0.22
KRM-23	0.19	0.12	0.15	0.1	0.1	1.07	0.32	0.83	0.53	0.22
KRM-24	0.12	0.1	0.11	0.08	0.09	0.78	0.2	0.9	0.67	0.16
KRM-25	6.49	0.12	0.17	0.16	0.12	1.21	11.03	1	0.02	3.37
NKT-38	0.16	0.12	0.09	0.08	0.13	0.64	0.27	1.08	0.5	0.2
NKT-40	0.42	0.14	0.12	0.17	0.22	0.85	0.71	1.57	0.4	0.35
NKT-42	7.38	0.11	0.14	0.35	0.36	0.99	12.55	3.27	0.05	3.8
NKT-44	0.31	0.11	0.12	0.1	0.18	0.85	0.53	1.64	0.32	0.27
NKT-46	1.21	0.16	0.16	0.09	0.11	1.14	2.06	0.69	0.07	0.77
								>0.5 non allophanic		2% for andic soil properties

1.11 References

ALLEN, B.L., and HAJEK, B.F., 1989, Mineral Occurrence in Soil Environments, *in* Dixon, J.B., and Weed, S.B., eds., Minerals in soil environments: Madison, Wisconsin, p. 199-278.

ARISTIZÁBAL, E., ROSER, B., and YOKOTA, S., 2005, Tropical chemical weathering of hillslope deposits and bedrock source in the Aburrá Valley, northern Colombian Andes: Engineering Geology, v. 81, p. 389-406.

BARKER, C.E., and PAWLEWICZ, M.J., 1986, The correlation of vitrinite reflectance with maximum paleotemperature in humic organic matter, *in* Buntebarth, G., and Stegena, L., eds., Paleogeothermic: New York, USA, Springer-Verlag, p. 79-93.

BARNHISEL, R.I., and BERTSCH, P.M., 1989, Chlorites and Hydroxy Interlayered Vermiculite and Smectite, *in* Dixon, J.B., and Weed, S.B., eds., Minerals in soil environments: Madison, Wisconsin, p. 729-788.

BESTLAND, E.A., 2002, Fossil Andisols Identified with Mass-Balance Geochemistry (Oligocene John Day Formation, Oregon, U.S.A.): Journal of Sedimentary Research, v. 72, p. 673-686.

BICE, K., ARTHUR, M., and MARINCOVICH, L., 1996, Late Paleocene Arctic Ocean shallow-marine temperatures from mollusc stable isotopes: Paleoceanography, v. 11, p. 241-249.

BIRD, K.J., and MOLENAAR, C.M., 1992, The North Slope foreland basin, Alaska, Foreland Basins and Foldbelts, American Association of Petroleum Geologists (AAPG.), p. 363-393.

BIRKELAND, P.W., 1999, Soils and Geomorphology, p. 433.

BISCAYE, P.E., 1965, Mineralogy and Sedimentation of Recent Deep-Sea Clay in the Atlantic Ocean and Adjacent Seas and Oceans: Geological Society of America Bulletin, v. 76, p. 803-832.

BLAKE, G.R., and HARTGE, K.H., 1986, Bulk density, Methods of soil analysis. Part 1. Physical and mineralogical methods, p. 363-375.

BORCHARDT, G., 1989, Smectites, *in* Dixon, J.B., and Weed, S.B., eds., Minerals in soil environments: Madison, Wisconsin, Soil Sci., p. 675-727.

BRANDLEN, E., 2008, Paleoenvironmental reconstruction of the Late Cretaceous (Maastrichtian) Prince Creek Formation, near the Kikak-Tegoseak dinosaur quarry, North Slope, Alaska: Fairbanks, Unpublished Master's Thesis University of Alaska Fairbanks, p. 225.

BRIMHALL, G.H., and DIETRICH, W.E., 1987, Constitutive mass balance relations between chemical composition, volume, density, porosity, and strain in metasomatic hydrochemical systems: Results on weathering and pedogenesis, Geochimica et Cosmochimica Acta, p. 567-587.

BRIMHALL, G.H., CHRISTOPHER J., L., FORD, C., BRATT, J., TAYLOR, G., and WARIN, O., 1991a, Quantitative geochemical approach to pedogenesis: importance of parent material reduction, volumetric expansion, and eolian influx in lateritization, Geoderma, p. 51-91.

BRIMHALL, G.H., CHADWICK, O.A., LEWIS, C.J., COMPSTON, W., WILLIAMS, I.S., DANTI, K.J., DIETRICH, W.E., POWER, M.E., HENDRICKS, D., and BRATT, J., 1991b, Deformational mass transport and invasive processes in soil evolution.: Science (New York, N.Y.), v. 255, p. 695-702.

BRONGER, A., 2003, Correlation of loess–paleosol sequences in East and Central Asia with SE Central Europe: towards a continental Quaternary pedostratigraphy and paleoclimatic history: Quaternary International, v. 106-107, p. 11-31.

BURNS, W.M., HAYBA, D.O., ROWAN, E.L., and HOUSEKNECHT, D.W., 2005, Estimating the Amount of Eroded Section in a Partially Exhumed Basin from Geophysical Well Logs : An Example from the North Slope: North, v. 1732D, p. 18 p.

BURT, R., 2004, Soil Survey Laboratory Methods Manual: Soil Survey Investigations Report, v. 42, p. 735.

CHITTLEBOROUGH, D.J., OADES, J.M., and WALKER, P.H., 1984, Textural differentiation in chronosequences from eastern australia, III. evidence from elemental chemistry, Geoderma, p. 227-248.

CONRAD, J.E., MCKEE, E.H., and TURRIN, B.D., 1990, Age of tephra beds at the Ocean Point Dinosaur Locality, North Slope, Alaska, based on K–Ar and 40Ar/39Ar analysis, p. C1-C12.

CUADROS, J., and ALTANER, S., 1998, Characterization of mixed-layer illite-smectite from bentonites using microscopic , chemical , and X-ray methods : Constraints on the smectite-to-illite transformation mechanism: American Mineralogist, v. 83, p. 762-774.

De CARITAT, P., BLOCH, J.D., and LONGSTAFFE, F.J., 1994, Compositional trends of a Cretaceous foreland basin shale (Belle Formation, Western Canada Sedimentary Basin): Diagenetic and depositional Controls: Clay Minerals, v. 29, p. 503-526.

D'AMORE, D.V., STEWART, S.R., and HUDDLESTON, J.H., 2004, Saturation, Reduction, and the Formation of Iron–Manganese Concretions in the Jackson-Frazier Wetland, Oregon, Soil Science Society of America Journal, p. 1012.

DRIESE, S.G., MORA, C.I., COTTER, E., and FOREMAN, J.L., 1992, Paleopedology and Stable Isotope Chemistry of Late Silurian Vertic Paleosols, Bloomsburg Formation, Central Pennsylvania: Journal of Sedimentary Research, v. 62, p. 825-841.

ESSINGTON, M.E., 2004, Soil and water chemistry. An integrative approach, p. 534.

FANNING, D.S., and FANNING, M.C.B., 1989, Soil: morphology, genesis, and classification, Wiley.

FIORILLO, A.R., HASIOTIS, S.T., KOBAYASHI, Y., and TOMSICH, C.S., 2009, A pterosaur manus track from Denali National Park, Alaska Range, Alaska, United States: Palaios, v. 24, p. 466-472.

FIORILLO, A.R., MCCARTHY, P.J., and FLAIG, P.P., 2010a, Taphonomic and sedimentologic interpretations of the dinosaur-bearing Upper Cretaceous Strata of the Prince Creek Formation, Northern Alaska: Insights from an ancient high-latitude terrestrial ecosystem: Palaeogeography, Palaeoclimatology, Palaeoecology, v. 295, p. 376-388.

FIORILLO, A.R., MCCARTHY, P.J., FLAIG, P.P., BRANDLEN, E., NORTON, D.W., ZIPPI, P., JACOBS, L., GANGLOFF, R.A., and FARLOW, J.O., 2010b, Paleontology and paleoenvironmental interpretation of the Kikak-Tegoseak Quarry (Prince Creek Formation: Late Cretaceous), northern Alaska: a multi-disciplinary study of a high-latitude ceratopsian dinosaur bonebed, *in* Ryan, M.J., Chinnery-Allgeier, B.J., and Eberth, D.A., eds., New Perspectives On Horned Dinosaurs The Royal Tyrrell Museum Ceratopsian Symposium, Indiana University Press, p. 456-477.

FLAIG, P.P., 2010, Depositional environments of the Late Cretaceous (Maastrichtian) dinosaur-bearing Prince Creek Formation: Colville River region, North Slope, Alaska., p. 311.

FLAIG, P.P., RD, B., MCCARTHY, P.J., and FIORILLO, A.R., 2011, A tidally-influenced, high-latitude alluvial/coastal plain: the Late Cretaceous (Maastrichtian) Prince Creek Formation, North Slope, Alaska: SEPM Special Publication, v. 97, p. 233-264.

FLAIG, P.P., MCCARTHY, P.J., and FIORILLO, A.R., 2013, Anatomy, evolution and paleoenvironmental interpretation of an ancient arctic coastal plain: Integrated paleopedology and palynology from the Upper Cretaceous (Maastrichtian) Prince Creek Formation, North Slope, Alaska: SEPM Special Publication, v. 104, p. 179-230.

FOSCOLOS, A.E., RUTTER, N.W., and HUGHES, O.L., 1977, The use of pedological studies in interpreting the Quaternary history of central Yukon.: Geological Survey of Canada, Bulletin, v. 271, p. 1-48.

HILLIER, S., 2003, Quantitative analysis of clay and other minerals in sandstones by X-ray powder diffraction (XRPD), *in* Worden, R., and Morad, S., eds., Clay Mineral Cements in Sandstones: International Association of Sedimentologists, International Association of Sedimentologists Special Publication 34, p. 213-251.

HUGGETT, J.M., and CUADROS, J., 2005, Low-temperature illitization of smectite in the late eocene and early oligocene of the Isle of Wight (Hampshire basin), U.K.: American Mineralogist, v. 90, p. 1192-1202.

JOHNSON, M.J., and HOWELL, D.G., 1996, Thermal maturity of sedimentary basins in Alaska-An overview: United States Geological Survey Bulletin, v. 2142, p. 131.

KAHLE, M., KLEBER, M., and JAHN, R., 2002, Review of XRD-based quantitative analyses of clay minerals in soils: the suitability of mineral intensity factors: Geoderma, v. 109, p. 191-205.

KODAMA, H., N., SHIMODA, M.S., and BRYDON, J.E., 1976, Mixed-layer kaolinite-montmorillonite from soils near Dawson, Yukon Territory: Canadian Mineralogist, v. 14, p. 159-163.

LAVES, D., and JÄHN, G., 1972, Zur quantitativen röntgenographischen Bodenton-Mineralanalyse: Arch. Acker-u. Pflanzenbau u. Bodenkd., v. 16.

LAWVER, L.A., GRANTZ, A., and GAHAGAN, L.M., 2002, Plate kinematic evolution of the present Arctic region since the Ordovician". In: Tectonic evolution of the Bering Shelf-Chukchi Sea-Arctic margin and adjacent landmasses: Geol. Soc. Am. Special Paper, v. 360, p. 333-358.

LINDBO, D.L., STOLT, M.H., and VEPRASKAS, M.J., 2010, Redoximorphic Features, Interpretation of Micromorphological Features of Soils and Regoliths, Elsevier, p. 129-147.

MACK, G., JAMES, W.C., and MONGER, H.C., 1993, Classification of paleosols: Geological Society of America, Bulletin, p. 129-136.

MAXWELL, D.T., and HOWER, J., 1967, High-grade diagenesis and low-grade metamor-phism of illite in the precambrian belt series: The American Mineralogist, v. 52, p. 843-857.

MAYNARD, J.B., 1992, Chemistry of Modern Soils as a Guide to Interpreting Precambrian Paleosols, The Journal of Geology, p. 279-289.

MCCARTHY, P.J., MARTINI, I.P., and LECKIE, D.A., 1997, Pedosedimentary history and floodplain dynamics of the Lower Cretaceous upper Blairmore Group, southwestern Alberta, Canada, Canadian Journal of Earth Sciences, p. 598-617.

MCCARTHY, P.J., and PLINT, A.G.U.Y., 2003, Spatial variability of palaeosols across Cretaceous interfluves in the Dunvegan Formation , NE British Columbia , Canada : palaeohydrological , palaeogeomorphological and stratigraphic implications: Sedimentology, p. 1187-1220.

MCKEAGUE, J.A., 1978, Manual on soil sampling and methods of analysis., Can. Soc. Soil Sci.: Ottawa, Canada, Can. Soc. Soil Sci.

MEUNIER, A., 2005, Clays, p. p 472.

MONTAÑEZ, I.P., TABOR, N.J., NIEMEIER, D., DIMICHELE, W.A., FRANK, T.D., FIELDING, C.R., ISBELL, J.L., BIRGENHEIER, L.P., and RYGEL, M.C., 2007, CO2-forced climate and vegetation instability during Late Paleozoic deglaciation.: Science (New York, N.Y.), v. 315, p. 87-91.

MOORE, D.M., and REYNOLDS, R.C., JR, 1997, X-ray Diffraction and the Identification and Analysis of Clay Minerals, p. 378.

MULL, C.G., HOUSEKNECHT, D.W., and BIRD, K.J., 2003, Revised Cretaceous and Tertiary stratigraphic nomenclature in the Colville Basin, Northern Alaska: U. S. Geological Survey Professional Paper. 2003.

NAIDU, A.S., BURRELL, D.C., and WOOD, D.H., 1971, Clay Mineral Composition and Geologic Significance of Some Beaufort Sea Sediments: Journal of Sedimentary Petrology, v. 41, p. 691-694.

NETTLETON, W.D., OLSON, C.G., and WYSOCKI, D.A., 2000, Paleosol classification: Problems and solutions: CATENA, v. 41, p. 61-92.

OLSSON, S., and KARNLAND, O., 2011, Mineralogical and chemical characteristics of the bentonite in the A2 test parcel of the LOT field experiments at Äspö HRL, Sweden: Physics and Chemistry of the Earth, v. 36, p. 1545-1553.

PARFITT, R.L., and CHILDS, C.W., 1988, Estimation of formas of Fe and Al: A Review, and Analysis of Contrasting Soils by Dissolution and Moessbauer methods: Australian journal of soil research, v. 26, p. 121-144.

PARRISH, D.D., LAW, K.S., STAEHELIN, J., DERWENT, R., COOPER, O.R., TANIMOTO, H., VOLZ-THOMAS, A., GILGE, S., SCHEEL, H.-E., STEINBACHER, M., and CHAN, E., 2012, Long-term changes in lower tropospheric baseline ozone concentrations at northern mid-latitudes: Atmospheric Chemistry and Physics Discussions, v. 12, p. 13881-13931.

PARRY, W.T., JASUMBACK, M., and WILSON, P.N., 2002, Clay Mineralogy of Phyllic and Intermediate Argillic Alteration at Bingham, Utah: Economic Geology, v. 97, p. 221-239.

PHILLIPS, R.L., 2003, Depositional environments and processes in Upper Cretaceous nonmarine and marine sediments, Ocean Point dinosaur locality, North Slope, Alaska: Cretaceous Research, v. 24, p. 499-523.

PINHEIRO, J., SALGUERO, M.T., and RODRIGUEZ, A., 2004, Genesis of placic horizons in Andisols from Terceira Island Azores—Portugal: Catena, v. 56, p. 85-94.

POLLASTRO, R.M., 1993, Considerations and applications of the illite/smectite geothermometer in hydrocarbon-bearing rocks of Miocene to Mississippian age: Clays and Clay Minerals, v. 41, p. 119-133.

POPPE, L.J., and ELIASON, A.E., 2009, A BASIC program to calculate gravitational and centrifugal parameters, Geological Society of America.

REYNOLDS, R.C., 1985, NEWMOD a computer program for the calculation of one-dimensional diffraction patterns of mixed-layer clays: 9 Brook Rd., Hanover, New Hampshire 03755, USA., Reynolds, R.C.

REYNOLDS, R.C., 1980, Interstratified clay minerals: in Crystal Structures of Clay Minerals and Their X-ray Identiftcation, *in* Brindley, G.W., and Brown, G., eds., Crystal Structures of Clay Minerals and Their X-ray Identification: London, Mineralogical Society, p. 249-303.

ROBINSON, M.S., 1989, Kerogen microscopy of coal and shales from the North Slope of Alaska, Alaska Division of Geological and Geophysical Surveys Public Data File, p. 89-22.

SHELDON, N.D., and TABOR, N.J., 2009, Quantitative paleoenvironmental and paleoclimatic reconstruction using paleosols: Earth-Science Reviews, v. 95, p. 1-52.

SHOJI, S., NANZYO, M., and DAHLGREN, R.A., 1993, Volcanic Ash Soils, p. 288.

SINGER, A., 1980, The paleoclimatic interpretation of clay minerals in soils and weathering profiles: Earth-Science Reviews, v. 15, p. 303-326.

SINGER, A., 1984, The Paleoclimatic Interpretation of Clay Minerals in Sediments a Review: Earth-Science Reviews, v. 21, p. 251-293.

SOIL SURVEY STAFF, 1975, Soil Taxonomy, p. 754.

SOIL SURVEY STAFF, 1999, Soil taxonomy: A basic system of soil classification for making and interpreting soil surveys, p. 869.

SPICER, R.A., 2003, Changing climate and biota, p. 85-162.

SPICER, R.A., and HERMAN, A.B., 2010, The Late Cretaceous environment of the Arctic: A quantitative reassessment based on plant fossils: Palaeogeography, Palaeoclimatology, Palaeoecology, v. 295, p. 423-442.

ŚRODOŃ, J., 1984, X-ray Powder Diffraction Identification of Illitic Materials: Clays and Clay Minerals, v. 32, p. 337-349.

ŚRODOŃ, J., 1999, Nature of mixed-layer clays and mechanisms of their formation and alteration: Annual Review of Earth and Planetary Sciences, v. 27, p. 19-53.

ŚRODOŃ, J., DRITS, V.A., MCCARTY, D.K., HSIEH, J.C.C., and EBERL, D.D., 2001, Quantitative X-Ray Diffraction Analysis of Clay-Bearing Rocks from Random Preparations: Clays and Clay Minerals, v. 49, p. 514-528.

ŠUCHA, V., ŚRODOŃ, J., CLAUER, N., ELSASS, F., EBERL, D.D., KRAUS, I., and MADEJOVÁ, J., 2001, Weathering of smectite and illite-smectite under temperate climatic conditions: Clay Minerals, v. 36, p. 403-419.

TOMSICH, C.S., MCCARTHY, P.J., FOWELL, S.J., and SUNDERLIN, D., 2010, Paleofloristic and paleoenvironmental information from a Late Cretaceous (Maastrichtian) flora of the lower Cantwell Formation near Sable Mountain, Denali National Park, Alaska: Palaeogeography, Palaeoclimatology, Palaeoecology, v. 295, p. 389-408.

TRIBUTH, H., 1991, Qualitative und ‘‘quantitative’’ Bestimmung der Tonminerale in Bodentonen, *in* Tributh, H., and Lagaly, G., eds., Identifizierung und Charakterisierung von Tonmineralen. Berichte der Deutschen Ton- und Tonmineralgruppe: Giessen, Germany, p. 37-85.

UGOLINI, F.C., and DAHLGREN, R.A., 2002, Soil Development in Volcanic Ash, p. 69-81.

VAN BREEMEN, N., and BUURMAN, P., 2002, Soil formation, p. 415.

VAN OLPHEN, H., FRIPIAT, J.J., CO-OPERATION, O.F.E., DEVELOPMENT, and SOCIETY, C.M., 1979, Data handbook for clay materials and other non-metallic minerals: providing those involved in clay research and industrial application with sets of authoritative data describing the physical and chemical properties and mineralogical composition of the available reference materials, Pergamon Press.

VEPRASKAS, M.J., and LINDBO, D.L., 2012, Redoximorphic features as related to soil hydrology and hydric soils, p. 143-172.

VEPRASKAS, M.J., 1996, Redoximorphic Features for Identifying Aquic Conditions, N.C. Agricultural Research Service, N.C. State University, p. 33.

VITALI, F., LONGSTAFFE, F.J., MCCARTHY, P.J., PLINT, A.G., and CALDWELL, W.G.E., 2002, Stable isotopic investigation of clay minerals and pedogenesis in an interfluve paleosol from the Cenomanian Dunvegan Formation, N.E. British Columbia, Canada: Chemical Geology, v. 192, p. 269-287.

WADA, K., 1989, Allophane and imogolite, *in* Dixon, J.B., and Weed, S.B., eds., Minerals in soil environments: Madison, Wisconsin, p. 1051-1087.

WEIR, A.H., ORMEROD, E.C., and EL MANSEY, I.M.I., 1975, Clay Mineralogy Western of Sediments of the Nile Delta: Clay Minerals, v. 10, p. 369-386.

WILSON, M.J., 1999, The origin and formation of clay minerals in soils: past, present and future perspectives: Clay Minerals, v. 34, p. 7-25.

WINCHESTER, J.A., and FLOYD, P.A., 1977, Geochemical discrimination of different magma series and their differentiation products using immobile elements: Chemical Geology, v. 20, p. 325-343.

ZEHETNER, F., MILLER, W.P., and WEST, L.T., 2003, Pedogenesis of Volcanic Ash Soils in Andean Ecuador: Soil Science Society of America Journal, v. 67, p. 1797-1809.

ZIEGLER, A.M., SCOTESE, C.R., and BARRETT, S.F., 1983, Mesozoic and Cenozoic paleogeographic maps, *in* Brosche, P., Sundermann, J., ed., Tidal friction and the earth's rotation II: Berlin, Springer-Verlag, p. 240-252.

1.12 Appendices

Apendix 1.12.1. Summary of the clay mineral identification lab methods

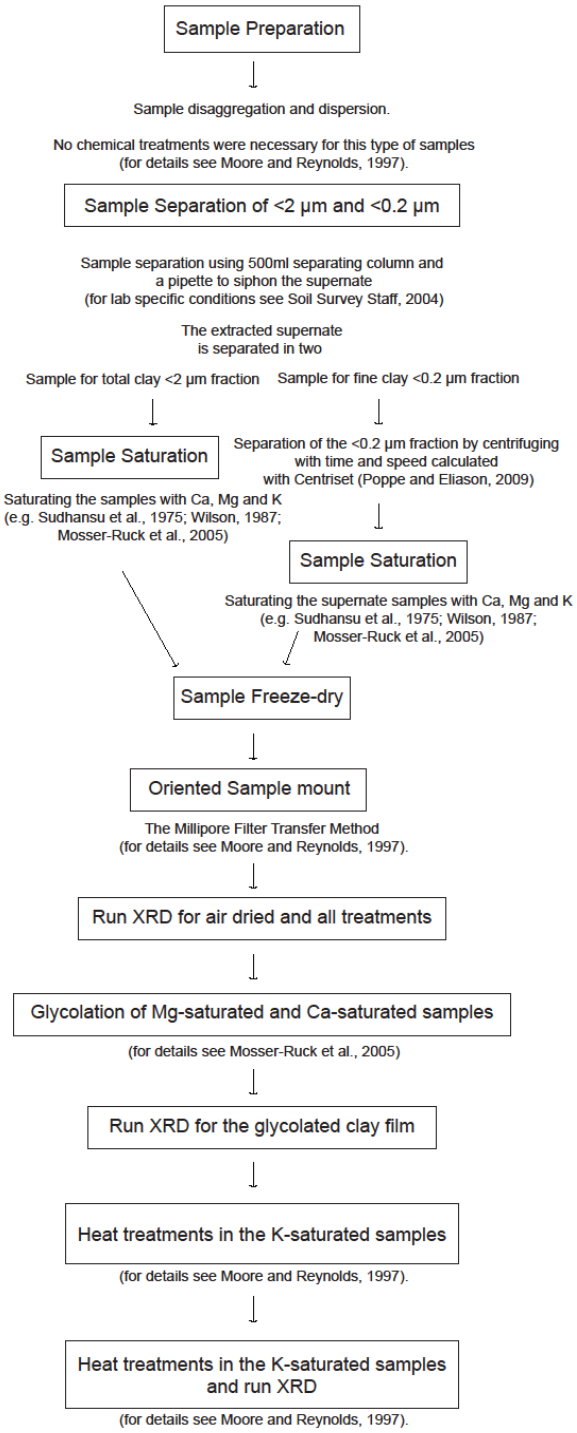

Apendix 1.12.2. Summary of the mineral intensity factors (MIF), d spacing (Å) and reflections used in this study.

	Reflection	d (Å)	MIF (literature)	Reference
illite	I: 001	10	1	Biscaye 1965
smectite	S:001	17	4	Biscaye 1965
kaolinite	K:001	7.2	2	Biscaye 1965
chlorite	Chl:002	7.1	2	Biscaye 1965
Quartz	Qtz:003	4.26	0.43	Laves and Jähn (1972); Tributh (1991)
illite/smectite	I/S: 002/003	~5.6	1.58	Gjems (1967) in Tributh (1991).

Chapter 2. Determining Late Maastrichtian Climate of the Lower Cantwell Formation, Alaska: Terrestrial Isotopic Evidence of Warmer Conditions[1]

2.1 Abstract

$\delta^{13}C$ isotope analysis of terrestrial organic matter and a new U-Pb age of 69.5 ± 0.7 Ma indicate that the Late Cretaceous lower Cantwell Formation, central Alaska, registers the Middle-Maastrichtian Event (MME) global warming episode. We explore carbon stable isotope ratios in fossil wood and bulk samples to better reconstruct the paleoclimate history and to establish stratigraphic correlation between this high latitude formation and other terrestrial and marine sequences. A measured section at the East Fork of the Toklat River extends from the Campanian-Maastrichtian boundary (~72 Ma) to the middle Maastrichtian (~69 Ma) and includes a bentonite layer with the new age determination. At 69.5 ± 0.7 Ma our $\delta^{13}C$ dataset records a ~3‰ positive excursion. Stable isotope excursions from sites around the world indicate an episode of rapid warming at this time, known as the Middle-Maastrichtian Event (MME). The chronostratigraphic constraints on deposition of this section (~72 to ~ 69 Ma) allow us to correlate the positive $\delta^{13}C_{wood}$ excursion (~3‰) with terrestrial and marine $\delta^{13}C$ stratigraphies from West Texas, and Tercis les Bains, Gubbio, to identify the MME. A mean annual precipitation of ~ 517.92± 134.44 mm/yr was obtained using $\delta^{13}C$ from organic matter. The new age, new C-isotope record and calculated precipitation values at the East Fork Toklat River section may serve as a reference for further paleoclimatic investigations and stratigraphic correlation with other terrestrial $\delta^{13}C$ records, of which there are few at present.

[1] SUSANA SALAZAR JARAMILLO, SARAH J. FOWELL, MACIEJ SLIWINSKI, PAUL J. MCCARTHY, JEFF BENOWITZ. 2014. "Determining Late Maastrichtian climate of the lower Cantwell Formation, Alaska: terrestrial isotopic evidence of warmer conditions" Cretaceous Research.

2.2 Introduction

During the Late Cretaceous the long-term global cooling trend (Li and Keller, 1999), was interrupted at ~69 Ma by an intense greenhouse event indentified in the terrestrial record as the Middle Maastrichtian Event (MME) (Nordt et al., 2003; Dworkin et al., 2005). The warming event (MME) occurred during the early Maastrichtian and lasted <1 m.y. (Bralower et al., 2002). In the marine record, the overall magnitude of the fluctuation is 0.6 ‰ to 1.5‰ and appears as a two-step rise (positive excursions) (Voigt et al., 2012). The MME is characterized by a rapid warming of deep and surface waters of 2–3°C (Keller, 2001; Bralower et al., 2002; Frank et al., 2005). Based on chemostratigraphic correlation, the terrestrial greenhouse episode associated with the Mid-Maastrichtian Event (MME) is represented by a two-step positive excursion in the $\delta^{13}C$ isotopic record (Nordt et al., 2003).

There has been limited isotopic work investigating the effects of the MME on the terrestrial environment (e.g. Nordt et al., 2003; Dworkin et al., 2005). Investigations on carbon isotopes in fossil wood provide the possibility of identifying excursions related to climate change conditions (e.g. Gröcke et al., 2005; Gröcke et al., 2006) and the possibility of correlating marine and terrestrial sequences (e.g. Gröcke et al., 1999; Gröcke, 2002). The importance of Late Cretaceous high latitude formations with a well preserved floral and faunal fossil record (Fiorillo et al., 2009; Fiorillo and Adams, 2012; Tomsich et al., 2010) make the lower Cantwell Formation (Fig. 2.9.1) a critical target to reconstruct ancient paleoclimatic conditions in this Cretaceous sub-arctic region. The new U-Pb age of 69.5 ± 0.7 Ma that brackets the $\delta^{13}C$ fluctuations in wood and bulk organic matter between ~72 to ~ 69 Ma allows chemostratigraphic correlation with other terrestrial and marine $\delta^{13}C$ curves, offering a climatic context for the lower Cantwell Formation. We found a significant positive $\delta^{13}C_{wood}$ excursion that, when compared with stable C isotopic curves of the same time period, correlates with the MME climate episode (e.g. Bralower et al., 2002; Nordt et al., 2003; Frank et al., 2005; Dworkin et al., 2005) (Fig. 2.9.5).

We studied a high resolution multi-proxy sediment record from sections of the lower Cantwell Formation exposed along the East Fork of the Toklat River to 1) reconstruct the depositional environment using sedimentary facies analysis, 2) determine the time of deposition of the lower Cantwell Formation at this locality; and 3) produce a $\delta^{13}C$ isotope stratigraphy (bulk organic matter and isolated wood fragments) for comparison with other Late Cretaceous records.

The similarity between our most prominent $\delta^{13}C$ shift with other reference sites (e.g. West Texas, Tercis les Bains, Gubbio) at ~ 69 Ma allows us to conclude that this greenhouse climate episode (MME) is likely registered at the East Fork of the Toklat River in the lower Cantwell Formation (Fig. 2.9.5).

2.3 Geologic Setting

Southern Alaska is the product of collisional events that added juvenile crust to western North America (Trop and Ridgway, 2007). The Cantwell Formation (Fig. 2.9.1) is located in the Cantwell Basin (Ridgway et al., 1997), developed during the Mesozoic accretion of the Wrangellia composite terrane to the North American Cordilleran margin (Trop and Ridgway, 2007). The Cantwell Formation is bounded to the south by the strike-slip Denali fault and to the north by the predominately thrust-faulted Hines Creek fault (Ridgway et al., 1997, Nokleberg et al., 2013). The Cantwell Basin, in which the Cantwell Formation was deposited, was at an approximate paleolatitude of 64 ^{o} N (Hillhouse and Coe, 1994).

The Cantwell Formation is subdivided into two lithologic units, a lower sedimentary unit and an upper volcanic unit (Ridgway, et al., 1997; Trop and Ridgway, 2007), separated by an angular unconformity broadly constrained as a 10–20 Ma hiatus (Cole et al., 1999). The lower Canwell Formation is a Late Cretaceous sedimentary unit composed of nonmarine to marginal-marine conglomerate, sandstone, siltstone, shale, minor coal and oncolitic limestone, mudstones and local paleosols (Wolfe and Wahrhaftig, 1970; Ridgway et al., 1997; Ridgway, et al., 2002). The upper Cantwell Formation is a volcanic

unit of Paleocene-Eocene age which consists of andesite, basalt, rhyolite, pyroclastic rocks, conglomerate, sandstone, siltstone and shale with the oldest volcanic rocks dated at 61.9 ± 0.3 Ma (whole gas) with a plateau age of 59.8 ± 0.2 Ma ($^{40}Ar/^{39}Ar$ whole rock; Cole et al., 1999). There are also older K-Ar age determinations on upper Cantwell Formation volcanic rocks of 61.0 ± 2.8 Ma (whole rock) and 64.6 ± 3.4 Ma (hornblende) (e.g. Csejtey et al., 1992). Given that these K-Ar ages are within error of the more precise $^{40}Ar/^{39}Ar$ age determination that takes into account both excess ^{40}Ar and alteration, we prefer the newer radiometric age determination as the maximum age of the upper Cantwell Formation. The extensive volcanism, belonging to the volcanic unit, was likely synchronous with localized extension attributable to strike-slip faulting (Ridgway et al., 2002).

In the lower Cantwell Formation, sedimentation occurred mainly in stream-dominated alluvial fan, axial braided stream, and lacustrine settings (Ridgway, et al., 1997). The thermal maturity of the organic matter at the East Fork indicated by Tmax is 497 °C (Stanley, 1987).

The lower and upper age brackets of the lower Cantwell Formation have been a subject of much debate. Previous age determinations have been based on conflicting interpretations of the paleofloral (palynology and leaf fossil) record and K-Ar radiogenic age determinations on granite stocks that intrude the lower Cantwell Formation. Based on newer palynological analyses it was determined the lower Cantwell Formation was deposited during the late Campanian and early Maastrichtian (Ridgway, et al., 1997). Our data yields a $^{206}Pb/^{238}U$ crystallization age of 69.5 ± 0.7 (Fig. 2.9.3) constraining the age of the lower Cantwell Formation at the East Toklat River section to early Maastrichtian, very close to the early Maastrichtian-late Maastrichtian boundary (69.23 Ma) (Gradstein et al., 2004).

2.4 Methods

2.4.1. Sedimentology

The sedimentology of the lower Cantwell Formation was analyzed in detail at the East Fork of the Toklat River (see Fig. 2.9.2). Stratigraphic sections were measured with a Jacob Staff and Brunton Compass. The S-2 section, at 122.45 m thick, contained leaf beds, dinosaur tracks, pedogenic features (burrows, root traces, and redoximorphic features), and a bentonite layer, and it was selected for detailed facies analysis and stable isotope analyses. The facies analysis (Table 2.10.1; Table 2.10.2) was carried out using a facies classification modified from Miall (1996).

2.4.2. Bentonite U/Pb Zircon Age

Four liters (~2 kg) of an altered ~10 cm thick white bentonite was collected from the lower Cantwell Formation at the East Fork of the Toklat River site (~95m) (Fig2.9.2). Zircon grains were isolated and prepared using standard mineral separation procedures described by Donelick et al. (2005) and summarized below. The bentonite sample was crushed to 2-3 mm, sieved through 300 µm nylon mesh, and the <300 µm size fraction was washed. Zircons were separated using lithium metatungstate, a Frantz magnetic separator, diodomethane, and hand-panning separation procedures. The zircon separate was mounted in epoxy and polished to expose grains. LA-ICP-MS (laser ablation–inductively coupled plasma–mass spectrometry) data collection was performed at the Geoanalytical Laboratory, Washington State University, Pullman, Washington, U.S.A. LA-ICP-MS analysis was performed using a New Wave YP213 213 nm solid state laser ablation system and a Thermo Scientific Element2 magnetic sector mass spectrometer.

Zircon U–Pb age standards with accepted ages of 1099.00 Ma (primary standard) and 1065.40 Ma (secondary standard) were scanned repeatedly as unknowns during the analysis to calibrate fractionation factors and absolute errors. Results were smoothed for each scan according to standard procedures, and all calculated ages for the zircon

standards were applied to construct a fractionation factor correction curve to account for error resultant of cumulative radiation damage. Concordance was monitored separately for each ablation spot. Ages for the ratios $^{207}Pb/^{235}U$, $^{206}Pb/^{238}U$, and $^{207}Pb/^{206}Pb$ were calculated for each data scan (25 to 32 individual scans performed on each spot) and checked for concordance; concordance here was defined as congruence of all three ages at the 2σ level. If the number of concordant data scans for a spot was greater than zero, the more precise age from the concordant-scan-weighted ratio $^{207}Pb/^{235}U$, $^{206}Pb/^{238}U$ or $^{207}Pb/^{206}Pb$, was chosen as the preferred age. $^{206}Pb/^{238}U$ ratios were used to calibrate ages for grains younger than 1.1 Ga, and $^{207}Pb/^{235}U$ ratios were used to calculate ages for grains older than 1.1 Ga. Asymmetrical negative and positive errors for each age were calculated by subtracting and adding, respectively, the isotopic ratio errors in the appropriate age equation (Chew and Donelick, 2012). The results for the measured isotope ratios and preferred ages are listed in Appendix 2.12.1. Positive errors may reflect localized anomalous concentration of uranium within a grain. In addition, the amount of error was limited to 10% at the 2σ level, a cut-off that is commonly, but not universally, used in the detrital zircon research community to filter zircon grains that may have experienced Pb loss and/or unaccounted for common Pb (e.g. Bradley et al., 2009). The remaining probable ages were used to calculate the weighted mean age for the sample using Isoplot (Ludwig, 2003). The individual U-Pb grain age results were plotted as histograms showing the error distribution about the mean (green line = age determination of sample as shown in Fig. 2.9.3).

2.4.3. Carbon and Nitrogen Isotopes and Total Organic Carbon

92 samples from bulk sediment were collected throughout the 122.45 m measured section (Fig. 2.9.2), with a sampling interval of 1m or less. Bulk samples were treated with 10% HCl for 24 hours and water washed. For the wood samples, about 4g of bulk sediment was crushed to <1 mm using a clean hammer. The samples were treated with 10% HCl to remove carbonate and with 49% HF to remove silicates. Then samples were washed with

de-ionized water several times to neutralize the acid. Oven-dried samples were examined under a stereomicroscope and 28 wood fragments were collected for isotopic analysis.

$\delta^{15}N$ and $\delta^{13}C$ values were measured usingEA (Elemental Analyser)-IRMS (Isotope-ratio mass spectrometry). Stable isotope values were obtained using Costech Elemental Analyzer (ESC 4010) and Thermo Conflo III interface with a DeltaV Mass Spectrometer. All samples were processed at the Alaska Stable Isotope Facility Lab, University of Alaska Fairbanks. Samples where weighed and placed in tin capsules. These tin capsules were closed, and combusted in the EA autosampler. N_2 and CO_2 combustion gases were separated chromatographically and then transferred to the IRMS, where the isotopes were measured. $\delta^{15}N_{air}$ and $\delta^{13}C_{PDB}$ values are reported with reference to international isotope standards. The 29 and 44 m/z peaks are used to quantify the N and C content of the samples, respectively.

2.4.3.1. Precipitation Estimates from $\delta^{13}C$ Stable Isotopes

Estimates of mean annual precipitation (MAP) from organic matter in bulk organic matter and wood were carried out using the Diefendorf et al., (2010) and Kohn (2010) equations. These equations are simple functions that allow MAP to be estimated from $\delta^{13}C$ of terrestrial organic matter. The estimation of MAP from carbon isotope compositions of plant tissues is based on the Farquhar et al., (1989) conceptual model that describes the isotopic fractionation (Δ) of C_3 plants during carbon assimilation.

(1)

$$\Delta_{leaf} = \frac{\delta^{13}C_{atm} - \delta^{13}C_{leaf}}{1 + \delta^{13}C_{leaf}/1000}$$

We use the Diefendorf et al., (2010) equation:

(2)

$$\Delta_{leaf} = 5.54(\pm 0.22) * \log_{10}(\mathrm{MAP}) + 4.07(\pm 0.70)$$

and Kohn (2010) equation:

(3)

$$\Delta_{leaf} = 2.01 - 1.98\times10^{-4}\ \text{Altitude(m)} + 5.88\log_{10}\left(\text{MAP} + 300, \frac{\text{mm}}{\text{yr}}\right) - 0.0129\,\text{Abs(latitude,°)}$$

According to paleomagnetic reconstructions this region lay at a paleolatitude of ~64ºN (Hillhouse and Coe, 1994). We assumed an altitude between 0-500 MASL (meters above sea level). For $\delta^{13}C$ of atmospheric CO_2, we assumed $\delta^{13}C_{atm} = -6.6‰$, which has been reported for the Late Cretaceous (Ghosh et al., 2001; Ghosh et al., 2005). For the Kohn equation we used an error propagation formula.

2.5 Results

2.5.1. Sedimentology

Using a facies classification scheme modified from Miall (1996) (Table 2.10.1), ten lithofacies were identified and grouped into five facies associations (FA) (Fig 2.9.2; Table 2.9.2).

2.5.1.1. Facies Association 1 (FA1): Horizontally Bedded Sandstone with Shale Lenses.

FA1 is characterized by horizontally bedded sandstone with narrow shale lenses (Facies Fl), interbedded with subordinate sandstone and fine-grained lithofacies (Sh, Fsm, Fc) (Figs 2.9.2; Table 2.10.1, 2.10.2). This succession typically consists of Fsm (silt, shale) at the bottom and Fl (or Sh) at the top. The shale lenses are up to 5mm thick and display planar lamination. Coarsening-up successions are common where facies Fc, Fsm and Sh are present. Individual FA1 sandbodies are between 1-3.5 m thick. Sandstones are very fine- to medium-grained. Individual beds of Fl are highly rooted and bioturbated which may obscure the lamination in sandstones. Plant roots are present in growth position. Transported wood casts and coalified tree trunks are common. Loadcasts are also

common. Horsetail fossil remains are present. Pedogenic features like weak platy structure, iron cemented beds, drab-gray colors and organi-rich horizons are observed in Fsm. FA1 is only present at the base of the stratigraphic section, and is present in close association with FA2.

2.5.1.2. Interpretation

Horizontal sandstone with narrow shale lenses is interpreted as levee deposits based on the sedimentology and association with other overbank elements (see e.g. Brierley et al., 1997; Fielding, 1986; Bown and Kraus, 1987) (Fig. 2.9.2; Table 2.10.1, 2.10.2). Alternation of coarse and fine-grained layers reflects periodic inundation and overbank flooding. In levees, thin rhythmically interbedded deposits are interpreted to reflect rising- and waning-stage deposits (Brierley et al., 1997), and the horizontal shale laminations (Sh) can be interpreted as a change in the flow regime and a decrease in energy of deposition (Ferguson and Brierley, 1999). Coarse-grained sediment is deposited during flood stage while fine-grained sediment is deposited from suspension as the flood recedes. Upward-coarsening indicates progradation of coarser natural levee deposits over fine-grained floodplains (Hudson, 2005). Organic-rich beds develop when plant debris settles and the sediment becomes waterlogged during lower-stage periods. Levees are only sporadically inundated (Brierley et al., 1997), therefore FA1 is subjected to redox procesess related to oscillations of the water table. Soils developed in levees are weakly developed and somewhat poorly drained (e.g. Aslan and Autin, 1998) or moderately well-drained when lithofacies Sh is at the top of FA1.

2.5.1.3. Facies Association 2 (FA2): Interbedded Tabular Sandstone and Mudstone.

FA2 consist of facies Sm, Sr, Fsm, Fc and Fb (Fig.2.9.2; Table 2.10.1, 2.10.2). The main characteristic of this association is the rhythmic alternation of facies Sm (or Sr) and Fsm. Sandstones range from very fine- to medium-grained. Sand bodies in FA2 range from 2-6 m thick. Individual tabular sand beds vary between a few centimeters and 2 m-thick. The tabular bodies are interbedded with beds of overbank fines (Fsm) up to 4 m thick.

Contacts tend to be sharp. Fc (carbonaceous mudstone) is typically at the top of the successions forming a boundary between this facies association and other elements (e.g. levee, floodplain, crevasse channel and other crevasse splay deposits). Transported wood, roots, burrows, nodules and Fe-oxide accumulations are common. Fossil leaves are common. Siderite is present in some sandstones. Flame structures are also present. FA2 is present in close association with FA1 and FA5.

Facies Fb (bentonite) is a rare but important lithofacies within FA2. The bentonite bed is 10 cm thick and has sharp upper and lower contacts. This bed can also be recognized in outcrops ~50 m away. The main minerals present are quartz, k-feldspar, and zircon. The clay fraction consists mainly of montmorillonite with some illite and chlorite (Chapter 1).

2.5.1.4. Interpretation

Interbedded tabular sandstones and mudstones of this facies association are interpreted as crevasse splays (Fig. 2.9.2; Table 2.10.1, 2.10.2). The alternation of sandstone with siltstone and mudstone has been identified as a typical feature of crevasse splay deposits (Nadon, 1994; Mjos et al., 1993) that indicates intermittent flow conditions associated with flood flows. Crevasse splay deposits are sheet-like sandstones with sharp basal contacts (Elliot, 1986 in Mjos et al., 1993) commonly interbedded with fine-grained mudrocks (Mjos et al., 2009). Sediment is introduced into the backswamp by crevasse channels and is deposited by a loss of flow power (Miall, 1996). The interfingering of Fsm and Sm reflects periodic changes in flow conditions. Facies Fsm is interpreted as suspension load deposits (Hornung and Aigner, 1999) and, together with facies Sm, they form a composite crevasse splay. Individual zones of facies Fsm are interpreted as backswamps. Facies Sm represents rapid sedimentation and dewatering that is typical of crevasse splay deposits (Hornung and Aigner, 1999). Successions of FA2 may pass upward into levees, crevasse channels or floodplains. The presence of carbonaceous mudstone, bioturbation, root beds and pedogenic features at the top of some splays indicates splay abandonment. Crevasse Splays are the main element in the East Fork

Toktlat River section. As in levees, periodic flooding events generate oscillations in the water table and redoxymorphic pedogenic features develop in FA2.

The S-2-82 bentonite bed (Fig. 2.9.2) is a non-reworked, airfall volcanic ash, deposited during an explosive period of rhyolitic volcanic activity. After intense weathering and prolonged alteration, the volcanic ash was altered to bentonite. This interpretation is supported by its' the montmorillonte composition.

2.5.1.5. Facies Association 3 (FA3): Cross-bedded Sandstone – Fines (Siltstone and Mudstone) and/or Massive Sandstone

FA3 consist of facies Sm, St, Ss, Fsm and Fc (Fig. 2.9.2; Table 2.10.1, 2.10.2). The main characteristic of this facies association is the fine- to medium-grained sandstone of facies St (cross-bedding) or facies Ss (pebble lags) interbedded with facies Sm or Fsm. Coarse sand of St (cross-bedded sand) and Ss (lag materials and poorly sorted sand) comprises the fill of the channel (mixed-load).Sandstones vary from very fine- to very coarse-grained. FA3 may be up to 2m-thick. Individual beds of facies St are a maximum of 2m thick and can show either fining-upward or interbbeding with facies Sm and Fsm. Beds of facies Ss may be interbedded with Fsm. Facies Fc may be present at the top or basal contacts of FA3. Dinosaur tracks, burrows, root traces, transported coalified tree trunks (~30cm diameter), needle-shaped leaves (conifers) and siderite nodules are common. Bioturbation at the base of Ss beds is common. In outcrop, the boundaries of the FA3 pinch-out laterally. FA3 is in close association with FA5.

2.5.1.6. Interpretation

FA3 is interpreted as crevasse channels (Fig. 2.9.2; Table 2.10.1, 2.10.2). FA3 occurs as both single and multistorey units (as part of a composite crevasse splay succession). Facies St (channel fill) overlain by Fsm (floodplain fines) in a rhythmic sequence is interpreted as a multi-story record of flood events. A fining upward trend, from channel-fill to floodplain deposits is interpreted as a change in the flow regime from upper to lower flow conditions as flood energy dissipates. After crevassing, facies Ss indicates

rapid deposition of poorly sorted bed load (Hornung and Aigner, 1999). Finer-grained facies than those in the main channels are to be expected, as these channels represent a "stripping" of the top of the flow in the main channel as the result of overbank flow and incision (Miall, 1996). FA3 corresponds to small channels that incise levee deposits and backswamps as crevasse splay deposits form. The relationship with other facies associations indicates that they are minor crevasse channels. Minor crevasse channels are interpreted to have been cut by erosive, turbulent flows emanating from small openings in distributary channel banks formed during channel flood stage (Fielding, 1986). Crevasse channels serve as conduits to deliver sediment from the larger channels onto the floodplain. The presence of roots throughout these crevasse channel sandstones indicates episodic flow in crevasse channels. Plants became established when the channels were dry or carried very low flow (Nadon, 1994). In general, crevasse splays and crevasse channels are the main depositional elements in the East Fork Toktlat River section, which may suggest seasonal flooding or, alternatively, frequent crevassing of channels in response to flashy flow conditions.

2.5.1.7. Facies Association 4 (FA4): Coarse Pebbly Cross-Bedded Sandstone:

FA4 consist of facies St with subordinate lithofacies Ss (Fig. 2.9.2; Table 2.10.1, 2.10.2). The main characteristics of FA4 are sandstones that fine upward, with trough cross-bedding. Coarse-grained and pebbly sandbodies are present at the base of FA4. The sandstone varies from medium- to very coarse-grained. The beds have clear fining-upward trends. The thickness of FA4 ranges between 2-4 m and typically occurs as single story units. Lags of facies Ss are present at the bottom of some beds. Pebbles are well-rounded (~3cm diameter). FA4 and FA3 are both channelized, however, FA4 is less abundant than FA3, it is thicker, and it lacks overbank fines. The beds are highly rooted. FA4 is typically interbedded with FA 5.

2.5.1.8. Interpretation:

Coarse pebbly, cross-bedded sandstone is interpreted as a major channel based on the dimensions, sedimentary structures and fining-upward character (Fig. 2.9.2; Table 2.10.1, 2.10.2). Coarse cross-bedded sandstone (St) and Ss (lag materials and poorly sorted sand) comprises the fill of the channel. Channel-fills generally fine upward, reflecting progressively weaker flows during filling (Bridge, 2006). FA4 is usually overlain or underlain by FA5. Fine-grained lithologies that cap major channel deposits are interpreted as abandonment facies. Thicker, fine-grained intervals enclosed within major channel facies are interpreted as slough channel or abandonment deposits within channel belts (Fielding, 1986). The presence of roots throughout the channel sandstones is interpreted to be the result of episodic or ephemeral flow in the channels. Plants became established when the channels were dry and/or carried very low flow. When flow increased and sediment was transported, the plants, mostly *Equisetum*, either grew to keep pace with the sediment influx or were buried (Nadon, 1994).

2.5.1.9. Facies Association 5 (FA5): Fine-Grained Overbank Sediments:

FA5 consist of Fsm and Fc. Single Fsm beds are up to 4m thick (Fig. 2.9.2; Table 2.10.1, 2.10.2). Laminations may be present. Fc (carbonaceous mudstone) appears sheet-like and is composed of coalified plant material. Fc is common at the top of some of the successions. Single beds of Fc range from 3-15 cm thick. Pedogenetic features include soil structure, redoximorphic features, and siderite. Ferruginous nodules and horizonization are common. The roots are oxidized and are in growth position. Horizons can be separated by more oxidized (reddish) conditions or by changes in the amount of organic matter.

2.5.1.10. Interpretation:

Fine-grained sediments are interpreted as backswamp, floodplain ponds and ephemeral sheet flood deposits with weak pedogenic development (Fig. 2.9.2; Table 2.10.1, 2.10.2). FA5 occurs as single and multistory units. All the FA5 features are drainage-related.

Waterlogged conditions favor peat accumulation and backswamp development. Oscillation of the water table and periodic flooding from the channels, on the other hand, resulted in the formation of ponds, swamps, sheet floods and fine-grained suspension deposits on floodplains with weak pedogenic development.

2.5.2. Bentonite U/Pb Zircon Age

Sixty-five zircons were picked from the bentonite, located a ~95m in the measured section (Fig. 2.9.2), for analysis (appendix 1). Fifty-four zircons give concordant analyses. One zircon grain had a U-Pb age determination of 149.85 ± 8.8 (2σ) and is inferred to be detrital and not representative of the crystallization age of the bentonite unit. Five zircon grains had errors of over 10% and, hence, were discarded. Additionally, two analyses were statistically excluded from the main cluster because they have modified error bars that do not overlap the weighted average age (Fig. 2.9.3).

Excluding these three zircon analyses, our best estimate for the age of this bentonite from the lower Cantwell Formation at the East Fork of the Toklat River, based on forty-six single grain zircon analyses, is 69.5 ± 0.7 Ma (with 95% confidence level and MSWD = 2.0).

2.5.3. Carbon Isotopes and Total Organic Carbon

$\delta^{13}C$, TOC (%) and C/N ratio results for bulk organic matter ($\delta^{13}C_{bulk}$) and wood ($\delta^{13}C_{Wood}$) samples are given in Table 2.10.3 and shown in fig. 2.9.4. Bulk organic matter $\delta 13C_{bulk}$ values exhibit a range between -22.95‰ and -27.10‰. Wood fragments exhibit $\delta^{13}C_{Wood}$ values between -22.42‰ and -27.85‰. The average and standard deviations of the bulk and wood populations are -25.99‰ (± 1.3‰) and -25.17‰ (± 0.73‰), respectively (Table 2.10.4).

C/N ratios range between 6 and 24 for bulk samples and between 13 and 55 for wood. As shown in Fig. 2.9.6 and Table 2.10.3, C/N ratios of bulk samples are in the range between

lacustrine algae and C_3 plants, while wood samples plot mostly in the C_3 land plants area (Meyers, 1997). The detailed results of isotopic analyses are given in appendix 2.12.2.

TOC (%) in bulk samples ranges between 0.3% and 19%. In wood, TOC (%) ranges between 4.52% and 68.67%.

The most positive $\delta^{13}C$ bulk values correlate with relatively high C/N values and high TOC (%) values (Fig. 2.9.4, table 2.10.3). More positive $\delta^{13}C_{bulk}$ values are generally found in samples collected from carbonaceous mudstone beds, except sample S-2-63 (sandstone) located at 61.8 m (Fig. 2.9.4). The $\delta^{13}C_{Wood}$ values are an average of ~0.32‰ more positive than $\delta^{13}C_{bulk}$ but most of the isotopic shifts are present in both curves (same general trend), showing a coupling between bulk and wood samples (Fig. 2.9.4).

2.6 Discussion

2.6.1. Depositional Environment

At the East Fork of the Toklat River, deposition was dominated by low-energy depositional processes. Overall, the facies associations (Fig.2.9.2) indicate that the section is consistent with an overbank environment dominated by levees, small crevasse channels, crevasse splays and backswamps with small channel bodies (Miall, 1996). The alternation of fine-grained and organic-rich layers (carbonaceous mudstone) indicates that peat formation was interrupted by frequent sediment input from low energy fluvial processes (e.g. Kirschbaum and McCabe, 1992; Nyambe, 1999).

Paleosol features are developed in all facies associations. Pedogenic development could be recognized based on pedofeatures like organic matter content, color, root traces, burrows and redoximorphic features. Paleosols and pedogenic features can be used for interpreting depositional and hydrologic histories of ancient alluvial deposits. For example, paleosol development may be an indication of well vegetated floodplains

produced by channels of normally low sinuosity (e.g. Nanson and Crocke, 1992) which may be the case for the measured section at the East Fork of the Toklat River. In weakly developed paleosols, for example, each soil profile could represent a single depositional episode where rapid sedimentation prevented cumulative soil development (Kraus and Aslan, 1993). Frequent sedimentation on the floodplain could be the result of overbank flooding (e.g. Vis et al., 2010) or crevassing and avulsion (e.g. Aslan and Autin, 1999).

Backswamps (carbonaceous mudstone) form when there is a reduction in energy from the proximal to distal floodplain and fine-grained deposits accumulate from suspension (Fryirs and Brierley, 2013; Vis et al., 2010). Carbonaceous mudstone is deposited from suspension during floods (Nyambe, 1999) as dense swamp vegetation traps the suspended sediments favoring organic-rich, mud deposition (Fryirs and Brierley, 2013). Periodic flooding could also result in organic matter accumulation. For example, in Holocene sediments of the Lower Tagus Valley (Portugal), the thick organic matter-rich deposits resulted from a high local groundwater table due to damming of the tributary (Vale de Atela Valley) entrance by more rapid aggradation in the main Valley (Tagus Valley). The continuous Tagus Valley aggradation causes a continuous rise of the groundwater table and accumulation of organic deposits (Vis et al., 2010).

In contrast, Davies-Vollum and Wing (1998) suggested that, channel avulsion, after climatic or tectonic forcing, is the main mechanism controlling carbonaceous bed deposition. Aslan and Autin (1999) also suggest that instead of a traditional model of fine-grained floodplain construction by repeated episodes of overbank flooding, crevassing and avulsion are the dominant processes of construction of fine-grained floodplains during periods of rapid floodplain aggradation. Crevassing and avulsion can occur regardless of trunk-channel flooding (Aslan and Autin, 1999). According to Davies-Vollum and Wing (1998) the accumulation of organic rich sediments (carbonaceous mudstone) is periodically interrupted by the distal portions of high-discharge flood events that input fine-grained sediment to the lowest parts of the floodplain. They also suggest that the clastic influxes preserve leaves local to the

backswamp environment in less organic-rich sediment and form fossil-bearing silty-claystones. Our measured section has leaf beds S-2-5 (5.3m), S-2-69 (67.5m) and S-2-83 (61.05m) in interbedded siltstones and very-fine sandstones deposited above the carbonaceous bed and these may have formed in a similar manner to that suggested by Davies-Vollum and Wing (1998).

At the East Fork of the Toklat River, the poor drainage evidenced by redoximorphic pedogenic features described above and the organic matter-rich accumulation evidenced by the frequency of carbonaceous mudstone (backswamps) (Fig. 2.9.2) can be explained by continuous rise of the groundwater table. Nanson and Crocke (1992) classified floodplains into three main classes based on stream power and sediment character: High-energy non-cohesive floodplains; medium-energy non-cohesive floodplains; and low-energy cohesive floodplains. Based on the sedimentary characteristics, the overbank deposits of our measured sections could be categorized as low-energy cohesive floodplains.

Furthermore, at the suborder level Nanson and Crocke (1992) use the following factors: (1) valley confinement; (2) channel cutting and filling; (3) braid-channel accretion; (4) lateral point-bar accretion; (5) overbank vertical-accretion; (6) anabranching; (7) scroll-bar formation; (8) counterpoint accretion; and (9) organic accumulation. In our measured section, the geomorphic units (levees, crevasse splays, crevasse channels and backswamps) associated with fine-grained sediments of low energy rivers and the lack of evidence of main (large) channels suggests a laterally-unconfined river formed on very low slope (e.g Brierley and Fryirs, 2005). Multichanneled networks of smaller sinuous and/ low sinuosity channels are common in these low energy rivers (Brierley and Fryirs, 2005).

According to previous studies, sedimentation in the lower Cantwell Formation was predominantly by stream-dominated alluvial fans, axial braided streams, and lacustrine environments within a thrust-top basin (Ridgway et al., 1997). Based on the description of the facies associations at East Fork of the Toklat River, the S-2 section has similar

characteristics to the distal alluvial fans, perhaps with small lacustrine deposits or ponds, described by Ridgway et al., (1997).

Given the general configuration of the basin and depositional environments outlined by Ridgway et al., (1997) the distal part of an alluvial fan seems a plausible depositional setting for the section measured at the East Fork of the Toklat River. The distal part of an alluvial fan is a likely setting where small sinuous and/or low sinuosity channels would be present and we would also expect a high water table, frequent channel avulsions (?) and significant accumulatiosn of organic matter.

Although our measured section may have formed under a number of circumstances, there are similarities in lithofacies and pedogenic features with both the vertically accreting fine grained floodplains of anastomosing rivers and/or the distal part of an alluvial fan where low sinuosity channels would also be present. But neither one can be fully explained with the limited field data at this one site. The last one can be used to develop a single hypothesis that can explain most of the section features in the context of Ridgway et al., (1997) model.

If avulsion is the dominant mechanism of lateral channel motion in our section then, according to Jerolmack and Mohrig, (2007), an anabranching river is likely to occur. If additionally we assume that the measured section is located at the distal part of an alluvial fan, we can highlight that rapidly aggrading alluvial fans, deposited by tributaries entering an alluvial valley, provided local elevations of base level and caused upstream anastomosis (Smith 1973 in Makaske, 2001).

Based on these ideas, a hypothesis of the environmental conditions responsible for the deposition of the East Fork Toklat River section is summarized below. When the stream-dominated alluvial fan enters into the braided stream valley, on the fan toe, rapid aggradation of the fan could provide local elevation of the base level and cause anastomosis. This process could be accompanied by avulsion and represent a fluvial cycle. At the end of each cycle, weakly developed paleosols form in the areas closer to

the crevasse channels, crevasse splays and levees while in the distal parts backswamps developed. In this reducing environment, organic matter accumulation is favored. The organic layer accumulation (carbonaceous mudstone) is interrupted by the sediment input caused by a new fluvial cycle. As pointed out by Davies-Vollum and Wing (1998) the clastic influxes preserved leaves that were local to the backswamp environment in less organic-rich sediment.

2.6.2. The Age of the Lower Cantwell Formation

The age of the lower Cantwell Formation has been a matter of debate. Attempts to bracket the minimum age of the lower Cantwell Formation have dealt with indirect geological evidence, such as the ages of the overlying volcanic rocks of the upper Cantwell Formation, but there is a documented unconformity between the two formations (Cole et al., 1999). Earlier studies assigned an early Tertiary age to the formation based on the plant fossil record (Wolfe and Wahrhaftig, 1970). More recently, Ridgway et al., (1997) found various species of *Aquilapollenites* and *Cranwellia* in the palynological record, indicating that the lower Cantwell Formation was deposited during the late Campanian and early Maastrichtian. Ridgway et al. (1997) also determined an age span of Late Campanian to early Maastrichtian for deposition of the lower Cantwell Formation at the East Fork of the Toklat River. In the Sable Mountain section, the presence of rare *Aquilapollenites conatus* and abundant forms of *Corylites*, especially *Corylites beringianus*, suggest that the entire succession is of mid- to Late Maastrichtian age (Tomsich et al., 2010).

According to Ridgway et al., (1997) the palynological data agree with previous K-Ar ages obtained from biotites, 71.9 ± 2.7 Ma, and 78.7 ± 3.6 Ma (see Sherwood and Craddock, 1979) from granitic stocks that intrude the lower Cantwell Formation. Additionally, the presence of *Kurtzipites andersonii* in the lower Cantwell Formation (Ridgway et al., 1997) can be used as a reference since it has a geologic range of ~72.4Ma to ~71.1Ma (~ 1.3 Ma age range) (Braman and Sweet, 2012).

The differences in the age estimates reflect the lack of reliable isotopic dates for the sedimentary lower Cantwell Formation. At the East Fork of the Toklat River section, we report the first numerical age for the S-2-82 bed (at ~95m depth) and thereby constrain the age of the Lower Cantwell Formation (Fig. 2.9.4). The age of a bentonite interlayered with the sedimentary strata represents both the depositional age of the volcanic ash and a maximum age for the overlying sediments. The bentonite bed S-2-82 has a U-Pb age of 69.50 ± 0.7 (2σ) (fig. 2.9.3). The volcanic source of the ~69.5 Ma volcanic ash (bentonite) is unknown, but itwas likely derived from the Alaska Range magmatic arc that was active south of the Cantwell Basin during this time period (Trop and Ridgway, 2007). The results from the U-Pb analyses on single zircon crystals demonstrate that the majority of the concordant zircons belong to one population. Hence, the S-2-82 bentonite bed probably represents one single ashfall event.

This radiometric age places the lower Cantwell Formation at the East Fork of the Toklat River in the early Maastrichtian, very close to the Early Maastrichtian-Late Maastrichtian boundary (69.23 Ma) (Gradstein et al., 2004). The palynologic age of Late Campanian-Early Maastrichtian (Ridgway et al., 1997) gives a maximum age of ~72 Ma for the base of our measured section and the U-Pb age of 69.57 ± 0.69 (2σ) located at ~95m gives a maximum age for the upper section. The two ages bracket the stratigraphic section between ~72 and ~ 69 Ma (Fig. 2.9.4).

2.6.3. Correlation with the Prince Creek Formation

The Prince Creek Formation is a Maastrichtian alluvial-deltaic coastal plain succession that was deposited in the Colville Basin, an east-west-trending, asymmetrical foreland basin to the north of the Brooks Range mountain belt (Fig. 2.9.1). During the Late Cretaceous, the Prince Creek Formation was located between 83° and 85° N paleo-latitude (Ziegler et al., 1983; Lawver et al., 2002). The foreland basin-fill was deposited from Middle Jurassic through Tertiary (Bird and Molenaar, 1992) and consists of interbedded, very fine- to fine-grained sandstone, conglomerate, organic-rich siltstone,

and coal with thin bentonites and tuffs, and abundant remains of both vertebrates and plants (Mull et al., 2003). This formation is interpreted as a large, tidally influenced alluvial/deltaic depositional system consisting of meandering trunk channels, meandering and anastomosing distributary channels and mud-rich floodplain deposits with paleosols (Flaig et al., 2011). The age of the Prince Creek Formation bonebeds is between 68 and 71 Ma, based on the $^{40}Ar/^{39}Ar$ and K-Ar dating of numerous tephras at Ocean Point (Conrad et al., 1990). The most recent $^{40}Ar/^{39}Ar$ age from glass in tuff from the Prince Creek Formation yields a 69.2 ± 0.5 Ma age (Flaig, 2010).

The lower Cantwell Formation bentonite U-Pb zircon 69.5 ± 0.7 Ma age and the 69.2 ± 0.5 Ma $^{40}Ar/^{39}Ar$ age from glass in tuff from the Prince Creek Formation (Flaig, 2010) overlap within analytical error (0.3 ± 1.19 Ma), showing that these two distal sedimentary beds are coeval. The different latitudes of these two lower Maastrichtian units, the presence of dinosaur remains and tracks, diverse invertebrate traces, and plant fossils gives a unique opportunity for faunal, floral and climatic comparisons between the Lower Cantwell Formation and the Prince Creek Formation. Correlation of the two formations also allows estimation of latitudinal mean annual temperature (MAT) and mean annual precipitation (MAP) gradients across Alaska (from ~64° to 84°N) during the late Cretaceous.

2.6.4. Carbon Isotopes and Total Organic Carbon

Five of the bulk samples (total=92) and nine of the wood samples (total=28) from the East Fork of the Toklat River record $\delta^{13}C$ values more positive (>-25‰) than the $\delta^{13}C$ Mesozoic C_3 plants average (-27‰) (Gröcke, 2002) and can be considered positive excursions. The coupling between $\delta^{13}C_{Wood}$ and $\delta^{13}C_{bulk}$ (Fig. 2.9.4) indicate that these positive excursions are probably being affected by $\delta^{13}C$ fluctuation in CO_2 in the global ocean-atmospheric reservoir (e.g Gröcke 2002., Hasegawa et al., 2003) rather than palaeoenvironmental or paleoecological factors.

$\delta^{13}C_{bulk}$ values lie between -22.95‰ and -27.10‰ (average -26.10 ± 0.3‰) and $\delta^{13}C_{Wood}$ values between -22.42‰ and -27.85‰. These values are within the range for living terrestrial plants with C_3 photosynthesis (Gröcke, 2002; Meyers, 1997) and within the Late Cretaceous $\delta^{13}C$ range for C_3 plants of -20‰ and -28‰ (Bocherens et al., 1994). According to Bocherens et al. (1994), values of $\delta^{13}C$ around -20‰ are at the very upper limit for C_3 plants and values higher than -23‰ are rather unusual in modern C_3 plants, occurring only in plants growing under stress, such as water stress or salt stress. In our samples, there is no evidence of brackish influence in the sedimentological record which suggests that water-stress is not the explanation for the positive values. Four (S-2-4; S-2-54; S-2-56; S-2-62) of five $\delta^{13}C_{bulk}$ positive shifts coincide with carbonaceous mudstone facies (Table 2.10.3). However, in the $\delta^{13}C_{wood}$ only one positive excursion (S-2-62) of nine coincides with carbonaceous mudstone facies (Table 2.10.3). This indicates that the positive excursions are not being controlled by the depositional environment (carbonaceous mudstone).

Other variables that can drive $\delta^{13}C$ towards more positive values are the source of the organic matter and/or selective partial degradation of the organic matter due to diagenesis (e.g. Gröcke 1998; Gröcke 2002).

2.6.4.1. Shifts in δ13C and Taphonomic-Diagenetic Controls

Shifts in $\delta^{13}C$ can occur when the original $\delta^{13}C$ values differ according to the plant constituent (e.g. leaf, seed, wood) that is being preserved or the chemical component of that constituent (e.g. cellulose, lignin, lipids) (Gröcke, 2002). The components, in order of highest resistance to degradation and, thus, greater preservation potential in sedimentary rocks, are lignin, lipids, cellulose, proteins and carbohydrates (Gröcke, 2002). The plant constituents, and the chemical components of those constituents, indirectly identified by C/N ratios (Fig. 2.9.6) and kerogen types (Stanley, 1987), are discussed in order to evaluate bias due to the source of the organic matter.

2.6.4.1.1. Bulk Sample Organic Matter:

In the bulk sample the positive excursions in the carbonaceous mudstone may reflect an increased contribution of organic matter from fossil remains with higher $\delta^{13}C$ than the other non-carbonaceous samples. Some chemical components that have higher $\delta^{13}C$ values are cellulose, carbohydrates and/or hemicellulose (Meyers, 1997; Gröcke, 2002). Carbonaceous mudstone is interpreted as backswamps (Table 2.10.2) and higher C% and anoxic conditions are consistent with this environment (e.g. Meyers and Lallier-Vergès, 1999). In the backswamp environment not only is lignin a major constituent of the coal-like carbonaceous mudstone (e.g. Hatcher et al., 1992) but lignin and lignocellulosic detritus derived from vascular plants tends to have a higher rate of preservation (Benner et al., 1984). For older specimens, cellulose and carbohydrates may be altered or not preserved (Gröcke 1998). Furthermore, lignocelluloses derived from herbaceous plants seem to degrade more rapidly than lignocelluloses derived from hardwoods (Benner et al., 1984). In fact, previous studies of organic matter from stratigraphic sections on the East Fork of the Toklat River indicate that mudstone kerogens are mainly type III (Stanley, 1987). Type III kerogen is dominated by ligno-cellulosic material (Tyson, 1984) and typifies woody plant matter (Meyers, 1997). Consequently, previous studies support the hypothesis that ligno-cellulose is the main chemical component in the bulk samples of the carbonaceous mudstone.

2.6.4.1.2. Wood Separates:

Separation of wood from bulk avoids variations caused by different types of organic matter. Bulk wood is composed of a ligno-cellulose complex constituting polysaccharides, cellulose and hemicellulose, and lignin (Poole et al., 2004).

The wood samples are likely the remains of conifers for the following reasons: angiosperm wood is generally more ^{13}C depleted (more negative values ~ -24‰ to ~ -30‰) relative to conifer wood (~ -19‰ to ~ -27‰) (Poole and van Bergen, 2006), and we report wood values between ~ -22‰ to ~ -27‰ (Table 2.10.3); our most positive

$\delta^{13}C$ wood values (~ -22‰) are consistent with enriched $\delta^{13}C$ values reported from Cretaceous conifer wood (van Bergen and Poole 2002); and studies of the coeval coal beds and fossil record in the Late Cretaceous Prince Creek Formation, North Slope, Alaska, indicate that the vegetation was dominated by conifers (Spicer et al.,1992).

2.6.4.1.3. Diagenesis:

Bulk organic matter in carbonaceous mudstone and wood are mainly ligno-cellulosic in composition. The ligno-cellulose complex of the bulk wood is composed of polysaccharides, cellulose and hemicellulose, and lignin. Hemicellulose, cellulose and lignin have different $\delta^{13}C$ of ~ -23‰, ~ -25‰ and ~ -28‰, respectively (Poole et al., 2004). Important isotopic changes can occur during the early diagenesis of lignified plant tissues. In ancient wood, for example, the remaining tissues are enriched in lignin and consistently depleted in ^{13}C relative to modern counterparts (Benner et al., 1987). Other studies suggest that in older sediments fossil wood shows apparent general ^{13}C enrichment over time. Van Bergen and Poole (2002) found $\delta^{13}C$ values of approx. -21.3‰ in Cretaceous woods and attributed the isotope variation to chemical alteration of lignin in conifer specimens causing enrichment of $\delta^{13}C$ values (van Bergen and Poole, 2002).

Lignin has values ~ -28‰ (Gröcke, 2002; Poole et al., 2004) unless chemical alteration enriches ^{13}C (van Bergen and Poole, 2002). However, as discussed earlier, $\delta^{13}C_{wood}$ and $\delta^{13}C_{bulk}$ range (Table 2.10.3) most of the isotope shifts (negative and positive) are shown in both the $\delta^{13}C_{bulk}$ and $\delta^{13}C_{Wood}$ values, demonstrating a coupling between bulk and wood samples (Fig. 2.9.4). Hence, chemical alteration of lignin is not a suitable explanation for the positive excursions.

Additionally, some studies suggest that despite the loss of organic matter during early diagenesis, sedimentary organic matter seems to undergo little change (Meyers, 1994; Meyers, 1997). Anoxic conditions tend to preserve the original $\delta^{13}C$ values (Lehman et al., 2002). During early diagenesis, there is a selective degradation of the organic matter.

However, it is unlikely that the $\delta^{13}C$ excursions are the result of selective partial degradation of the organic matter in a few horizons.

At the East Fork of the Toklat River, the organic matter is ligno-cellulosic in composition that was deposited in anoxic conditions, making it resistant to further diagenesis. In any case, the consistency between $\delta^{13}C_{bulk}$ and $\delta^{13}C_{Wood}$ values suggest that, despite diagenesis, the excursions are real and variations due to diagenesis are small compared to fluctuations of the primary isotope signal.

In summary, the carbonaceous mudstone has a higher proportion of ligno-cellulose material with higher $\delta^{13}C$ than the other non-carbonaceous samples. The preservation of ligno-cellulose over other organic matter components in the carbonaceous mudstone can be explained by the anoxic depositional environment (backswamp). The non-carbonaceous siliciclastic rocks have more mixed organic matter. Despite an offset between $\delta^{13}C_{bulk}$ and $\delta^{13}C_{Wood}$ values, there is consistency between most of the peaks (fig. 2.9.4), which suggests that the main fluctuations cannot be explained by variations in the mixing of organic matter or selective degradation of the organic matter.

2.6.4.2. $\delta^{13}C$ Shifts Related to Changes in the Paleo Athmospheric CO_2

The coupling between $\delta^{13}C_{Wood}$ and $\delta^{13}C_{bulk}$ indicate that the positive excursions are probably caused by $\delta^{13}C$ fluctuation in CO_2 in the global ocean-atmospheric reservoir (e.g Gröcke 2002., Hasegawa et al., 2003). Such changes in composition of atmospheric CO_2 can be used for chemostratigraphic correlation (Arens et al., 2000).

Nordt et al. (2003) identified an intense greenhouse event, the Middle Maastrichtian Event (MME) at ~69 Ma. The MME has been reported in isotopic records from marine sediments (Keller, 2001; Bralower et al., 2002; Frank et al., 2005), and paleosol carbonates (Dworkin et al., 2005; Nordt et al., 2003). In the marine record, this event is characterized by rapid, 2-3°C warming of deep and surface waters at ~69 Ma (Keller, 2001; Bralower et al., 2002; Frank et al., 2005). In the $\delta^{13}C$ marine record, the overall magnitude of the fluctuation is 0.6 ‰ to 1.5‰, and it is represented by two positive

excursions (Voigt et al., 2012). Nordt et al., (2003), in the terrestrial record, interpret the two positive excursions as greenhouse episodes associated with the Mid-Maastrichtian Event (MME).

Another event, the Campanian-Maastrichtian Boundary Event (CMBE or CMB) at ~72 Ma, has also been reported in marine sediments, where it is characterized by a negative $\delta^{13}C$ excursion (Jung et al., 2012; Voigt et al. 2010). Thibault et al. (2012a and b) describes an overall negative $\delta^{13}C$ excursion (CMB) at the Campanian-Maastrichtian Boundary that is characterized by three negative excursions (CMBa, CMBb, CMBc). The CMBE corresponds to the third excursion, CMBc (Thibault et al., 2012b) at ~72Ma (Thibault et al. 2012a). On the other hand, Voigt et al., (2012) describe the Campanian-Maastrichtian Boundary as five small-scale positive excursions (CMBE-1; CMBE-2; CMBE-3; CMBE-4 and CMBE-5).

We compare our $\delta^{13}C$ (wood and bulk) records with data from carbonate paleosols in West Texas (Nordt et al., 2003), marine carbonates from Tercis les Bains (France), Gubbio (Italy), Lägerdorf-Kronsmoor-Hemmoor section (northern Germany), stevns-1 (Denmark) (Voigt et al., 2012) and the Indian Ocean (ODP Hole 762C) (Thibault et al., 2012a and b) in order to assess whether the MME and the CMBE are recorded in our measured section (Fig. 2.9.4). The main positive excursion in our measured section occurs between 100 and 95m. Values change from -26.51‰ at ~100 m to -22.42‰ at ~95 m and to -24.70‰ at 88.65 m. As this positive excursion (~3‰) occurred at ~69 Ma, it may be correlative with one of the MME $\delta^{13}C$ excursions recorded in paleosol carbonate (Nordt et al., 2003) and one of the marine MME excursions of the Voigt et al. (2012) (Fig. 2.9.5).

Another feature of our record is a negative excursion. $\delta^{13}C_{Wood}$ shows the most negative value, -27.84‰, at ~52.5 m (Fig. 2.9.5). Combined with the set of four positive excursions between 53 and 60 m, this excursion may represent the CMBE (lower pink area of Fig. 2.9.5). According to Voigt et al. (2012), the CMBE is represented by five small-scale positive excursions.

When compared with both terrestrial and marine carbonates, the magnitude of the $\delta^{13}C$ wood excursions of our samples are considerably greater. Gröcke et al., (1999) also report larger excursions in the $\delta^{13}C$ values of marine and terrestrial organic matter (particularly wood) compared to carbonates.

Both the magnitued of the excursions and the available age constraints indicate that the MME is present at the East Fork measured section.

The age of the two positive excursions that represents the MME (Fig. 2.9.5) are estimated from the confidence interval of the radiometric U-Pb age of 69.5± 0.7 Ma. The confidence interval at 95% confidence level is between 70.19Ma and 68.81Ma.(Pink upper area of Fig.2.9.5).

The presence of CMBE excursions is more dubious. The ~69 Ma MME lasted <1 m.y. (Bralower et al., 2002). According to the Jung et al. (2012) age model, the CMBE negative carbon-isotope excursion occurred between ~72.1 and ~70.5 Ma (1.6 Ma in duration), while Thibault et al. (2012a) estimate a minimum age of 71.94 Ma and a maximum age of 72.16 Ma (0.22 Ma in duration). At the East Fork section, the most negative value, -27.84‰ at ~52.5 m, and four positive excursions above, between 53 and 60 m, are constrained only indirectly by a relative age. As discussed earlier, the presence of *Kurtzipites andersonii* in the lower Cantwell Formation (Ridgway et al., 1997) can be used as a reference since it has a geologic range of ~72.4Ma to ~71.1Ma (~ 1.3 Ma age range) (Braman and Sweet, 2012). Hence the negative excursion and the set of four positive ones can be bracketed between 72.4 Ma and ~71.1 Ma, which is approximatly the same CMBE time interval (Jung et at. 2012; Thibault et al. 2012a).

2.6.4.3. Mean annual Precipitation in the Cantwell Formation

Arens et al. (2000) and Jahren et al. (2008) have suggested that the $\delta^{13}C$ value of land plant carbon ($\delta^{13}C$ plant) preserved in the geologic record should reflect the $\delta^{13}C$ value of atmospheric CO_2 at the time during which the plants grew ($\delta^{13}C$ atmosphere), based on a meta-analysis of modern plant data. The isotopic composition of bulk organic carbon in

the sediments approximates the many-species average sample that best minimizes physiological vital effect bias (Arens and Jahren, 2000). Contributions from multiple species and many individual plants can be extracted from a few cubic centimeters of many terrestrial rocks, making such rocks the optimal substrate for $\delta^{13}C$ atmospheric reconstruction (Jahren et al., 2008).

Based on a regression of $\delta^{13}C$ plant value and $\delta^{13}C$ atmospheric value Arens et al., (2000) used an inverse solution to reconstruct the $\delta^{13}C$ value of the atmosphere, where:

(4)

$$\delta^{13}C \text{ atmosphere} = (\delta^{13}C \text{ plants} + 18.67) / 1.1$$

We estimated the $\delta^{13}C$ of atmospheric CO_2 ($\delta^{13}C$ atmosphere) using Arens et al., (2000) equation. The mean $\delta^{13}C$ value for the organic matter in the Lower Cantwell Formation is ~ -26‰. Therefore -6.6‰ is the average $\delta^{13}C$ value of atmospheric CO_2 for the period between ~72 and ~69 Ma based on equation (4). A value of -6.6‰ is also reported by Ghosh et al., (2001) for the Late Cretaceous Lameta Formation.

The Diefendorf et al. (2010) equation (2) yields a growing season average MAP of 603.41 mm/yr, and the Kohn (2010) equation (3) yields an average MAP of 517.92± 134.44 mm/yr. We prefer the data obtained with Kohn´s equation over Diefendorf et al.´s equation for two reasons: 1) the Kohn (2010) regression has a better R^2 than that of Diefendorf et al., (2010); and 2) altitude and latitude are variables that can be choosen in the Kohn (2010) equations while in Diefendorf et al. (2010) altitude and latitude are constants that are assigned according to geographic zone and/or plant functional type.

The precipitation value of 517.92 ± 134.44 mm/yr is higher than the growing season MAP of 229.4 ± 334.5mm obtained on the basis of CLAMP Analysis (Tomsich et al., 2010).

2.7 Conclusions

Based on the facies association analysis we interpret the depositional environment of the East Fork of the Toklat River as being part of the distal part of an alluvial fan. The depositional environment agrees with the characteristics of the distal alluvial fan and the lacustrine deposits described by Ridgway et al., (1997). The distal part of an alluvial fan is also a likely setting where anastomosis could have taken place and is one possibility to explain the continuous rise of the water table, avulsion (?) and significant organic matter accumulation processes.

The new U-Pb age of 69.5 ± 0.7 Ma from a bentonite horizon constrains the age of the upper section of the lower Cantwell Formation at the East Fork of the Toklat River. Together with the palynostratigraphic age of Late Campanian-Early Maastrichtian (Ridgway et al., 1997), the stratigraphic section can be bracketed between ~72 to ~ 69 Ma.

The average MAP value is 517.92± 134.44 mm/yr, based on the Kohn (2010) equation (3). These precipitation values are higher than the growing season MAP of 229.4±334.5mm obtained on Leaf Margin Analysis (Tomsich et al., 2010).

The coupling between $\delta^{13}C_{Wood}$ and $\delta^{13}C_{bulk}$ indicate that the positive excursions are driven by $\delta^{13}C$ fluctuations in CO_2 in the global ocean-atmospheric reservoir rather than the result of digenetic or taphonomic controls.

The record of $\delta^{13}C$ fossil wood reveals excursions that can be correlated with excursions in other Late Cretaceous marine and terrestrial records (West Texas, Tercis les Bains, Gubbio). The main features of the $\delta^{13}C$ wood record are: 1) a positive $\delta^{13}C_{Wood}$ excursion (-22.42‰) at 95.6 m depth right below the 69.5 ± 0.7 Ma bentonite layer and 2) a negative excursion (-27.84‰) at ~52.5 m overlain by four positive excursions between 53 and 60 m. Radiometric age control and chemostratigraphic correlation suggest that the initial positive excursion is related to an intense greenhouse event that occured in the Mid-Maastrichtian. The negative excursion and the overlying positive

excursions occurred between 72.4Ma and ~71.1Ma, based on the presence of *Kurtzipites andersonii* in the lower Cantwell Formation (Ridgway et al., 1997). The timing, magnitude, and direction of the $\delta^{13}C$ excursions suggest that they may be interpreted as short-term variations recorded at the Campanian-Maastrichtian Boundary in marine and terrestrial sections (Thibault et al. 2012b; Jung et al., 2012; Voigt et al. 2012).

2.8 Acknowledgments

Financial support for this research was provided by the University of Alaska Museum of the North. The authors wish to thank Colciencias Colombia for economic support. The authors also wish to thank Nadine Reitman, Alexander de Moor and Todd Jacobus for the field support. Special thanks for Carla Susanne Tomsich for her support and assistance with data analyses and interpretations.

2.9 Figures

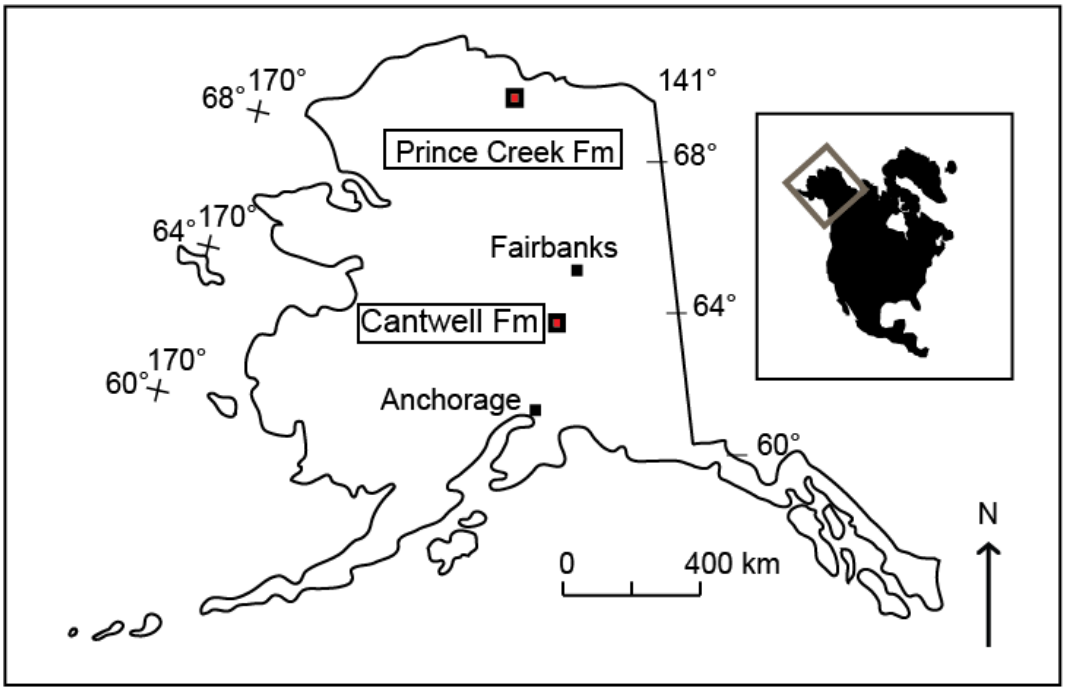

Fig. 2.9.1. Location area of the Cantwell Formation and the coeval Prince Creek Formation.

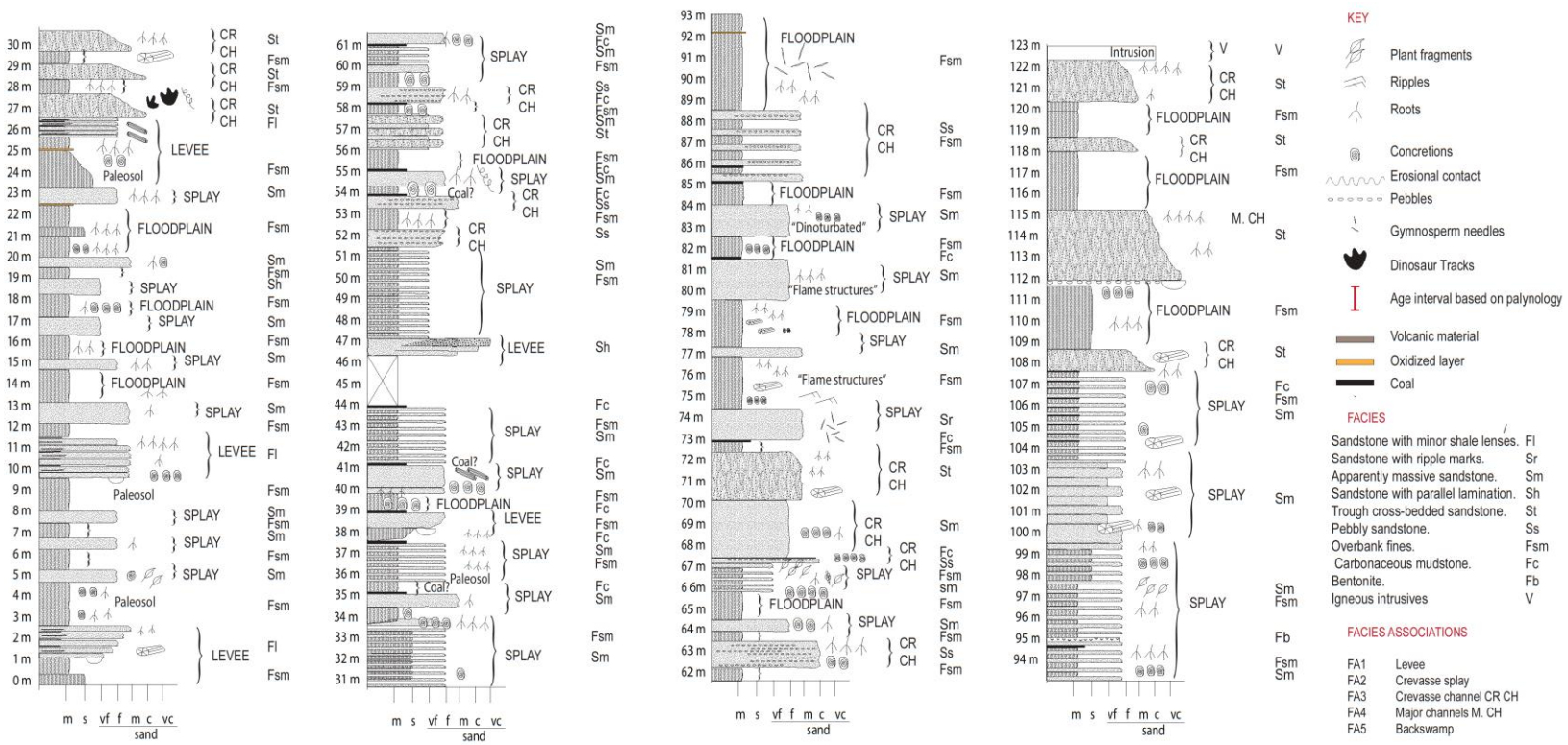

Fig. 2.9.2. Detailed stratigraphy of the East Fork Toklat River section. Facies and facies associations are summarized next to the column. Explanation of abbreviations in tables 2.10.1 and 2.10.2.

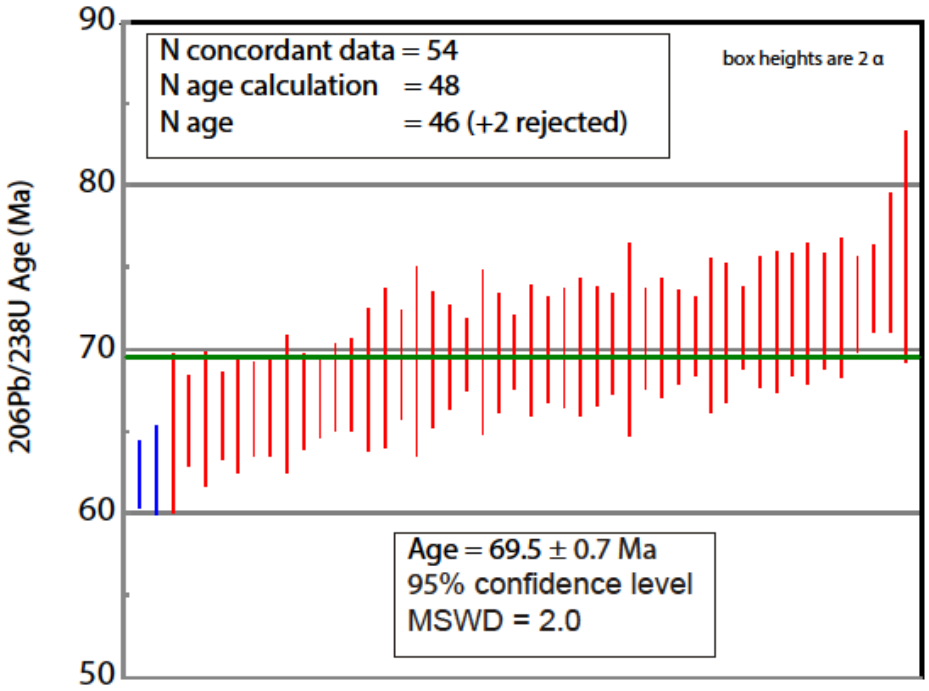

Fig. 2.9.3. Age of the bentonite of the measured section at ~95m depth.

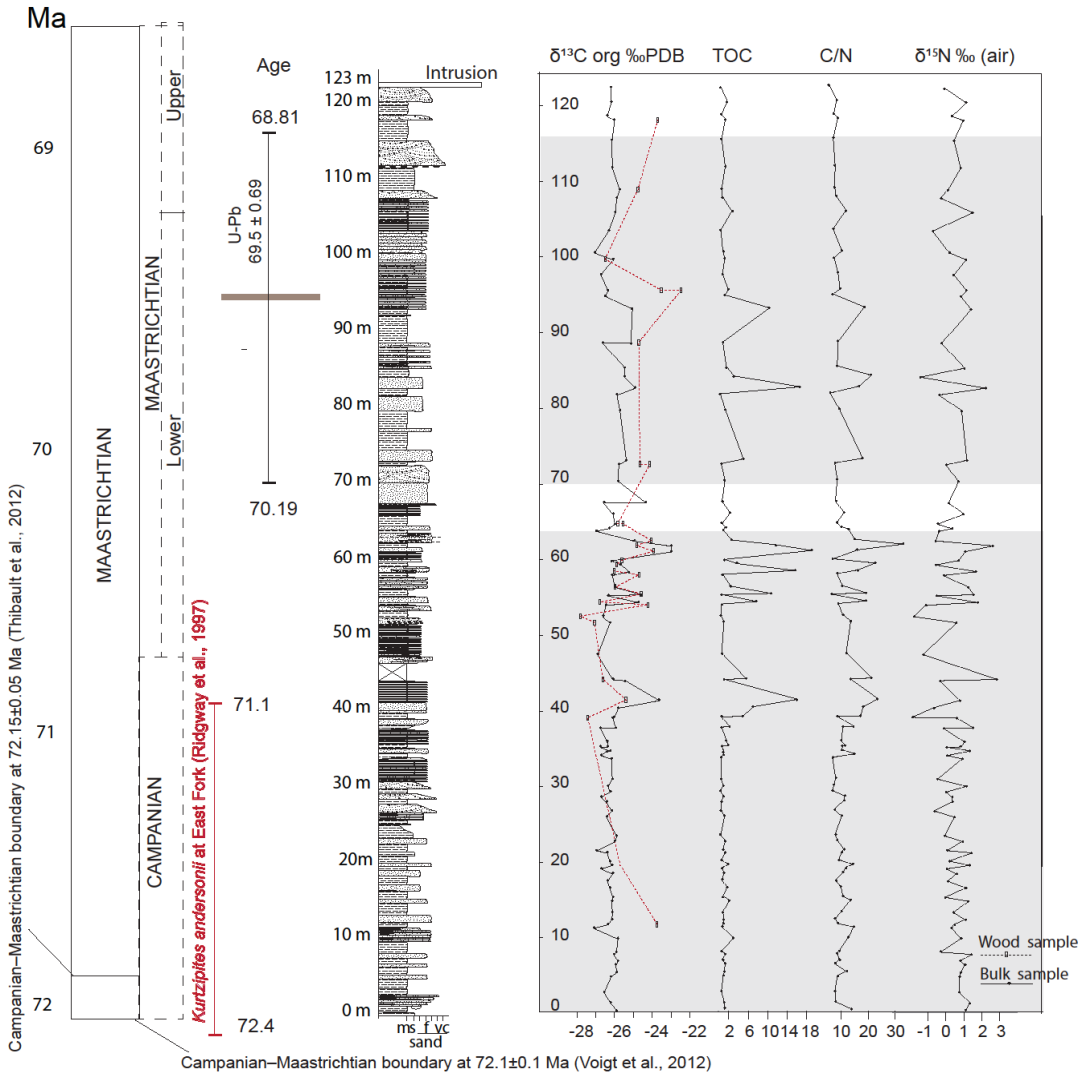

Fig. 2.9.4. Summary of the age interval, stratigraphy, $\delta^{13}C$ values, C%, C/N and $\delta^{15}N$ values for the measured section.

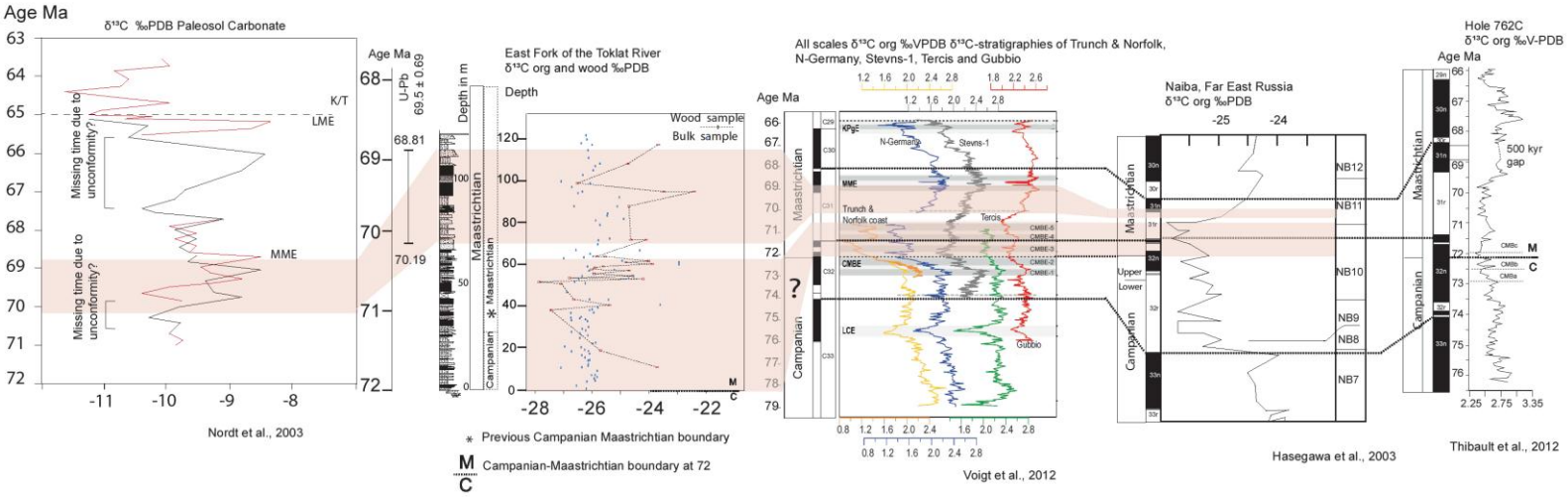

Fig. 2.9.5. Chemostratigraphic correlation of the $\delta^{13}C$ values of the measured section at East Fork Toklat River (this study) with stratigraphies of West Texas, Tercis les Bains, Gubbio, Hole 762C to identify the MME.

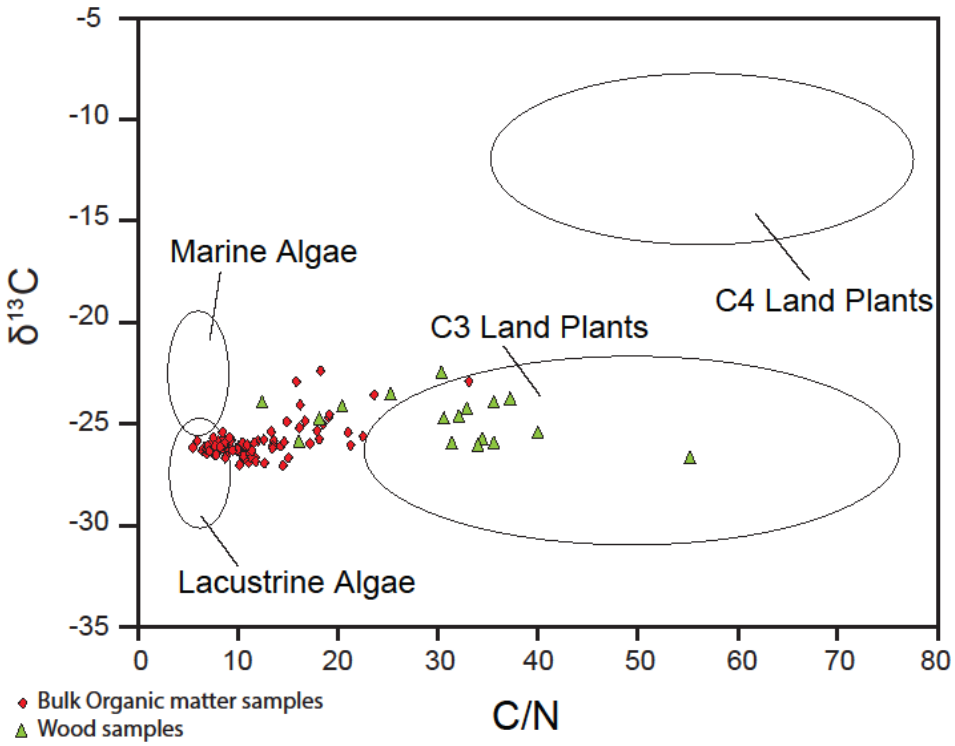

Fig. 2.9.6. C/N ratio and isotopic $\delta^{13}C$ value identifiers of bulk organic matter produced by marine algae, lacustrine algae, C_3 land plants, and C_4 land plants (Meyers, 1997). The figure shows a more mixed bulk sample in the area of lacustrine algae and the wood separates in the area of C_3 land plants.

2.10 Tables

Table 2.10.1. Lithofacies identified in the Lower Cantwell Formation at the East Fork of the Toklat River.

Facies (F) name	Symbol	Description	Process
Sandstone with minor shale lenses.	Fl	Very fine to medium sand. Shale lenses of 5 mm thick. Packages are 1-2-m-thick. Transported wood, horstails, iron nodules and abundant root traces. Load cast is present at the bottom of some packages. Some packages grade upward into progressively coarser ones.	Vertical accretion.
Sand with ripple marks.	Sr	The sand grain size range from very fine to medium. Packages are at least 1-m-thick. Conifer leaves (6.5 cm) are common. Ripple marks are present.	Lower flow regime.
Apparently massive sand.	Sm	Massive or structured beds with lenticular form. Very fine to medium sand. Packages are 1-5-m-thick. Some packages are fine sandstone interbedded with medium sandstone. Abundant root traces. Iron nodules, angiosperm leaves, conifer needles, borrows, flame structures, horstails and bioturbation are common.	Postdepositional modification of laminated sand? Bank collapse in small channels? Sediment gravity flow?
Sand with parallel lamination.	Sh	Parallel laminated sand. Very fine to medium sand. The packages are maximum 1-m-thick. Abundant root traces. Load cast present at the bottom of some packages. Some packages grade upward into progressively coarser ones. Well-rounded clasts up to 3 cm in diameter present in some beds.	Transition from subcritical to supercritical flow
Trough cross-bedded sandstone.	St	Medium to very coarse sand. Lag deposits of fine conglomerate are present in some beds at the base. Beds are 0.5m-4m-thick. Some cross-bedded sandstone is interbedded with massive or laminated sandstone. Beds grade upward into progressively finer ones. Transported wood, burrows, iron nodules and root traces are common. Dinosaur tracks are present in one of the beds. Some strata in the outcrop pinch-out laterally.	3-D dunes migrating downstream within channels. Low flow regime.

Table 2.10.1. Lithofacies identified in the Lower Cantwell Formation at the East Fork of the Toklat River (continued).

Facies (F) name	Symbol	Description	Process
Pebbly sandstone.	Ss	Grain size ranges from very fine to very coarse sand. Beds are maximum 1m-thick. Some packages are interbedded with mudstone. The pebbles are: well-rounded; ~3cm diameter and form horizontal lamination. Bioturbation is present at the base of some beds. Iron nodules, conifer needles and root traces are common. Some beds show a "platy" structure. Some packages grade upward into progressively coarser ones.	Rapid deposition. May comprise the fill of channels.
Overbank fines.	Fsm	Siltstone, claystone, mudstone. This material is organic rich. Weathering develops a platy structure at the top of some beds. Packages are up to 4m thick. Iron oxide accumulations between the layers (like placic horizons). Transported wood, burrows, and iron nodules are very common. Root traces are very abundant. Root beds are at the top of the layers. The roots are oxidized and in growing position. The root traces are also in the same bed with abundant plant remains and big wood fragments and/or flame structures. Pedogenic features: soil structure, soil nodules, placic horizon, siderite, and horizonization.	Floodplain deposit more distant of the fluvial channel.The rootbeds are interpreted as paleosols. Weak paleosol development indicates proximity to the channel compare to more developed paleosols. Redoximorphic features indicate variations in soil saturation caused by seasonal fluctuations of the water table. Warm to cool temperate paleoclimate (mean annual soil temperature 5-20 degrees C) (Driese et al., 1995).
Carbonaceous mudstone.	Fc	Organic rich mudstone with coaly appearance. Contain iron oxide nodules and siderite concretions. Beds are 3-15cm thick. Typically occurs at the top of any bed with abundant root traces, bioturbation, leaves, and/or flame structures. Wood fragments are very common. Some wood looks vitrinized.	Peat formation after flooding. Swamp.
Bentonite.	Fb	White to light green ash altered to bentonite. Layers are few cm thick.	Deposition of ash on low energy area after volcanism.
Intrusives	V	Dikes and sills mainly of basaltic composition. They are of Tertiary age (Cole et al., 1999).	Igneous process.

Table 2.10.2. Facies associations identified in the Lower Cantwell Formation at the East Fork of the Toklat River.

Facies association (FA)	**Symbol**	**Facies grouped in the FA**	**Interpretation**	**Lithology**
Horizontal sandstone with narrow shale lenses	FA1	Fl, Sh, Fsm, Fc	Levee	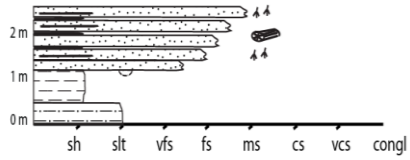
Interbedded tabular sandstone and fines	FA2	Sr, Sm, Fsm, Fc, Fb	Crevasse splay	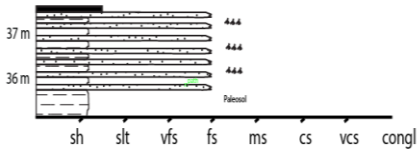
Structured sandstone – fines and/or massive sandstone	FA3	Sm, St, Ss, Fsm, Fc	Crevasse channel	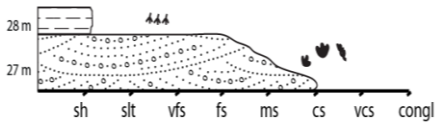
Coarse pebbly-structured sandstone	FA4	St, Ss	Major channels	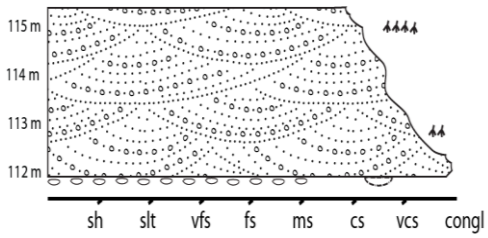
Fine-grained	FA5	Fsm, Fc	Backswamp paleosols, floodplain weakly developed paleosols, marsh, lakes, ponds.	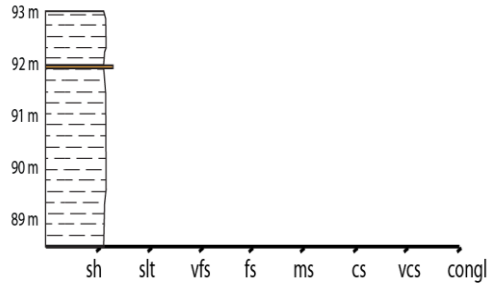

Table 2.10.3. $\delta^{13}C$, TOC (%) and C/N ratio values at the East Fork of the Toklat River section S-2.

Sample Name Bulk organic matter	Depth (m)	C (%)	$\delta^{13}C$ PDB (‰)	C/N ratio
S-2-3	2.7	0.51	-26.56	7.7
S-2-4	4.75	0.93	-26.18	8.59
S-2-5	5.3	1.15	-25.88	12.01
S-2-6	6.35	1.26	-25.93	7.7
S-2-7	6.85	0.8	-25.82	9.39
S-2-8	7.7	1.34	-26.03	8.51
S-2-9	8	0.61	-25.9	9.31
S-2-10	9.8	2.92	-25.82	12.65
S-2-11	11.2	0.66	-27.1	14.55
S-2-12	11.65	0.82	-26.35	8.75
S-2-13	12.3	1.03	-26.13	7.92
S-2-14	13.25	0.84	-26.12	10.15
S-2-15	14.75	2.13	-26.14	13.51
S-2-16	15.25	0.86	-26.08	10.73
S-2-17	16.5	1.64	-26.25	9.91
S-2-18	17.4	0.67	-26.37	7.98
S-2-19	18.4	1.03	-26.09	10.7
S-2-20	19.05	0.67	-26.72	11.76
S-2-21	19.5	2	-26.13	14.3
S-2-22	20.05	0.57	-26.25	9.13
S-2-23	21.15	1.34	-26.39	10.27
S-2-24	21.45	0.85	-26.95	11.12
S-2-25	22.65	1.34	-25.98	8.68
S-2-26	23.4	0.41	-25.89	7.81
S-2-27	25.9	1.15	-26.42	10.21
S-2-28	26.7	0.43	-26.14	7.39
S-2-29	27.9	0.57	-26.43	11.11
S-2-30	28.55	1	-26.72	11.36
S-2-31	29.2	0.34	-26.23	6.79
S-2-32	29.95	0.93	-26.34	7.3
S-2-33	30.9	0.44	-26.12	7.95
S-2-34A	33.6	0.43	-26.16	6.75
S-2-35	34.05	1	-26.72	15.1
S-2-36	34.65	0.89	-26.41	10.31
S-2-36N	34.65	1.71	-26.23	Too low Nitrogen levels
S-2-37	35.15	0.66	-26.74	10.61
S-2-38	35.2	1.83	-26.37	11.44
S-2-39	35.85	1.53	-26.38	10.06
S-2-40	37.65	0.58	-26.75	10.71
S-2-41	37.7	2.18	-25.94	14.66
S-2-42	39	0.56	-26.08	8.83
S-2-43	39.1	4.83	-26.01	17.24

Table 2.10.3. $\delta^{13}C$, TOC (%) and C/N ratio values at the East Fork of the Toklat River section S-2 (continued).

Sample Name Bulk organic matter	Depth (m)	C (%)	$\delta^{13}C$ PDB (‰)	C/N ratio
S-2-44	40.35	6.99	-25.8	18.18
S-2-46	41.35	16.04	-23.61	23.66
S-2-47	43.95	1.22	-25.43	13.37
S-2-48	44.1	5.48	-26.08	21.31
S-2-49	47.4	0.59	-26.9	11.82
S-2-50	51.6	1.02	-26.24	13.5
S-2-51	52.45	0.52	-26.61	10.59
S-2-53	53.95	0.57	-26.46	9.02
S-2-54A	54.3	7.65	-24.72	19.12
S-2-55	55.2	0.62	-26.34	6.48
S-2-56	55.35	10.64	-24.58	19.19
S-2-57	56.3	2.38	-25.97	10.47
S-2-58	57.9	0.72	-26.12	8.49
S-2-59	58.4	15.65	-25.23	16.2
S-2-60	59.3	3.7	-25.66	22.55
S-2-61	59.85	1.13	-26.17	7.14
S-2-62	61.05	18.99	-22.95	15.88
S-2-63	61.8	11.65	-22.95	33.15
S-2-64	62.45	2.53	-24.93	14.93
S-2-65	63.75	0.82	-26.98	12.7
S-2-66	64.1	1.33	-26.29	10
S-2-67	64.65	0.62	-25.98	8.45
S-2-68	66	2.25	-26.08	10.96
S-2-69	67.5	0.65	-26.56	7.87
S-2-69B	67.5	7.9	-24.32	21.82
S-2-70	70.35	1.24	-25.8	8.53
S-2-71C	72.55	0.48	-25.78	7.63
S-2-72	73.15	4.98	-25.38	17.96
S-2-74	79.7	1.28	-25.71	9.18
S-2-75	81.8	0.3	-25.88	5.98
S-2-76	82.7	16.74	-24.9	16.76
S-2-77	84.15	3.03	-25.47	21.06
S-2-78	85.35	1.54	-25.45	8.5
S-2-79B	88.65	0.77	-26.63	8.89

Table 2.10.3. Continuation $\delta^{13}C$, TOC (%) and C/N ratio values at the East Fork of the Toklat River section S-2 (continued).

Sample Name Bulk organic matter	**Depth (m)**	**C (%)**	**$\delta^{13}C$ PDB (‰)**	**C/N ratio**
S-2-79C	88.65	3.81	-25.12	12.95
S-2-80	93.15	10.31	-25.04	18.53
S-2-81	94.85	1.23	-26.5	6.91
S-2-82	95.6	1.87	-26.35	9.51
S-2-86	103.5	0.4	-26.31	6.91
S-2-87	105.95	2.6	-25.96	11.67
S-2-88	107.85	0.71	-25.89	8.03
S-2-89	108.95	0.57	-25.73	7.58
S-2-90	111.85	1.29	-26.12	7.75
S-2-91	115.5	0.57	-26.14	7.02
S-2-92	118.15	1.3	-26	8.72
S-2-93	118.7	0.46	-26.39	7.17
S-2-94	120.5	1.7	-26.17	8.28
S-2-95	122.45	0.34	-26.2	5.52
S-2-12W	11.65	53.54	-23.72	almost too low nitrogen levels
S-2-21W	19.5	68.67	-25.7	45.15
S-2-42 Q+W	39	7.81	-27.44	Too low Nitrogen levels
S-2-46 W	41.35	63.67	-25.39	34.57
S-2-48 W	44.1	88.57	-26.64	40.11
S-2-50 W+S	51.6	20.33	-27.08	Too low Nitrogen levels
S-2-51 Q+W	52.45	37.15	-27.85	Too low Nitrogen levels
S-2-53W	53.95	41.64	-24.21	55.29
S-2-54B W	54.3	71.28	-26.78	Too low Nitrogen levels
S-2-56 W	55.35	75.46	-24.58	33.03
S-2-57 W	56.3	73.27	-25.92	32.22
S-2-58 W	57.9	37.36	-24.7	31.53
S-2-59 W	58.4	81.38	-26.01	30.73
S-2-60 W	59.3	42.25	-25.9	34.14
S-2-61 W	59.85	63.17	-25.61	Too low Nitrogen levels
S-2-62W	61.05	45.2	-23.89	35.72
S-2-63 W	61.8	83.7	-24.81	Too low Nitrogen levels
S-2-64 W	62.45	58.82	-24.02	Too low Nitrogen levels
S-2-67 W	64.65	53.92	-25.54	Too low Nitrogen levels
S-2-67 wood	64.65	1.35	-25.83	12.59

Table 2.10.3. $\delta^{13}C$, TOC (%) and C/N ratio values at the East Fork of the Toklat River section S-2 (continued).

Sample Name Bulk organic matter	**Depth (m)**	**C (%)**	**$\delta^{13}C$ PDB (‰)**	**C/N ratio**
S-2-71B Wood	72.55	24.42	-24.11	16.27
S-2-71A Q+W	72.55	4.52	-24.64	Too low Nitrogen levels
S-2-82A Wood	95.6	38.47	-23.49	30.49
S-2-84W	99.7	67.53	-26.51	almost too low nitrogen levels
S-2-89W	108.95	68.2	-24.74	almost too low nitrogen levels
S-2-92 Wood	118.15	25.07	-23.68	25.41

Table 2.10.4. Summary of organic matter components and facies to identify any relationship between depositional environment and origin of the organic matter.

	Wood	**Bulk sample**	**Carbonaceous Mudstone**	**Siliceous sedimentary rocks (bulk sample)**	
				Siltstone, claystone, mudstone	**Sandstones**
Facies			Fc	Fsm	Fl, Sr, Sm, Sh, St, Ss
Main type of organic matter	C_3 plants		C_3plants	Mixed OM – C_3plants	Mixed OM – C_3 plants
Sedimentary environment	Found in all the sedimentary environments.		Backswamp	Floodplain ponds and ephemeral sheet floods.	Crevasse splays, crevasse channels, levees, major channels.
C (%)	47%	2.44%	8.83%	1. 28 - 3.14%	0.62 - 2.15 %
$\delta^{13}C$	-25.17‰ (± 1.3‰)	-25.99‰ (± 0.73‰)	-25. 09‰	-26.04‰	-26.16‰
C/N	30.83	11.35	17.67	8.32 - 12.38	7.84 - 14.59
Kerogen Type (based on literature)	Wood, Type III ? (Meyers, 1997)		Type III? (Coal values from Stanley)	Type III and IV (Stanley,1990)	
Organic matter constituents (based on literature)	Carbohydrates in wood (Meyers, 1997), Ligno-cellulosic material (Tyson, 1984). More ligning in older sediments? (Meyers and Ishiwatari, 1993)		Hemicellulose? Based on δ13C (Gröcke, 2002). C/N values>14, cellulosic plant material (Meyers and Ishiwatari, 1993).	Carbohydrates ? based on δ13C (Gröcke, 2002),	C/N values>14, cellulosic plant material (Meyers and Ishiwatari, 1993). Carbohydrates ? based on δ13C (Gröcke, 2002)
Redox environment	Reducing		Strongly reducing?	Strongly reducing – Mildly reducing	Mildly reducing (alternation oxidation - reducing?)

2.11 References

ARENS, N.C., JAHREN, A.H., and AMUNDSON, R., 2000, Can C_3 plants faithfully record the carbon isotopic composition of atmospheric carbon dioxide ? Can C_3 plants faithfully record the carbon isotopic composition of atmospheric carbon dioxide ?: Paleobiology, v. 26, p. 137-164.

ARENS, N.C., and JAHREN, A.H., 2000, Carbon Isotope Excursion in Atmospheric CO 2 at the Cretaceous-Tertiary Boundary: Evidence from Terrestrial Sediments Carbon Isotope Excursion in Atmospheric CO 2 at the Cretaceous-Tertiary Boundary : Evidence from: Palaios, v. 15, p. 314-322.

ASLAN, A., and AUTIN, W.J., 1998, Holocene flood-plain soil formation in the southern lower Mississippi Valley: Implications for interpreting alluvial paleosols: GSA Bulletin, v. 110, p. 433-449.

ASLAN, A., and AUTIN, W.J., 1999, Evolution of the Holocene Mississippi River floodplain, Ferriday, Louisiana; insights on the origin of fine-grained floodplains: Journal of Sedimentary Research, v. 69, p. 800-815.

BENNER, R., FOGEL, M.L., SPRAGUE, E.K., and HODSON, R.E., 1987, Depletion of 13C in lignin and its implications for d13C isotope studies: Nature, v. 329, p. 708-710.

BENNER, R., MACCUBBIN, A.E., and HODSON, R.E., 1984, Anaerobic Biodegradation of the Lignin and Polysaccharide Components of Lignocellulose and Synthetic Lignin by Sediment Microflora Anaerobic Biodegradation of the Lignin and Polysaccharide Components of Lignocellulose and Synthetic Lignin by Sediment Micr: Appl. Environ. Microbiol., v. 47, p. 998-1004.

BIRD, K.J., and MOLENAAR, C.M., 1992, The North Slope foreland basin, Alaska, Foreland Basins and Foldbelts, American Association of Petroleum Geologists (AAPG.), p. 363-393.

BOCHERENS, H., FRIIS, E.M., MARIOTTI, A., and PEDERSEN, K.R., 1994, Carbon isotopic abundances in Mesozoic and Cenozoic fossil plants: Palaeoecological implications: Lethaia, v. 26, p. 347-358.

BOWN, T.M., and KRAUS, M.J., 1987, Integration of channel and floodplain suites, I. Developmental sequence and lateral relations of alluvial paleosols: Journal of Sedimentary Petrology, v. 57, p. 587-601.

BRADLEY, D., HAEUSSLER, P., O'SULLIVAN, P., FRIEDMAN, R., TILL, A., and TROP, J., 2009, Detrital zircon geochronology of Cretaceous and Paleogene strata across the south-central Alaskan convergent margin, in Haeussler,: Studies by the U.S. Geological Survey in Alaska, 2007: U.S. Geological Survey Professional Paper, v. 1760-F, p. 36.

BRALOWER, T.J., SILVA, I.P., and MALONE, M.J., 2002, New evidence for abrupt climate change in the Cretaceous and Paleogene: An Ocean Drilling Program expedition to Shatsky Rise, northwest Pacific: GSA TODAY, p. 4-10.

BRAMAN, D.R., and SWEET, A.R., 2012, Biostratigraphically useful Late Cretaceous–Paleocene Terrestrial palynomorphs from the Canadian Western Interior Sedimentary Basin: Palynology, v. 36, p. 8-35.

BRIDGE, J.S., 2006, Facies Models: Recent developments: SEPM Special Publication, v. 84, p. 85-170.

BRIERLEY, G.J., FERGUSON, R.J., and WOOLFE, K.J., 1997, What is a fluvial levee ?: Sedimentary Geology, v. 114, p. 1-9.

BRIERLEY, G.J., and FRYIRS, K.A., 2005, Geomorphology and river management: applications of the river styles framework, John Wiley & Sons.

CHEW, D.M., and DONELICK, R.A., 2012, Combined apatite fission track and U-Pb dating by LAICPMS and its application in apatite provenance analysis. Short, *in* Can., S.M.A., ed., Quantitative Mineralogy and Microanalysis of Sediments and Sedimentary Rocks, p. 219-248.

COLE, R.B., RIDGWAY, K.D., LAYER, P.W., and DRAKE, J., 1999, Kinematics of basin development during the transition from terrane accretion to strike-slip tectonics, Late Cretaceous-early Tertiary Cantwell Formation, south central Alaska: Tectonics, v. 18, p. 1224-1244.

CONRAD, J.E., MCKEE, E.H., and TURRIN, B.D., 1990, Age of tephra beds at the Ocean Point Dinosaur Locality, North Slope, Alaska, based on K–Ar and 40Ar/39Ar analysis, p. C1-C12.

CSEJTEY, B., MULLEN, M.W., COX, D.P., and STRICKER, G.D., 1992, Geology and geochronology of the Healy Quadrangle, south-central Alaska., U.S. Geological Survey Miscellaneous Investigations 1191, p. 1-63.

DAVIES-VOLLUM, K.S., and WING, S.L., 1998, Sedimentological, Taphonomic, and Climatic Aspects of Eocene Swamp Deposits (Willwood Formation, Bighorn Basin, Wyoming): Palaios, v. 13, p. 28.

DIEFENDORF, A.F., MUELLER, K.E., WING, S.L., KOCH, P.L., and FREEMAN, K.H., 2010, Global patterns in leaf 13C discrimination and implications for studies of past and future climate: Proceedings of the National Academy of Sciences of the United States of America, v. 107, p. 5738-43.

DONELICK, R.A., O'SULLIVAN, P.B., and KETCHAM, R.A., 2005, Apatite fission-track analysis, Mineral Soc America, p. 49-94.

DWORKIN, S.I., NORDT, L., and ATCHLEY, S., 2005, Determining terrestrial paleotemperatures using the oxygen isotopic composition of pedogenic carbonate: Earth and Planetary Science Letters, v. 237, p. 56-68.

FARQUHAR, G.D., EHLERINGER, J.R., and HUBICK, K.T., 1989, Carbon Isotope Discrimination and Photosynthesis: Annu. Rev. Plant Physiol. Plant Mol. Biol, v. 40, p. 503-537.

FERGUSON, R.J., and BRIERLEY, G.J., 1999, Levee morphology and sedimentology along the lower Tuross River, south-eastern Australia: Sedimentology, v. 46, p. 627-648.

FIELDING, C.R., 1986, Fluvial channel, overbanks deposits from Westphalian of the Durham coalified, NE England: Sedimentology, v. 33, p. 119-140.

FIORILLO, A.R., and ADAMS, T.L., 2012, A Therizinosaur Track From the Lower Cantwell Formation (Upper Cretaceous) of Denali National Park, Alaska: Palaios, v. 27, p. 395-400.

FIORILLO, A.R., HASIOTIS, S.T., KOBAYASHI, Y., and TOMSICH, C.S., 2009, A pterosaur manus track from Denali National Park, Alaska Range, Alaska, United States: Palaios, v. 24, p. 466-472.

FLAIG, P.P., 2010, Depositional environments of the Late Cretaceous (Maastrichtian) dinosaur-bearing Prince Creek Formation: Colville River region, North Slope, Alaska., p. 311.

FLAIG, P.P., RD, B., MCCARTHY, P.J., and FIORILLO, A.R., 2011, A tidally-influenced, high-latitude alluvial/coastal plain: the Late Cretaceous (Maastrichtian) Prince Creek Formation, North Slope, Alaska: SEPM Special Publication, v. 97, p. 233-264.

FRANK, T.D., THOMAS, D.J., LECKIE, R.M., ARTHUR, M.A., BOWN, P.R., JONES, K., and LEES, J.A., 2005, The Maastrichtian record from Shatsky Rise (northwest Pacific): A tropical perspective on global ecological and oceanographic changes: Paleoceanography, v. 20, p. 14.

FRYIRS, K.A., and BRIERLEY, G.J., 2013, Geomorphic Analysis of River Systems: An Approach to Reading the Landscape, Wiley.

GHOSH, P., BHATTACHARYA, S.K., and GHOSH, P., 2005, Atmospheric CO_2 During the Late Paleozoic and Mesozoic : Estimates from Indian Soils: Ecological Studies, v. 177, p. 8-34.

GHOSH, P., GHOSH, P., and BHATTACHARYA, S.K., 2001, CO2 levels in the Late Palaeozoic and Mesozoic atmosphere from soil carbonate and organic matter, Satpura basin, Central India: Palaeogeography, Palaeoclimatology, Palaeoecology, v. 170, p. 219-236.

GRADSTEIN, F., OGG, J., and SMITH, A., 2004, The Cretaceous Period, *in* Felix M. Gradstein, J.G.O., and Alan G. Smith, ed., A geologic time scale 2004: New York, USA, Cambridge University Press,, p. 344-383.

GRÖCKE, D., PRICE, G., ROBINSON, S., BARABOSHKIN, E., MUTTERLOSE, J., and RUFFELL, A., 2005, The Upper Valanginian (Early Cretaceous) positive carbon–isotope event recorded in terrestrial plants: Earth and Planetary Science Letters, v. 240, p. 495-509.

GRÖCKE, D.R., 1998, Carbon-isotope analyses of fossil plants as a chemostratigraphic and palaeoenvironmental tool: Lethaia, v. 31, p. 1-13.

GRÖCKE, D.R., 2002, The carbon isotope composition of ancient CO2 based on higher-plant organic matter.: Philosophical transactions. Series A, Mathematical, physical, and engineering sciences, v. 360, p. 633-58.

GRÖCKE, D.R., HESSELBO, S.P., and JENKYNS, H.C., 1999, Carbon-isotope composition of Lower Cretaceous fossil wood : Ocean-atmosphere chemistry and relation to sea-level change: Geology, v. 27, p. 155-158.

GRÖCKE, D.R., LUDVIGSON, G.A., WITZKE, B.L., ROBINSON, S.A., JOECKEL, R.M., UFNAR, D.F., and RAVN, R.L., 2006, Recognizing the Albian-Cenomanian (OAE1d) sequence boundary using plant carbon isotopes: Dakota Formation, Western Interior Basin, USA: Geology, v. 34, p. 193.

HASEGAWA, T., PRATT, L.M., MAEDA, H., SHIGETA, Y., OKAMOTO, T., KASE, T., and UEMURA, K., 2003, Upper Cretaceous stable carbon isotope stratigraphy of terrestrial organic matter from Sakhalin, Russian Far East: a proxy for the isotopic composition of paleoatmospheric CO2: Palaeogeography, Palaeoclimatology, Palaeoecology, v. 189, p. 97-115.

HATCHER, P.G., FAULON, J.L., WENZEL, K.A., and CODY, G.D., 1992, A structural model for lignin-derived vitrinite from high-volatile bituminous coal (coalified wood): Energy & Fuels, v. 6, p. 813-820.

HILLHOUSE, J., and COE, R., 1994, Paleomagnetic data pom Alaska: The Geological Society of America, v. G-1, p. 797-812.

HORNUNG, J., and AIGNER, T., 1999, Reservoir and aquifer characterization of fluvial architectural elements : Stubensandstein , Upper Triassic , southwest Germany: Sedimentary Geology, v. 129, p. 215-280.

HUDSON, P.F., 2005, Natural Levees, *in* Trimble, S., ed., Encyclopedia of Water Science: New York, USA, Taylor & Francis, p. 1-4.

JAHREN, A.H., ARENS, N.C., HARBESON, S.A., and ARENS, N.C., 2008, Prediction of atmospheric d13 CO2 using fossil plant tussues: American Geophysical Union, p. 1-12.

JEROLMACK, D.J., and MOHRIG, D., 2007, Conditions for branching in depositional rivers: Geology, v. 35, p. 463.

JUNG, C., VOIGT, S., and FRIEDRICH, O., 2012, High-resolution carbon-isotope stratigraphy across the Campanian–Maastrichtian boundary at Shatsky Rise (tropical Pacific): Cretaceous Research, v. 37, p. 177-185.

KELLER, G., 2001, The end-cretaceous mass extinction in the marine realm: year 2000 assessment: Planetary and Space Science, v. 49, p. 817-830.

KIRSCHBAUM, M.A., and MCCABE, P.J., 1992, Controls on the accumulation of coal and on the development of anastomosed fluvial systems in the Cretaceous Dakota Formation of southern Utah: Sedimentology, v. 39, p. 581-598.

KOHN, M.J., 2010, Carbon isotope compositions of terrestrial C_3 plants as indicators of (paleo)ecology and (paleo)climate.: Proceedings of the National Academy of Sciences of the United States of America, v. 107, p. 19691-5.

KRAUS, M.J., and ASLAN, A., 1993, Eocene Hydromorphic Paleosols: significance for interpreting ancient floodplain processes: Journal of Sedimentary Petrology, v. 63, p. 453-463.

LAWVER, L.A., GRANTZ, A., and GAHAGAN, L.M., 2002, Plate kinematic evolution of the present Arctic region since the Ordovician". In: Tectonic evolution of the Bering Shelf-Chukchi Sea-Arctic margin and adjacent landmasses: Geol. Soc. Am. Special Paper, v. 360, p. 333-358.

LEHMAN, M.F., BERNASCONI, S.M., BARBIERI, A., and MCKENZIE, J.A., 2002, Preservation of organic matter and alteration of its carbon and nitrogen isotope composition during simulated and in situ early sedimentary diagenesis: Geochimica et Cosmochimica Acta, v. 66, p. 3573-3584.

LI, L., and KELLER, G., 1999, Variability in Late Cretaceous climate and deep waters: evidence from stable isotopes: Marine Geology, v. 161, p. 171-190.

LUDWIG, K.R., 2003, User's Manual for Isoplot 3.00: A Geochronological Toolkit for Microsoft Excel, Kenneth R. Ludwig.

MAKASKE, B., 2001, Anastomosing rivers: a review of their classification, origin and sedimentary products: Earth-Science Reviews, v. 53, p. 149-196.

MEYERS, P.A., 1994, Preservation of elemental and isotopic source identification of sedimentary organic matter, Chemical Geology, p. 289-302.

MEYERS, P.A., 1997, Organic geochemical proxies of paleoceanographic, paleolimnologic, and paleoclimatic processes: Organic Geochemistry, v. 27, p. 213-250.

MEYERS, P.A., and LALLIER-VERGÈS, E., 1999, Lacustrine sedimentary organic matter records of Late Quaternary paleoclimates: Journal of Paleolimnology, v. 21, p. 345-372.

MIALL, A.D., 1996, The geology of fluvial deposits: sedimentary facies, basin analysis, and petroleum geology, Springer.

MJOS, R., WALDERHAUG, O., and PRESTHOLM, E., 1993, Crevasse splay sandstone geometries in the Middle Jurassic Ravenscar Group of Yorkshire, UK: Spec. Publs Int. Ass. Sediment, v. 17, p. 167-184.

MJOS, R., WALDERHAUG, O., and PRESTHOLM, E., 2009, Crevasse splay sandstone geometries in the Middle Jurassic Ravenscar Group of Yorkshire, UK: Alluvial Sedimentation, International Association of Sedimentologists, Special Publication, v. 17, p. 167-184.

MULL, C.G., HOUSEKNECHT, D.W., and BIRD, K.J., 2003, Revised Cretaceous and Tertiary stratigraphic nomenclature in the Colville Basin, Northern Alaska: U. S. Geological Survey Professional Paper. 2003.

NADON, G.C., 1994, The Genesis and Recognition of Anastomosed Fluvial Deposits: Data from the St. Mary River Formation, Southwestern Alberta, Canada: SEPM Journal of Sedimentary Research, v. Vol. 64B, p. 451-463.

NANSON, G.C., and CROKE, J.C., 1992, A genetic classification of floodplains: Geomorphology, v. 4, p. 459-486.

NYAMBE, L.A., 1999, Sedimentology of the Gwembe Coal Formation (Permian), Lower Karoo Group, mid-Zambezi Valley, southern Zambia.: Spec. Publs int. Ass. Sediment., v. 28, p. 409-434.

NORDT, L., ATCHLEY, S., and DWORKIN, S., 2003, Terrestrial evidence for two greenhouse events in the latest Cretaceous: GSA TODAY.

POOLE, I., VAN BERGEN, P.F., KOOL, J., SCHOUTEN, S., and CANTRILL, D.J., 2004, Molecular isotopic heterogeneity of fossil organic matter: implications for δ13Cbiomass and δ13Cpalaeoatmosphere proxies: Organic Geochemistry, v. 35, p. 1261-1274.

POOLE, I., and VAN BERGEN, P.F., 2006, Physiognomic and chemical characters in wood as palaeoclimate proxies: Plant Ecology.

RIDGWAY, K.D., TROP, J.M., NOKLEBERG, W.J., DAVIDSON, C.M., and EASTHAM, K.R., 2002, Mesozoic and Cenozoic tectonics of the eastern and central Alaska Range: Progressive basin development and deformation in a suture zone: Geological Society of America Bulletin, v. 114, p. 1480-1504.

RIDGWAY, K.D., TROP, J.M., and SWEET, A.R., 1997, Thrust-top basin formation along a suture zone, Cantwell basin, Alaska Range: Implications for development of the Denali fault system: Geological Society of America Bulletin, v. 109, p. 505-523.

SHERWOOD, K.W., and CRADDOCK, C., 1979, General Geology of the Central Alaska Range Between the Nenana River and Mount Deborah, State of Alaska, Department of Natural Resources, Division of Geological and Geophysical Surveys.

SPICER, R.A., PARRISH, J.T., and GRANT, P.R., 1992, Evolution of vegetation and coal-forming environments in the Late Cretaceous of the North Slope of Alaska: Geological Society of America Special Papers., v. 267, p. 177-192.

STANLEY, R.G., 1987, Thermal maturity and petroleum-source potential of the Cantwell Formation (Paleocene), Alaska Range, p. 104-107.

THIBAULT, N., HUSSON, D., HARLOU, R., GARDIN, S., GALBRUN, B., HURET, E., and MINOLETTI, F., 2012a, Astronomical calibration of upper Campanian–Maastrichtian carbon isotope events and calcareous plankton biostratigraphy in the Indian Ocean (ODP Hole 762C): Implication for the age of the Campanian–Maastrichtian boundary: Palaeogeography, Palaeoclimatology, Palaeoecology, v. 337-338, p. 52-71.

THIBAULT, N., HARLOU, R., SCHOVSBO, N., SCHIØLER, P., MINOLETTI, F., GALBRUN, B., LAURIDSEN, B.W., SHELDON, E., STEMMERIK, L., and SURLYK, F., 2012b, Upper Campanian–Maastrichtian nannofossil biostratigraphy and high-resolution carbon-isotope stratigraphy of the Danish Basin: Towards a standard δ13C curve for the Boreal Realm: Cretaceous Research, v. 33, p. 72-90.

TOMSICH, C.S., MCCARTHY, P.J., FOWELL, S.J., and SUNDERLIN, D., 2010, Paleofloristic and paleoenvironmental information from a Late Cretaceous (Maastrichtian) flora of the lower Cantwell Formation near Sable Mountain, Denali National Park, Alaska: Palaeogeography, Palaeoclimatology, Palaeoecology, v. 295, p. 389-408.

TROP, J.M., and RIDGWAY, K.D., 2007, Mesozoic and Cenozoic tectonic growth of southern Alaska: A sedimentary basin perspective: Geological Society of America Special Papers, v. 431, p. 55-94.

TYSON, R.V., 1984, Palynofacies investigation of Callovian (Middle Jurassic) sediments from DSDP Site 534, Blake-Bahama Basin, Western Central Atlantic: Marine and Petroleum Geology, v. 1, p. 3-13.

VAN BERGEN, P.F., and POOLE, I., 2002, Stable carbon isotopes of wood: a clue to palaeoclimate?: Palaeogeography, Palaeoclimatology, Palaeoecology, v. 182, p. 31-45.

VIS, G.-J., BOHNCKE, S.J.P., SCHNEIDER, H., KASSE, C., COENRAADS-NEDERVEEN, S., ZUURBIER, K., and ROZEMA, J., 2010, Holocene flooding history of the Lower Tagus Valley (Portugal): Journal of Quaternary Science, v. 25, p. 1222-1238.

VOIGT, S., FRIEDRICH, O., NORRIS, R.D., and SCHÖNFELD, J., 2010, Campanian – Maastrichtian carbon isotope stratigraphy: shelf-ocean correlation between the European shelf sea and the tropical Pacific Ocean: Newsletters on Stratigraphy, v. 44, p. 57-72.

VOIGT, S., GALE, A.S., JUNG, C., and JENKYNS, H.C., 2012, Global correlation of Upper Campanian – Maastrichtian successions using carbon-isotope stratigraphy: development of a new Maastrichtian timescale: Newsletters on Stratigraphy, v. 45, p. 25-53.

WOLFE, J.A., AND WAHRHAFTIG, C., 1970, The Cantwell Formation of the central Alaska Range, *in* Cohee, G.V., Bates, R.G., and Wright, W.B., eds., U.S. Geological Survey Bulletin, p. 46.

ZIEGLER, A.M., SCOTESE, C.R., and BARRETT, S.F., 1983, Mesozoic and Cenozoic paleogeographic maps, *in* Brosche, P., Sundermann, J., ed., Tidal friction and the earth's rotation II: Berlin, Springer-Verlag, p. 240-252.

2.12 Appendices

Apendix 2.12.1. U/Pb Zircon data.

	Uranium and Thorium			**Isotopic Ratios**			**Age (Ma)**
Analysis Name	**[U] (ppm)**	**[Th] (ppm)**	**U/Th**	**207Pb/235Uc (±)**	**206Pb/238U (±)**	**207Pb/206Pb (±)**	**206Pb/238U (±)**
1267-01a1_1	166	89	1.85	0.0814	0.01074	0.05496	68.88 (4.8)
1267-01a1_2	330	82	4.04	0.0786	0.01028	0.05544	65.95 (2.6)
1267-01a1_3	198	123	1.61	0.08091	0.01082	0.05425	69.35 (4.1)
1267-01a1_4	75	31	2.41	0.17769	0.02352	0.0548	149.85 (8.8)
1267-01a1_5	128	110	1.16	0	0	0	53.61 (7.4)
1267-01a1_6	266	187	1.43	0.06942	0.00977	0.05153	62.68 (2.7)
1267-01a1_7	784	639	1.23	0.0728	0.01097	0.04814	70.33 (3.1)
1267-01a1_8	0	0	0	0	0	0	0.00 (0.0)
1267-01a1_9	154	139	1.11	0.07874	0.01126	0.0507	72.21 (4.3)
1267-01a1_10	0	0	0	0	0	0	0.00 (0.0)
1267-01a1_11	128	72	1.79	0.08143	0.01128	0.05236	72.31 (3.5)
1267-01a1_12	206	171	1.2	0.08059	0.01089	0.05365	69.85 (2.3)
1267-01a1_13	285	211	1.35	0.07154	0.01035	0.05011	66.40 (2.9)
1267-01a1_14	797	931	0.86	0.07075	0.00972	0.05279	62.36 (2.0)

Apendix 2.12.1. U/Pb Zircon data (continued).

	Uranium and Thorium			Isotopic Ratios			Age (Ma)
Analysis Name	**[U] (ppm)**	**[Th] (ppm)**	**U/Th**	**207Pb/235Uc (±)**	**206Pb/238U (±)**	**207Pb/206Pb (±)**	**206Pb/238U (±)**
1267-01a1_15	293	116	2.52	0.07217	0.01042	0.05023	66.83 (2.8)
1267-01a1_16	155	72	2.16	0.16347	0.0112	0.10581	71.83 (21.1)
1267-01a1_17	271	231	1.17	0.07419	0.01039	0.05178	66.65 (4.2)
1267-01a1_18	1603	1148	1.4	0.07036	0.01045	0.04885	66.99 (2.4)
1267-01a1_19	103	41	2.48	0.07864	0.01131	0.05044	72.49 (4.2)
1267-01a1_20	3476	3476	1	0.0741	0.01087	0.04946	69.67 (2.2)
1267-01a1_21	262	117	2.24	0.07285	0.01024	0.05161	65.66 (2.7)
1267-01a1_22	582	606	0.96	0.06934	0.01055	0.04765	67.67 (2.7)
1267-01a1_23	162	88	1.85	0.07515	0.01095	0.04978	70.19 (3.6)
1267-01a1_24	239	160	1.49	0.07383	0.01102	0.04858	70.67 (3.1)
1267-01a1_25	2659	6399	0.42	0.07566	0.01112	0.04934	71.30 (2.5)
1267-01a1_26	274	204	1.34	0.07376	0.0103	0.05194	66.05 (3.5)
1267-01a1_27	213	87	2.45	0.08595	0.01102	0.05658	70.64 (5.9)
1267-01a1_28	107	45	2.36	0.08752	0.01175	0.05402	75.31 (4.3)
1267-01a1_29	488	409	1.19	0.07486	0.01105	0.04915	70.82 (2.4)
1267-01a1_30	197	91	2.16	0.0748	0.01094	0.04958	70.15 (4.2)
1267-01a1_31	0	0	0	0	0	0	0.00 (0.0)
1267-01a1_32	266	188	1.41	0.07355	0.01092	0.04885	70.01 (3.3)
1267-01a1_33	381	384	0.99	0.07667	0.01084	0.05129	69.51 (3.2)
1267-01a1_34	261	135	1.93	0.07884	0.01103	0.05185	70.70 (3.7)
1267-01a1_35	357	264	1.35	0.07804	0.0115	0.0492	73.74 (2.6)
1267-01a1_36	146	80	1.81	0.07401	0.01091	0.04921	69.93 (4.0)
1267-01a1_37	244	90	2.71	0.09831	0.01201	0.05936	76.96 (8.7)
1267-01a1_38	120	83	1.45	0.08555	0.01118	0.05549	71.68 (4.0)
1267-01a1_39	171	108	1.59	0.07778	0.01025	0.05505	65.73 (4.1)
1267-01a1_58	0	0	0	0	0	0	0.00 (0.0)
1267-01a1_59	245	172	1.43	0.07318	0.01011	0.0525	64.84 (4.8)
1267-01a1_60	484	253	1.91	0.08285	0.01105	0.05436	70.87 (4.7)
1267-01a1_61	0	0	0	0	0	0	0.00 (0.0)
1267-01a1_63	167	107	1.56	0.07021	0.01092	0.04662	70.03 (3.6)
1267-01a1_64	144	54	2.67	0.10844	0.0119	0.0661	76.26 (7.0)
1267-01a1_65	354	262	1.35	0.07898	0.01135	0.05045	72.78 (2.9)

Apendix 2.12.2. Carbon and Nitrogen stable isotopes data.

Sample Name	Sample Wt.	N Signal (V)	C Signal (V)	Conc N (%)	Conc C (%)	δ^{15}N At-air (‰)	δ^{13}C PDB (‰)	Depth (m)	C/N
S-2-1	7.22	0.32	1.06	0.09	1.2	1.12	-25.88	0.4	13.62
S-2-2	7.83	0.55	1.07	0.14	1.11	1.33	-26.21	1.3	7.94
S-2-3	7.71	0.26	0.48	0.07	0.51	0.74	-26.56	2.7	7.7
S-2-4	6.29	0.34	0.72	0.11	0.93	0.76	-26.18	4.75	8.59
S-2-5	7.58	0.37	1.07	0.1	1.15	0.84	-25.88	5.3	12.01
S-2-6	7.05	0.58	1.1	0.16	1.26	1.07	-25.93	6.35	7.7
S-2-7	6.38	0.28	0.63	0.09	0.8	0.81	-25.82	6.85	9.39
S-2-8	6.97	0.55	1.15	0.16	1.34	1.43	-26.03	7.7	8.51
S-2-9	7.28	0.24	0.54	0.07	0.61	-0.28	-25.9	8	9.31
S-2-10	6.27	0.73	2.26	0.23	2.92	0.85	-25.82	9.8	12.65
S-2-11	6.95	0.16	0.56	0.05	0.66	0.33	-27.1	11.2	14.55
S-2-12	7.43	0.35	0.75	0.09	0.82	0.46	-26.35	11.65	8.75
S-2-13	7.08	0.46	0.9	0.13	1.03	1.08	-26.13	12.3	7.92
S-2-14	6.93	0.29	0.72	0.08	0.84	0.44	-26.12	13.25	10.15
S-2-15	7.75	0.62	2.04	0.16	2.13	1.26	-26.14	14.75	13.51
S-2-16	6.51	0.27	0.69	0.08	0.86	-0.05	-26.08	15.25	10.73
S-2-17	7.6	0.64	1.54	0.17	1.64	1.12	-26.25	16.5	9.91
S-2-18	6.75	0.29	0.56	0.08	0.67	0.12	-26.37	17.4	7.98
S-2-19	6.76	0.33	0.86	0.1	1.03	0.6	-26.09	18.4	10.7
S-2-20	7.69	0.22	0.64	0.06	0.67	0.04	-26.72	19.05	11.76
S-2-21	6.52	0.46	1.61	0.14	2	1.35	-26.13	19.5	14.3
S-2-22	7.55	0.24	0.53	0.06	0.57	0.22	-26.25	20.05	9.13
S-2-23	6.43	0.42	1.06	0.13	1.34	1.45	-26.39	21.15	10.27
S-2-24	6.35	0.25	0.67	0.08	0.85	0.08	-26.95	21.45	11.12
S-2-25	6.63	0.52	1.09	0.15	1.34	0.93	-25.98	22.65	8.68
S-2-26	7.9	0.21	0.4	0.05	0.41	-0.07	-25.89	23.4	7.81
S-2-27	6.19	0.35	0.88	0.11	1.15	0.49	-26.42	25.9	10.21
S-2-28	6.44	0.19	0.34	0.06	0.43	-0.64	-26.14	26.7	7.39
S-2-29	7.7	0.2	0.54	0.05	0.57	0.37	-26.43	27.9	11.11
S-2-30	7.02	0.31	0.87	0.09	1	0.34	-26.72	28.55	11.36
S-2-31	7.93	0.2	0.33	0.05	0.34	0.02	-26.23	29.2	6.79
S-2-32	6.64	0.43	0.76	0.13	0.93	1.16	-26.34	29.95	7.3
S-2-33	6.44	0.18	0.35	0.06	0.44	-0.46	-26.12	30.9	7.95
S-2-34A	7.18	0.23	0.38	0.06	0.43	0.93	-26.16	33.6	6.75
S-2-35	6.28	0.21	0.77	0.07	1	0.07	-26.72	34.05	15.1
S-2-38	6.94	0.56	1.57	0.16	1.83	0.84	-26.37	35.2	11.44
S-2-39	6.38	0.49	1.2	0.15	1.53	1.03	-26.38	35.85	10.06
S-2-40	7.31	0.2	0.52	0.05	0.58	-0.1	-26.75	37.65	10.71
S-2-41	7.26	0.55	1.95	0.15	2.18	1.5	-25.94	37.7	14.66

Apendix 2.12.2. Carbon and Nitrogen stable isotopes data (continued).

Sample Name	Sample Wt.	N Signal (V)	C Signal (V)	Conc N (%)	Conc C (%)	δ^{15}N At-air (‰)	δ^{13}C PDB (‰)	Depth (m)	C/N
S-2-42	7.06	0.23	0.49	0.06	0.56	0.6	-26.08	39	8.83
S-2-43	7.73	1.1	4.61	0.28	4.83	-1.86	-26.01	39.1	17.24
S-2-44	6.79	1.32	5.85	0.38	6.99	-0.68	-25.8	40.35	18.18
S-2-46	7.27	2.49	14.38	0.68	16.04	0.8	-23.61	41.35	23.66
S-2-47	7.31	0.34	1.1	0.09	1.22	-0.33	-25.43	43.95	13.37
S-2-48	6.95	0.9	4.7	0.26	5.48	2.83	-26.08	44.1	21.31
S-2-49	6.5	0.17	0.48	0.05	0.59	-1.26	-26.9	47.4	11.82
S-2-50	7.52	0.29	0.94	0.08	1.02	0.62	-26.24	51.6	13.5
S-2-51	6.79	0.17	0.43	0.05	0.52	-1.75	-26.61	52.45	10.59
S-2-53	7.99	0.25	0.56	0.06	0.57	-1.12	-26.46	53.95	9.02
S-2-54A	7.33	1.48	6.91	0.4	7.65	1.73	-24.72	54.3	19.12
S-2-55	6.94	0.34	0.53	0.1	0.62	-0.51	-26.34	55.2	6.48
S-2-56	6.93	1.94	9.09	0.55	10.64	1.52	-24.58	55.35	19.19
S-2-57	6.65	0.77	1.95	0.23	2.38	1.26	-25.97	56.3	10.47
S-2-58	6.78	0.29	0.6	0.08	0.72	-0.11	-26.12	57.9	8.49
S-2-59	7.29	3.56	14.06	0.97	15.65	1.69	-25.23	58.4	16.2
S-2-60	6.91	0.57	3.15	0.16	3.7	-0.55	-25.66	59.3	22.55
S-2-61	6.02	0.48	0.84	0.16	1.13	0.69	-26.17	59.85	7.14
S-2-62	6.57	3.97	15.38	1.2	18.99	1.06	-22.95	61.05	15.88
S-2-63	7.52	1.34	10.8	0.35	11.65	2.64	-22.95	61.8	33.15
S-2-64	7.63	0.65	2.38	0.17	2.53	-0.56	-24.93	62.45	14.93
S-2-65	7.17	0.23	0.73	0.06	0.82	-0.38	-26.98	63.75	12.7
S-2-66	7.48	0.5	1.23	0.13	1.33	0.37	-26.29	64.1	10
S-2-67	6.59	0.24	0.5	0.07	0.62	-0.45	-25.98	64.65	8.45
S-2-68	7.56	0.78	2.1	0.21	2.25	1	-26.08	66	10.96
S-2-69	6.6	0.28	0.53	0.08	0.65	0.16	-26.56	67.5	7.87
S-2-69B	7.12	1.3	6.93	0.36	7.9	1.04	-24.32	67.5	21.82
S-2-70	6.64	0.49	1.01	0.14	1.24	0.7	-25.8	70.35	8.53
S-2-71C	7.14	0.23	0.42	0.06	0.48	0.01	-25.78	72.55	7.63
S-2-72	7.95	1.11	4.87	0.28	4.98	1.17	-25.38	73.15	17.96
S-2-74	7.04	0.5	1.11	0.14	1.28	0.88	-25.71	79.7	9.18
S-2-75	7.41	0.19	0.27	0.05	0.3	-0.38	-25.88	81.8	5.98
S-2-76	7.99	4.03	16.49	1	16.74	2.21	-24.9	82.7	16.76
S-2-77	7.8	0.57	2.91	0.14	3.03	-1.42	-25.47	84.15	21.06
S-2-78	7.19	0.66	1.36	0.18	1.54	1.04	-25.45	85.35	8.5
S-2-79B	6.06	0.27	0.58	0.09	0.77	-0.24	-26.63	88.65	8.89
S-2-79C	7.4	1.1	3.47	0.29	3.81	1.42	-25.12	88.65	12.95
S-2-80	7.38	2.07	9.38	0.56	10.31	1.39	-25.04	93.15	18.53
S-2-81	6.8	0.61	1.03	0.18	1.23	0.82	-26.5	94.85	6.91
S-2-82	7.69	0.76	1.77	0.2	1.87	1.14	-26.35	95.6	9.51
S-2-83	7.16	0.31	0.66	0.08	0.75	0.43	-26.72	97.7	8.78
S-2-84	7.8	0.64	1.14	0.16	1.18	1.11	-26.06	99.7	7.3
S-2-85	7.01	0.29	0.71	0.08	0.82	0.21	-27.06	100.6	10.21
S-2-86	7.26	0.21	0.36	0.06	0.4	-0.73	-26.31	103.5	6.91

Apendix 2.12.2. Carbon and Nitrogen stable isotopes data (continued).

Sample Name	Sample Wt.	N Signal (V)	C Signal (V)	Conc N (%)	Conc C (%)	δ^{15}N At-air (‰)	δ^{13}C PDB (‰)	Depth (m)	C/N
S-2-87	7.76	0.87	2.48	0.22	2.6	1.48	-25.96	106	11.67
S-2-88	6.27	0.28	0.55	0.09	0.71	-0.28	-25.89	107.9	8.03
S-2-89	6.49	0.25	0.45	0.07	0.57	0.11	-25.73	109	7.58
S-2-90	7.09	0.6	1.13	0.17	1.29	0.82	-26.12	111.9	7.75
S-2-94	6.93	0.72	1.45	0.21	1.7	1.12	-26.17	120.5	8.28
S-2-95	6.51	0.2	0.27	0.06	0.34	-0.11	-26.2	122.5	5.52
					2.44	0.51	-25.99	0.73	11.35
S-2-12W	0.21	0.05	0.88	1.19	53.54	-0.12	-23.72	11.65	almost too low nitrogen levels
S-2-21W	0.46	0.17	2.48	1.84	68.67	0.76	-25.7	19.5	37.35
S-2-42 Q+W	0.23	0.03	0.55	0.28	7.81		-27.44	39	Too low Nitrogen levels
S-2-46 W	0.74	0.64	14.75	1.84	63.67	1.54	-25.39	41.35	34.57
S-2-48 W	0.06	0.06	1.6	2.21	88.57	1.43	-26.64	44.1	40.11
S-2-50 W+S	0.02	0.03	0.1	3.84	20.33		-27.08	51.6	Too low Nitrogen levels
S-2-51 Q+W	0.01	0.03	0.08	9.15	37.15		-27.85	52.45	Too low Nitrogen levels
S-2-53W	0.68	0.11	2.24	0.75	41.64	0.29	-24.21	53.95	55.29
S-2-54B W	0.02	0.04	0.44	4.48	71.28		-26.78	54.3	Too low Nitrogen levels
S-2-56 W	0.4	0.43	9.38	2.28	75.46	1.48	-24.58	55.35	33.03
S-2-57 W	0.54	0.57	12.23	2.27	73.27	0.62	-25.92	56.3	32.22
S-2-58 W	0.41	0.23	4.76	1.18	37.36	0.92	-24.7	57.9	31.53
S-2-59 W	0.13	0.17	3.37	2.65	81.38	0.65	-26.01	58.4	30.73
S-2-60 W	0.19	0.11	2.47	1.24	42.25	1.13	-25.9	59.3	34.14
S-2-61 W	0.04	0.04	0.85	1.94	63.17		-25.61	59.85	Too low Nitrogen levels
S-2-62W	1.33	0.35	4.72	1.27	45.2	1.26	-23.89	61.05	35.72
S-2-62W	1.33	0.35	4.72	1.27	45.2	1.26	-23.89	61.05	35.72
S-2-63 W	0.04	0.03	1.12	1.44	83.7		-24.81	61.8	Too low Nitrogen levels
S-2-64 W	0.08	0.05	1.43	1.23	58.82		-24.02	62.45	Too low Nitrogen levels
S-2-67 W	0.06	0.04	0.97	1.32	53.92		-25.54	64.65	Too low Nitrogen levels
S-2-67 wood	7.08	0.38	1.18	0.11	1.35	-1.54	-25.83	64.65	12.59

Apendix 2.12.2. Carbon and Nitrogen stable isotopes data (continued).

Sample Name	Sample Wt.	N Signal (V)	C Signal (V)	Conc N (%)	Conc C (%)	δ^{15}N At-air (‰)	δ^{13}C PDB (‰)	Depth (m)	C/N
S-2-71B Wood	6.24	4.73	18.78	1.5	24.42	0.68	-24.11	72.55	16.27
S-2-79C Wood	3.14	1.66	6.96	1.27	26.15	1.82	-24.7	88.65	20.58
S-2-82 Wood	7.22	4.12	18.43	1.13	20.72	2.2	-22.42	95.6	18.32
S-2-82A Wood	3.15	1.66	10.29	1.26	38.47	0.9	-23.49	95.6	30.49
S-2-84W	0.21	0.07	1.09	1.56	67.53	1.88	-26.51	99.7	almost too low nitrogen levels
S-2-89W	0.21	0.06	1.12	1.44	68.2	1.89	-24.74	109	almost too low nitrogen levels

Chapter 3. Multi-proxy Paleoclimatic Interpretation of the Paleo-arctic Prince Creek Formation, North Slope, Alaska[1]

3. 1 Abstract

Stable isotope and geochemical analyses of palynomorphs and clay minerals from the middle Maastrichtian Prince Creek Formation, on Alaska's North Slope, allow reconstruction of paleoprecipitation and estimation of meteoric water in the greenhouse arctic. A mean annual precipitation value of 1254 ±181 mm/yr, based on geochemical analyses, falls within the 745.56 – 1426.88 ± 221.38 mm/yr range derived from stable carbon isotope analysis of palynological separates. $\delta^{18}O$ values of smectite from bentonite beds cluster around ~ +5‰. The $\delta^{18}O$ value of meteoric water calculated from bentonitic smectite is ~ -24‰, assuming a mean annual temperature of 6.3°C. This indicates $\delta^{18}O$ -depleted precipitation, as expected for high latitudes during the Late Cretaceous. A ~69.2 Ma warm interval, known as the Mid-Maastrichtian Event (MME), has recently been identified in the lower Cantwell Formation, Denali National Park, Alaska, that is coeval with the Prince Creek Formation exposed along the Colville River on Alaska's North Slope.. The age, precipitation, temperature and meteoric water composition of the Prince Creek Formation, derived from analyses of bentonitic smectite, strongly supports the hypothesis that increased latent heat transport during the MME intensified the hydrological cycle and resulted in depleted $\delta^{18}O$ values of precipitation in the paleo-arctic.

3.2 Introduction

The Prince Creek Formation, North Slope, Alaska contains valuable information regarding Late Cretaceous paleoclimate in the paleo-arctic region (Fig.3.9.1). The

[1] SUSANA SALAZAR JARAMILLO, PAUL J. MCCARTHY, FRED LONSTAFFE, SARAH J. FOWELL. 2014. "Multi-proxy Paleoclimatic Interpretation of the Paleo-arctic Prince Creek Formation, North Slope, Alaska". Palaeogeography, Palaeoclimatology, Palaeoecology.

abundance of well preserved palynomorphs (Phillips, 2003; Frederiksen, 2002), leaves (Spicer and Herman, 2010) and paleosols (Flaig et al., 2011; Flaig et al., 2013) in the Prince Creek Formation provides the opportunity to employ multiple proxies to reconstruct temperature and precipitation of the Late Cretaceous (Maastrichtian) arctic and compare resulting estimates to previous reconstructions based on oxygen stable isotopes (Suarez et al., 2013), palynology (Frederiksen, 2002), paleosols (Flaig et al., 2013) and CLAMP analysis (Spicer and Herman, 2010).

Existing quantitative temperature and precipitation data are based entirely on paleobotanical data, including morphology of fossil leaves (Smiley, 1966; Spicer and Parrish, 1990a) and growth rings in fossil wood (Spicer and Parrish, 1990b; Spicer et al., 1992; Parrish and Spicer, 1988; Spicer and Herman, 2010). Reconstructions of Late Cretaceous paleoclimates indicate mean annual temperature (MAT) values between 2° and 8 °C (Parrish and Spicer, 1988; Spicer and Parrish, 1990a; Fiorillo et al., 2010b) and mean annual precipitation estimates between 500 and 1500 mm/yr (Spicer and Parrish 1990a) for North Slope ecosystems. Herman and Spicer (1996) provide evidence for a warm Arctic Ocean that remained above 0 °C even during the winter months. Spicer and Herman, (2010) used CLAMP (Climate Leaf Analysis Multivariate Program)-derived latitudinal temperature gradients for Arctic Ocean coastal environments at 70 Ma and 82°N to arrive at a mean annual temperature value of 6.3 ± 2.2°C, a warm month mean temperature of 14.5 ± 3.1°C and a cold month mean temperature no colder than -2.0 ± 3.9°C. Their CLAMP-derived estimates also indicate high humidity and precipitation values consistent with the existence of relatively warm air temperatures despite prolonged periods (up to 5 months) of winter darkness.

Estimates of meteoric water $\delta^{18}O$ based on two different proxies, paleosol siderite and phosphate from dinosaur tooth enamel, indicate extremely δO^{18}-depleted precipitation at high latitudes during the Late Cretaceous (Suarez et al., 2013). These results are consistent with an intensified hydrological cycle (e.g. higher precipitation flux) and

enhanced latent heat transport in the greenhouse arctic. (Ufnar et al., 2002; Ufnar et al., 2004a, b; Suarez et al., 2013).

$\delta^{18}O$ and $\delta^{13}C$ are quantitative tools that can be used as a paleohydrologic proxy. $\delta^{18}O$ values of clays have been used to determine the isotopic composition of meteoric water (e.g. Vitali et al., 2002), seawater (e.g. Cadrin et al., 1995) and temperatures of the water involved in clay genesis (e.g. Delgado and Reyes, 1996). $\delta^{13}C$ values of terrestrial organic matter have been used to calculate mean annual precipitation (MAP) (Kohn, 2010; Diefendorf et al., 2010). Estimation of MAP from carbon isotope composition of plant tissues is based on Farquhar et al.'s (1989) conceptual model that describes the isotopic fractionation (Δ) of C_3 plants during carbon assimilation. Changes in $\delta^{13}C$ values of terrestrial plant remains can be used to asses plant responses to environmental changes (Loader and Hemming, 2000) if it can be demonstrated that the isotopic composition of the preserved plant organs reflects the isotopic composition of whole plant tissue (e.g. Arens et al., 2000; Jahren, 2004; Descolas-Gros and Schölzel, 2007). However, shifts in $\delta^{13}C$ can also occur due to changes in the proportions of the plant organs (e.g. leaf, seed, wood) and the chemical composition of that organ (e.g. cellulose, lignin, lipids) (Gröcke, 2002). Separation and examination of the organic matter allows identification of the dominant plant organ (e.g. spores and pollen grains) and the chemical composition (e.g. sporopollenin), thus avoiding variations caused by different types of organic matter. If the products of photosynthesis used to form pollen grains reflect variations in the atmospheric CO_2 and meteoric water utilized by the plant, then the stable isotope ratios of pollen grains will record these changes (Loader and Hemming, 2000). Pollen is a suitable plant tissue for $\delta^{13}C$ analysis. It is more abundant than other plant tissues and can be separated from the sediment (Arens et al., 2000; Jahren, 2004). The chemical structure of sporopollenin (the structural constituent of the outer walls or exines, of pollen and spores from vascular plants) remains relatively stable over a wide range of temperatures (Fraser et al., 2014) and it has been shown to be relatively stable during diagenesis (van Bergen et al., 1993). Additionally, pollen extraction from rocks using the most common treatment (HF + HCL) seems to not affect $\delta^{13}C$ values and the carbon isotope values, of

pollen and leaf tissue of the same species are similar (isotope difference of ±3‰) (Jahren, 2004).

Independent estimates of temperature and precipitation can be derived from major element weathering indices (e.g. Chemical index of alteration, CIA-K; clayeness, Al/Si) (Sheldon and Tabor, 2009) and compared to estimates based on stable isotopes. Major element analyses of clay minerals from one paleosol profile (NKT) and two bentonite beds are compared to stable isotope analyses of clay minerals and palynomorphs to further constrain Late Cretaceous MAT and MAP of arctic ecosystems. The main goals of this paper are to document new and indepent proxies of temperature and precipitation for the Late Cretaceous (Maastrichtian) Prince Creek Formation in order to better understand conditions in the greenhouse arctic.

3.3 Geologic Setting

3.3.1.Stratigraphy

The Prince Creek Formation is a Late Cretaceous (Maastrichtian) alluvial-deltaic coastal plain succession that was deposited in the Colville Basin, an east-west-trending, asymmetrical foreland basin north of the Brooks Range mountain belt (Fig. 3.9.1). Deposition of the foreland basin-fill began during the middle Jurassic and continued through the Tertiary period (Bird and Molenaar, 1992). The Prince Creek Formation interfingers with, and is overlain by, marine and marginal-marine sediments of the Schrader Bluff Formation (Fig. 3.9.2; Mull et al., 2003; Phillips, 2003).

The entire Prince Creek Formation is Campanian to Paleocene in age, (Conrad et al.,1990; Moore et al., 1994; Bice et al., 1996). However, recent biostratigraphic and geochronologic analyses from exposures along the Colville River (Fig. 3.9.1) indicate an early Maastrichtian age for all of the samples included in our data set (Fiorillo et al., 2010a, b; Flaig, 2010; Flaig et al., 2011, 2013). The Prince Creek Formation was buried to depths of ~ 600 to 2000 m (Burns et al. 2005) and vitrinite reflectance values suggest

a maximum burial temperature of no more than ~ 48° C. (Barker and Pawlewicz., 1986; Robinson 1989; Johnson and Howell 1996).

3.3.2. Depositional Environments

The Prince Creek Formation consists of interbedded, very fine- to fine-grained sandstone, conglomerate, organic-rich siltstone, and coal, with thin bentonite and tuff layers and abundant remains of both vertebrates and plants (Mull et al., 2003). Detailed descriptions of facies and alluvial architecture of the Prince Creek Formation are presented elsewhere (Fiorillo et al., 2010a, b; Flaig et al., 2011), but a brief summary is provided here. The Prince Creek Formation is interpreted as a large, tidally influenced alluvial/deltaic depositional system consisting of meandering trunk channels, meandering and anastomosing distributary channels and mud-rich floodplain deposits with abundant paleosols (Phillips, 2003; Fiorillo et al., 2010a, b; Flaig et al., 2011, 2013). The depositional system grades northward into deltaic distributary channels and marginal marine interdistributary bays and tidal flats (Phillips, 2003; Fiorillo et al., 2010a ; Flaig et al., 2011).

3.3.2.1. Fluvial Channels.

The Prince Creek Fm. contains three distinct channel-forms. Medium- to fine-grained multi-story sandbodies that lack root traces and are capped with inclined heterolithic stratification (IHS) are interpreted as large meandering trunk channels. The presence of IHS, composed of rhythmically repeating sand and mud couplets, suggests a tidal influence (Flaig et al., 2011).

Single-story, fine-grained sandbodies, encased in floodplain fines, dominated by IHS and rooted throughout, are interpreted as small, meandering distributary channels (Flaig et al., 2011). Other small, very-fine to fine-grained, single-story, current-rippled and ubiquitously rooted sandbodies that are present in tiers at a single stratigraphic level are interpreted as laterally stable ribbon sandbodies (Flaig et al., 2011).

3.3.2.2. Floodplains and Biota.

Alluvial plains in the Prince Creek Formation are dominated by fine-grained sediment reflecting a variety of floodplain sub-environments. Small sheet-like sandstones and siltstones are interpreted as crevasse splays and levees (Flaig et al., 2011). Thin packages of interbedded, ripple cross-laminated, rarely rooted or burrowed siltstone and mudstone are interpreted as small floodplain lakes and ponds (Flaig et al., 2011). Organic-rich mudstone, carbonaceous shale, and coal (typically < 0.5 m thick) record organic deposition in swamps or on poorly drained floodplains. Thin (< 1 m thick) layers of tuff or bentonite are locally present.

Abundant and diverse biotic remains have been recovered from Prince Creek paleosols. Palynomorphs include: (1) *in-situ* and reworked peridinioid dinocysts and acritarchs; (2) brackish and freshwater algae such as *Botryococcus braunii, Pedisatrum, Sigmapollis psilatus,* and *Pterospermella*; (3) projectate pollen including *Aquilapollenites quadrilobus*, *Aquilapollenites aucellatus*, *Aquilapollenites scabridus*, and *Azonia cribrata*; (4) oculate pollen grains of *Wodehouseia edmontonicola*; (5) pollen from lowland trees, shrubs, and herbs dominated by *Cranwellia*, *Reticulatasporites*, *Perinopollenites*, and *Taxodiaceaepollenites*; (6) Bisaccate pollen; (7) fern and moss spores dominated by *Deltoidospora*, *Laevigatosporites*, *Lycopodiumsporites*, *Osmundacidites*, and *Psilatriletes*; and (8) fungal hyphae (Flaig, 2010).

3.3.2.2.1. North Kikak-Tegoseak Paleosol (NKT)

The NKT paleosol forms the upper part of a 4.5 m-thick cumulative paleosol succession (Fig. 1.9.3; Flaig et al., 2013). This paleosol consist of 80 cm of light olive-grey (5Y 5/2) blocky mudstone containing abundant carbonaceous root traces, overlain by 70 cm of dark yellowish-brown (10YR 4/2) blocky mudstone with few, very fine carbonaceous root traces. This is overlain by 80 cm of very dark grey (5Y 3/1) blocky mudstone with siderite nodules up to 2 cm in diameter and rare, very fine root traces. The upper surface

is truncated and the paleosol is capped by 20 cm of carbonaceous shale with abundant plant fragments. This paleosol is similar to an *Aquic Inceptisol* (Soil Survey Staff, 1999).

Palynomorph assemblages in the NKT paleosol are dominated by bisaccate (conifer) pollen, *Laevigatosporites* (ferns), and *in situ* and reworked peridinioid dinocysts, and the sedimentology indicates soil formation in a point bar setting (Flaig et al., 2011).

3.4 Methods

3.4.1. Palynological Separation for $\delta^{13}C$ Analysis

A palynomorph-rich organic residue was separated from the sediment via a modified version of the palynological processing methods summarized by Traverse (2007). Rock and sediment samples were mechanically disaggregated. Carbonate and silicate minerals were dissolved by immersion in HCl and HF, respectively (Traverse, 2007). No oxidation was necessary. Samples were rinsed and washed through a 250 μm sieve. Sodium polytungstate was used as a heavy liquid instead of zinc chloride (Traverse, 2007) in order to separate the organic fraction from remaining minerals. The resulting organic separates consisted mainly of amorphous organic matter (~50%), pollen and spores (~40%), and acritarchs (~10%). Isotopic analysis was conducted on this organic fraction.

3.4.2. $\delta^{13}C$ Stable Isotopes

Seven bulk sediment samples were collected from the NKT paleosol profile (Fig. 3.9.3). Bulk samples were treated with 10% HCl for 24 hours to eliminate carbonates. All samples were analyzed at the Alaska Stable Isotope Facility Lab, University of Alaska Fairbanks. $\delta^{15}N$ and $\delta^{13}C$ values were measured using Elemental Analyser-IRMS (Isotope-ratio mass spectrometry). Stable isotope values were obtained using a Costech Elemental Analyzer (ESC 4010) and a Thermo Conflo III interface with a DeltaV Mass Spectrometer. All samples where weighed and placed in tin capsules. These tin capsules

were closed and combusted in an EA autosampler. The N_2 and CO_2 combustion gases were separated chromatographically and then transferred to the IRMS, where the isotopes were measured. Values are reported in reference to international isotope standards $\delta^{15}N_{air}$ and $\delta^{13}C_{PDB}$. The 29 and 44 m/z peaks are used to quantify the N and C content of the samples, respectively.

3.4.3. MAP Estimates from $\delta^{13}C$ Stable Isotopes

Estimation of MAP from carbon isotope compositions of plant tissues is based on the Farquhar et al.'s (1989) conceptual model, which describes the isotopic fractionation (Δ_{leaf}) of C_3 plants during carbon assimilation (Eq. 1).

(1)

$$\Delta_{leaf} = \frac{\delta^{13}C_{atm} - \delta^{13}C_{leaf}}{1 + \delta^{13}C_{leaf}/1000}$$

For $\delta^{13}C$ of atmospheric CO_2 we assume a $\delta^{13}C$ value of -6.6‰, which has been reported for the Late Cretaceous (Ghosh et al., 2001; Ghosh et al., 2005). We substitute values from organic separates for $\delta^{13}C_{leaf}$, assuming that sporopollenin reflects the isotopic composition of whole plant tissue (e.g. Jahren, 2004; Descolas-Gros and Schölzel, 2007) or has a similar composition to that of leaves from the same plant (Mongrain, 2013). Estimates of MAP are based on the Diefendorf et al. (2010) and Kohn (2010) equations (equations 2 and 3, respectively). These equations are simple functions that allow MAP to be estimated from $\delta^{13}C$ of terrestrial organic matter.

Diefendorf et al. (2010) equation:

(2)

$$\Delta_{leaf} = 5.54(\pm 0.22) * \log_{10}(\mathrm{MAP}) + 4.07(\pm 0.70)$$

Kohn (2010) equation:

(3)

$$\Delta_{leaf} = 2.01 - 1.98\times10^{-4}\ \text{Altitude(m)} + 5.88\log_{10}\left(\text{MAP} + 300, \frac{\text{mm}}{\text{yr}}\right) - 0.0129\,\text{Abs(latitude,°)}$$

According to paleomagnetic reconstructions, this region lay between 83° and 85° N during the Late Cretaceous (Ziegler et al., 1983; Lawver et al., 2002). We used a value of 84±1°N. Since The Prince Creek Formation has been interpreted as a large alluvial/deltaic depositional system with meandering river channels grading northward into deltaic distributary channels and marginal marine interdistributary bays and tidal flats (Phillips, 2003; Flaig, 2010; Fiorillo et al., 2010b), we assumed an altitude near sea level. For the Kohn equation we used an error propagation formula.

3.4.4. MAP and MAT Estimates Using Geochemical Climofunctions:

Weathering indices are used to calculate paleotemperature and paleoprecipitation (e.g. Sheldon and Tabor, 2009) under the assumption that the degree of chemical weathering in soils increases with MAP and MAT (Kovács et al., 2013). Climofunctions based on weathering indices are independent proxies that can be used to test MAP and MAT values obtained from stable isotopes.

Abundances (in wt. %) of the light major oxides SiO_2, Al_2O_3, Fe_3O_3, Na_2O, MgO, P_2O_5, K_2O, CaO, MnO and TiO_2 were measured from bulk samples using a PANalytical Axios wavelength-dispersive X-ray fluorescence spectrometer (WD-XRF) at the University of Alaska Fairbanks Advanced Instrumentation Laboratory (AIL). Each analyte was calibrated against certified standard reference materials available from the United States Geological Survey and the United States National Institute of Standards and Technology. The accuracy of calibrations relative to reference materials is generally within 10%, whereas the precision (1σ) of replicate analyses (3x) of a representative sample is better than 0.01 wt.%. Samples were powdered using hardened steel vials from SPEX CertiPrep

Group and pressed into 35 mm diameter pellets using a polyvinyl alcohol binder. Major oxide concentrations were used for geochemical mass-balance calculations (Brimhall and Dietrich, 1987; Brimhall 1991a, b) after bulk density measurements were determined by the clod method (Blake and Hartge, 1986).

Our calculations are based on the CIA-K index (Maynard, 1992) (Eq. 4). The chemical index of alteration (CIA) uses the geochemistry of Al, Ca, K and Na; where each elemental concentration is converted to moles (Sheldon and Tabor, 2009). In other words, the CIA is a measurement of the weathering of feldspar minerals and their hydration to form clay minerals. As clay content increases Al should also increase, whereas Ca, K, and Na contents should decrease, leading to higher CIA values (Sheldon and Tabor, 2009). CIA-K has been used to estimate paleoclimatic conditions where pedogenic carbonate is absent (e.g. Hamer et al., 2007a, b).

(4)

$$\text{CIA-K} = 100 \times \frac{\text{Al}}{\text{Al} + \text{Ca} + \text{Na}}$$

Sheldon et al. (2002) found the following relationship between MAP (measured in Bw and Bt horizons) and the chemical index of alteration without K (CIA-K) in modern soils. This relationship has an R^2=0.73 and a standard error of ±181 mm:

(5)

$$\text{P} = 14.265 \times (\text{CIA-K}) - 37.632$$

The NKT paleosol is smectite-rich, and illitization of smectite is a significant pedogenic process which indicates an excess of K has been added to the paleosol (Salazar et al., 2014 in prep.). Consequently, we adopted the CIA-K (Maynard, 1992) in the climofunction (Eq. 5) to find MAP, since it removes K from the index.

Attempts to relate the molecular weathering ratio Na+K/Al (Eq. 6) to MAT (Eq. 6) indicate a less robust relationship (R^2=0.37) (Sheldon et al., 2002). This relationship is

best applied to paleosols formed in the temperature range of approximately 2°-20°C (Sheldon et al., 2002).

(6)

$$T\ (C°) = -18.516 \times (S) + 17.298$$

where S is the molecular ratio of potash and soda to alumina (Na+K/Al) and the standard error is ±4.4°C.

Alternatively, there is an Inceptisol-specific relationship between MAT and "clayeyness" (Al/Si) for the Bw or Bt horizon (Sheldon 2006; Sheldon and Tabor, 2009) (Eq. 7). This relationship has an R^2=0.96 and gives more robust results (Sheldon and Tabor, 2009). The results of paleotemperatures calculated with the Al/Si molecular ratio have shown to be consistent with independent estimates based on fossil floras and faunas (Hamer et al., 2007a., Sheldon and Tabor, 2009).

(7)

$$T\ (C°) = 46.94C\ + 3.99$$

where the standard error is ±0.6 °C (Sheldon, 2006).

3.4.5. $\delta^{18}O$ Stable Isotopes

Oxygen isotope measurements in nine clay samples were performed using a Prism II, dual-inlet, triple-collecting stable isotope ratio mass-spectrometer. The isotopic results are reported in the standard delta (δ) notation in parts per thousand (‰) relative to Vienna Standard Mean Ocean Water (VSMOW) (Coplen, 1994).

Seven clay samples are from the NKT paleosol profile (Fig. 3.9.3) and two samples are from bentonite layers (06KKT-20.5 and PFDV-17-5.7). Details of clay preparation are in chapter two. The XRD pattern in Fig. 3.9.4 shows the monomineralic character (pure montmorillonite) of the KKT bentonite sample.

Estimations of meteoric water from smectites developed *in situ* in bentonite layers were carried out using the relationship shown in equation (8).

(8)

$$\Delta_{smectite-H2O} = \delta^{18}O_{smectite} - \delta^{18}O_{H2O} \cong 1000 \ln \alpha_{smectite-H2O} = 2.6 \times \left(\frac{10^6}{T^2}\right) - 4.28$$

Where $1000 \ln \alpha_{smectite-H2O} = 2.6 \times \left(\frac{10^6}{T^2}\right) - 4.28$ is the fractionation factor between smectite and meteoric water (Savin and Lee, 1988). $\delta^{18}O_{smectite}$ represents the $\delta^{18}O$ V-SMOW that is measured in the soil sample. The temperatures (T) used for these calculations are taken from Spicer and Corfield (1992) and Spicer and Herman (2010).

3.5 Results

3.5.1. MAP Calculations

3.5.1.1. MAP Estimates from $\delta^{13}C$ Stable Isotopes

$\delta^{13}C$, TOC (%) and C/N ratio results for bulk organic matter ($\delta^{13}C_{bulk}$) and organic separates ($\delta^{13}C_{Pollen}$) are shown in table 3.10.1. For bulk samples, $\delta^{13}C_{bulk}$ values range between -25.03‰ and -27.45‰, C/N ratios range between 3 and 6, and C (%) ranges between 0.26% and 1.21%. For organic separates, $\delta^{13}C_{Pollen}$ values range between -25.24‰ and -28.12‰, C/N ratios range between 30 and 41 and TOC (%) ranges between 19.65% and 59.03%. The average and standard deviations of the bulk and organic separate populations are -25.77‰ (± 1‰) and -26.43‰ (± 1.19‰), respectively (Table 3.10.1).

The C/N ratios of the bulk samples fall in the range between lacustrine algae and C_3 plants, while the C/N ratios of the organic separates fall in the C_3 plants range (Fig. 3.10.5, Table 3.10.1).

Based on the Kohn (2010) equation, the average MAP value is 656.98± 221.38 mm/yr, the maximum value is 1426.88± 221.38 mm/yr and the minimum 275.12± 221.38 mm/yr. Based on the Diefendorf et al. (2010) equation, the average MAP is 525.91±0.92 mm/yr, the maximum value is 1135.38±0.92 mm/yr and the minimum value is 216.45±0.92 mm/yr (Table. 3.10.2).

Estimates of MAP based on the Kohn (2010) and Diefendorf et al. (2010) equations are compared in a plot of $\delta^{13}C$ vs. MAP (Fig. 3.9.6), which shows the inverse relationship between $\delta^{13}C$ (‰, V-PDB) and MAP values. The figure also shows that the Diefendorf et al. (2010) model predicts lower MAP values at more negative $\delta^{13}C$ (< -25.5‰) compared to the Kohn (2010) model (inset, Fig. 3.9.6).

The Kohn (2010) regression has an R^2 of 0.59, a significant improvement over the functional form used by Diefendorf et al., (2010) (R^2 of 0.34, including their altitude and latitude coefficients). Additionally, the Kohn (2010) equations (see equations 1 and 2 of Kohn´s paper) allow estimation of MAP from altitude, latitude and $\delta^{13}C$ or Δ_{leaf}, where altitude, latitude and $\delta^{13}C$ or Δ_{leaf} are variables. In contrast, Diefendorf et al. (2010) estimate MAP based on Δ_{leaf} with estimated or measured $\delta^{13}C_{atm}$, where altitude and latitude values are constantss that are given acording to the geographic zone and/or plant functional type.

3.5.1.2. MAP Estimates from CIA-K

MAP calculations from CIA-K (Sheldon et al., 2002) give an average value of 1254 ±181 mm/yr, a maximum value of 1278±181 mm/yr and a minimum value of 1208±181 mm/yr (Table. 3.10. 2).

3.5.2. MAT Calculations

The MAT values from palaeosols (Eq. 6) ranged from 12.59 to 13.3°C with an average of 12.7 (error ± 4.4°C). The MAT values based on Eq. 7 ranged from 15.7 to 17.0°C with an average of 14.5 (error ± 0.6°C) (Table 3.10.2).

3.5.3. $\delta^{18}O$ Composition of Smectite and Meteoric Water

$\delta^{18}O$ values of total clay from the NKT paleosol have an average -16.9‰, while smectite developed *in situ* from volcanic ash (bentonite) has an average $\delta^{18}O$ value of -24‰. Table 3.10.3 shows the estimated $\delta^{18}O$ of meteoric water derived from measured $\delta^{18}O$ values of smectite and equation (8). -2°C and 14.5°C are North Slope Late Cretaceous temperatures from Spicer and Corfield (1992) and Spicer and Herman (2010) used in meteoric water estimations (e.g. Ludvigson et al., 2013 and Suarez et al., 2013). Fig. 3.9.7. shows $\delta^{18}O_{H2O}$ (at -2°C, 6.3°C and 14.5°C) obtained from smectite (this study) compared to $\delta^{18}O_{H2O}$ (at -2°C, 6.3°C and 14.5°C) obtained from siderite (Suarez et al., 2013). Meteoric water data obtained from smectite in this study is 2‰ more negative compared to $\delta^{18}O$ meteoric water calculated from siderite (Suarez et al., 2013).

3.6 Discussion

3.6.1. MAP Estimates

Independent estimates of paleoprecipitation are obtained from $\delta^{13}C$ values of plant tissues (Diefendorf et al., 2010; Kohn, 2010) and from the chemical composition (CIA-K) of Bt or Bw horizons (e.g. Sheldon et al., 2002; Retallack, 2004) in the NKT paleosol.

3.6.1.1. MAP Using $\delta^{13}C$

Diefendorf et al. (2010) and Kohn (2010) describe the relationship between leaf carbon isotope fractionation (Δ_{leaf}) and mean annual precipitation (MAP) in ecosystems

dominated by C_3 plants (equations 2 and 3). We chose the data obtained with Kohn´s equation over the Diefendorf et al.´s equation (Table 3.10.2) for two reasons: 1) Kohn (2010) regression has a better R^2 compared to Diefendorf et al. (2010); and 2) altitude and latitude are variables that can be chosen in Kohn's (2010) equation while in Diefendorf et al. (2010) altitude and latitude are constants that are given acording to the geographic zone and/or plant functional type.

MAP estimates derived from $\delta^{13}C$ values using Kohn´s (2010) and Diefendorf et al.´s (2010) equations are increasingly different at low $\delta^{13}C$ values (Fig. 3.9.6; Table 3.10.2). Using Kohn´s equation, $\delta^{13}C$ values of ~ -27‰ yield MAP values of ~1000 mm/yr, while $\delta^{13}C$ values of ~ -25‰ yield MAP values of ~300 mm/yr (Table 3.10.2). The shift between -25‰ to -27‰ may reflect: 1) high abundance of carbohydrates and/or hemicellulose in the fossil material (Meyers, 1997; Gröcke, 2002); 2) an increase in the contribution of organic matter from algae (Maruoka et al., 2007); or 3) a change in environmental conditions such as ρCO_2, salinity, CO_2 recycling, and temperature (Gröcke, 2002).

3.6.1.1.1 Taphonomic and/or Diagenetic Controls on $\delta^{13}C$

The $\delta^{13}C$ values (-23 to -27‰) and the C/N ratios of the organic separates have C/N ratios >30 (Fig. 3.9.5) indicating that they consist primarily of C_3 plant remains (Gröcke, 1998). Algae typically have C/N ratios between 4 and 10 (Meyers, 1994; Meyers, 1997) and land plants have C/N ratios of 20 or greater (Meyers, 1994). In species of modern herbaceous C_3 plants (including Poaceae), the $\delta^{13}C$ mean value of pollen is -26.74‰ and the mean C/N ratios is 12 .11 (Descolas-Gros and Schölzel, 2007).

Study of kerogen from the Prince Creek Formation indicates that the organic matter consists of spores, pollen grains and cuticles (60-100%), wood (20-40%), and coal (1-20%). A few samples also contain amorphous organic matter (1-20%) (Lyle et al., 1980). According to Lyle et al. (1980), the summary of the visual kerogen data (type of organic matter) indicates that the spores, pollen grains and cuticles are indigenous, the wood is

half indigenous and half reworked, the coal is totally reworked and the amorphous organic matter is indigenous. This seems to suggest that despite the presence of little algal material in some samples (Flaig et al., 2013), the bulk of the organic mater is contributed by spores, pollen grains, and cuticles (Lyle et al., 1980; Flaig et al., 2013). These results indicate that the $\delta^{13}C$ values of organic separates from the Prince Creek Formation are good proxies for the $\delta^{13}C$ values of the leaf tissues of the terrestrial vegetation, because sporopollenin is the main chemical constituent of the organic separates. Recorded $\delta^{13}C$ shifts between -25‰ to -27‰ are unlikely to represent increased abundance of carbohydrates and/or hemicellulose, since these compounds are not resistant to the routine pollen-extraction procedures.

Thermal maturation can alter organic properties, including $\delta^{13}C$ values, during diagenesis (Hasegawa et al., 2003). As it is extremely unlikely that diagenesis affected only two horizons in the NKT paleosol, this can not explain the differences in $\delta^{13}C$ values. The Prince Creek Formation was buried to depths of ~ 600 to 2000 m (Burns et al., 2005) and vitrinite reflectance values suggest a maximum burial temperature of ~ 48° C (Barker and Pawlewicz., 1986; Robinson 1989; Johnson and Howell 1996). Burial temperatures were too low to have resulted in significant diagenetic changes.

Selective decomposition can also alter $\delta^{13}C$ values of total organic matter. This would have occurred during early diagenesis (Benner et al., 1987). However, the material used in this study is predominantly sporopollenin and thus resistant to further diagenesis (van Bergen et al., 1993).

3.6.1.1.2 $\delta^{13}C$ and Environmental Conditions

The most striking feature of the $\delta^{13}C$ values of the organic separates is their distinct grouping into $\delta^{13}C$ values of ~ -27‰ that yield MAP values ~1000 mm/yr and $\delta^{13}C$ values of ~ -25‰ that yield MAP values~300 mm/yr (Table 3.10.2). From section 3.6.1.1.1 we know that changes in the isotopic composition (shifts between -25‰ to -27‰) as the result of diagenetic and/or taphonomic controls are unlikely. This seems to

suggest that some environmental parameters may be controlling changes in the $\delta^{13}C$ values.

The average $\delta^{13}C$ value for Mesozoic C_3 plants is -27‰ (Gröcke, 2002) and the mean $\delta^{13}C$ value of pollen from modern species of herbaceous C_3 plants is -26.74‰ (Descolas-Gros and Schölzel, 2007). Therefore the shift from ~ -27‰ to -25‰ represents a positive excursion. Environmental parameters capable of producing a positive excursion are: increasing altitude, decreasing pCO_2, increasing salinity or decreasing water, increasing temperature, and increasing light (Gröcke, 1998).

It is unlikely that the shift in $\delta^{13}C$ values was due to increasing altitude. As the plant fragments are in situ (Lyle et al., 1980), they are derived from the same altitude, which we assume was near sea level.

Although changes in the isotopic composition and level of atmospheric CO_2 will cause excursions in the $\delta^{13}C$ values of plants (Gröcke, 1998), it is impossible to demonstrate a change in atmospheric CO_2 based on a few samples within a 2m-thick paleosol where there is no time control (Fig. 3.9.3).

Increasing temperature and increasing light could also result in a positive shift in $\delta^{13}C$ values, but their effect cannot fully explain the magnitude of the shift. The same is true for salt-stress (i.e. brackish or marine incursion). Even though one sample, NKT 40 (with a $\delta^{13}C$ value of -25.19‰), has acritarchs from a brackish environment (Flaig et al., 2013, p. 216-218), a $\delta^{13}C$ shift from ~ -27‰ to -25‰ cannot be fully explained by such an incursion.

Previous studies indicate that the Prince Creek Formation paleosols are part of an alluvial/deltaic depositional environment (Phillips, 2003; Fiorillo et al., 2010a, b; Flaig et al., 2011, 2013) and were subject to wetting and drying cycles (e.g. Fiorillo et al. 2009; Fiorillo et al. 2010b; Flaig, 2010; Flaig et al., 2011). Chapter 1 “Origin of Clay Minerals in Alluvial Paleosols, Prince Creek Formation, North Slope Alaska: Influence of Volcanic Ash on Pedogenesis in the Late Cretaceous Arctic” further supports this

hypothesis. Water stress and salt stress can cause positive $\delta^{13}C$ shifts (Bocherens et al., 1994; Gröcke, 2002). Hence, values of ~ -25‰ in samples NKT 36, NKT 38, NKT 40 and NKT 42 may be less negative due to water-stress (i.e. drought). Aridity could shift $\delta^{13}C$ values from "normal" (~ -27‰) to dry (~ -25‰).

In conclusion, we choose a $\delta^{13}C$ value of ~ -27‰ since it coincides with the average $\delta^{13}C$ value for Mesozoic C_3 plants (-27‰) (Gröcke, 2002) and the mean $\delta^{13}C$ value of pollen from modern species of herbaceous C_3 plants (-26.74‰) (Descolas-Gros and Schölzel, 2007). The $\delta^{13}C$ values of ~ -27‰ yield MAP values between 978.76 – 1426.88 ± 221.38 mm/yr (average 1144.39± 221.38 mm/yr) using the Kohn (2010) equation (Table 3.10.2).

3.6.1.2. MAP Using CIA-K

MAP estimates based on CIA-K are similar for all of the NKT horizons, with an average value of 1254 ±181 mm/yr (Table 3.10.2). It has to be pointed out that MAP estimates based on CIA-K are not usually applied to soils from swamps, bogs and other waterlogged ground (Sheldon et al., 2002). Despite the fact that the NKT paleosol is similar to an *Aquic Inceptisol* (waterlogged soil) (Flaig et al., 2011), MAP estimates based on CIA-K show robust results when applied to poorly drained paleosols. For example, Hamer et al. (2007a) calculated MAP and MAT values from Bt horizons in paleosols. Aqualf-like and poorly drained Entisols developed in altered channel and overbank deposits that interfinger with lacustrine facies (Hamer et al., 2007a).

We apply the precipitation climofunction (Eq. 5) to the NKT paleosol, which consists predominantly of Bw and Bt horizons (Fig. 3.9.3). This is important because the most robust climofuntion (Eq. 5) is based on the chemical composition of the subsurface (Bt or Bw) horizon (Sheldon et al., 2002). Fig. 3.9.8A. shows the relationship between MAP and CIA-K.

MAP estimates based on the climofunction using CIA-K (Eq. 5) yield an average value of 1254.87± 181 mm/yr that is similar to the 1144.39± 221.38 mm/yr average calculated from the Kohn (2010) equation. Whereas MAP estimated from $\delta^{13}C$ is a more direct

proxy than MAP estimated from a climofunction using the CIA-K index; comparison of the results provides independent confirmation of two MAP proxies.

3.6.1.3. MAT Using Major-Element Chemical Analyses

We obtained a MAT of 12±4.4°C using the empirical relationship (Sheldon et al., 2002; Sheldon and Tabor, 2009) shown in equation (6) and a MAT of 15.7±0.6°C using equation (7) (Sheldon, 2006; Sheldon and Tabor, 2009). Even though these values are supposedly estimates of MAT, they are closer to the 14.5°C CLAMP-derived maximum warm month mean temperature estimates of Spicer and Herman, (2010) for the Campanian–Maastrichtian North Slope of Alaska. Compared to average MAT estimates of 6.3 ± 2.2°C (Spicer and Herman, 2010), equations 6 and 7 overstimate the MAT. One possible reason for this discrepency is that temperatures based on the degree of chemical weathering in soils may not be a suitable approach for these paleosols. The [K + Na]/Al molecular ratio is an indirect measurement of salinity and the Al/Si ratio is a proxy for hydrolysis and clay-mineral formation as Al accumulates in clays relative to the siliceous parent material (Sheldon and Tabor, 2009; Gastaldo et al., 2014). During the process of pedogenic illitization, K is being added to the illite/smectite mixed-layered clay (See Chapter 1). Assuming that the degree of chemical weathering in soils increases with MAT (Kovács et al., 2013), the climofunction that relates MAT to the [K + Na]/Al ratio may be unsuitable for the NKT paleosol because new K has been added to the system.

Similarly, the measurement of the “clayness” is not a good proxy for paleosols for which parent material is alluvial clay (See Chapter 1). In that case, the degree of chemical weathering won’t be directly related to MAT. This could explain the poor relationship between “clayness” and MAT shown in Fig. 3.9.8B.

3.6.1.4. Oxygen-Isotopic Composition of Water Involved in Smectite Genesis

$\delta^{18}O$ isotopes obtained from smectites are presented in table 3.10.3. $\delta^{18}O$ values are measured in two types of samples, soil samples of detrital origin that are mainly smectitic, and monomineralic bentonites (pure montmorillonite) developed in situ

(Salazar et al., 2013 in prep.). The values calculated from detrital smectite average -16.9‰, for an estimated MAT of 6.3°C (table 3.10.3). The $\delta^{18}O$ values of meteoric water calculated from bentonitic smectite (06KKT-20.5 and PFDV-17-5.7) are -26.1‰, -24‰ and -22.11‰ for temperatures of -2°C, 6.3°C and 14.5°C, respectively (See table 3.10.3 for the whole temperature range between -2 to 14.5°C). We emphasize results for -2°C, 6.3°C and 14.5°C to make a direct comparison with Suarez et al., (2010) (Fig. 3.9.7).

When the smectite samples (06KKT-20.5 and PFDV-17-5.7) are compared with siderite from geographically equivalent outrops (PFDV-16-18.75 and PFDV-16-20.10 of Suarez et al., 2013) the water isotopic compositions differ by 2‰ (Table 3.10.3; Fig. 3.9.7). Hence values from samples developed in situ (bentonites) are preferred, because they corroborate water isotopic compositions from siderite and dinosaur-ingested water (Suarez et al., 2013) are derived from pure montmorillonite developed *in situ* (Salazar et al., in prep.) (Fig. 3.9.4), and were formed from volcanic ash under atmospheric conditions. Higher $\delta^{18}O$ values of meteoric water derived from NKT smectite are probably due to the fact they contain a mixture of detrital and pedogenic clay.

According to Suarez et al. (2013), the combination of siderite and dinosaurian data suggest that the Prince Creek Formation regional palaeohydrology consisted of meteoric water that averaged ~ -21‰ with an orographically influenced $\delta^{18}Ow$ snowmelt composition of ~ -28‰ and near-coastal precipitation of ~ -19‰. Suarez et al., (2013) suggest that the low $\delta^{18}O$ of meteoric water from the Prince Creek Formation was the result of increased rainout effects due to an intensified hydrological cycle that enhanced latent heat transport. They futher suggest that the increased latent heat transport may be due to a short-term global warming event (the Middle Maastrichtian Event).

The Middle Maastrichtian Event (MME) is characterized by rapid warming of deep and surface waters (2–3°C) at ~69 Ma (Keller, 2001; Bralower et al., 2002; Frank et al., 2005). This greenhouse episode has also been identified in terrestrial records (Nordt et al., 2003; Dworkin et al., 2005). In the Cantwell Formation, located at a paleolatitude of

~64ºN (Hillhouse and Coe, 1994), the MME is recorded as a pair of positive excursions in the $\delta^{13}C$ values of wood (Salazar et al., 2014 in prep). That the Prince Creek Formation and the Cantwell Formation are coeval is indicated by a 69.2 ± 0.5 Ma $^{40}Ar/^{39}Ar$ age from glass in Prince Creek Formation tuff (Flaig, 2010) and a 69.5± 0.7 Ma U-Pb age from zircons in Cantwell Formation bentonite (Salazar et al., 2014 in prep).

Meteoric water $\delta^{18}O$ values of ~ -24‰ (from 06KKT-20.5 and PFDV-17-5.7) are derived from smectite with a MAT of 6.3°C. We chose 6.3 °C because it is the same temperature used by Suarez et al. (2013) and allows a direct comparison of meteoric water found in siderite and dinosaur tooth enamel with the meteoric water found in smectite. These values corroborate Suarez et al.'s evidence of extremely $\delta^{18}O$ -depleted precipitation at high latitudes during the Late Cretaceous and supports the hypothesis that these values were caused by increased rainout effects from an intensified hydrological cycle during the MME.

3.7 Conclusions

Geochemical and stable isotope analyses in organic separates and clays provide independent proxies of MAT and MAP for the Late Cretaceous arctic. The temperature obtained from a climofunction based on the [K + Na]/Al ratio has limitations in soils where K has been added to the system. The temperature obtained from a climofunction based on the Al/Si ratio has limitations in paleosols with clay as parent material. Therefore we conclude that MAT estimates of 12 ± 4.4°C and15.7 ± 0.6°C substantially overestimate Maastrichtian MATs on Alaska's North Slope.

$\delta^{18}O$ values of ~ -24‰ for meteoric water are consistent with previous results (Suarez et al., 2013). The 69.2 ± 0.5 Ma $^{40}Ar/^{39}Ar$ age of the Prince Creek Formation (Flaig, 2010) correlates with a short-term global warming event, which is also recorded in the coeval Cantwell Formation of central Alaska (Salazar et al., 2013 in prep).

MAP estimates based on both $\delta^{13}C$ values and the CIA-K approach indicate that precipitation in the Prince Creek Formation was between 745.56 and 1426.88 ± 221.38

mm/yr. Elevated MAP estimates are interpreted as a consequence of the high pCO_2 during a global warming event (Sloan and Rea, 1995). The $\delta^{18}O$-depleted nature of meteoric water is consistent with higher tempertaures and precipitation compared to present values (Smith, 1993), supporting the hyphotesis that increased latent heat transport during the MME resulted in $\delta^{18}O$ depleted precipitation at high latitudes during the Late Cretaceous (Suarez et al., 2013).

3.8 Acknowledgments

Financial support for this research was provided by the University of Alaska Museum of the North and the Clay Minerals Society. The authors wish to thank Colciencias Colombia for economic support and Fred Longstaffe at University of Western Ontario, Canada for the oxygen isotopic analyses. The authors also wish to thank Andrés Ochoa for their assistance with data analyses and Peter Flaig for providing all the paleosol samples and Figures.

3.9 Figures

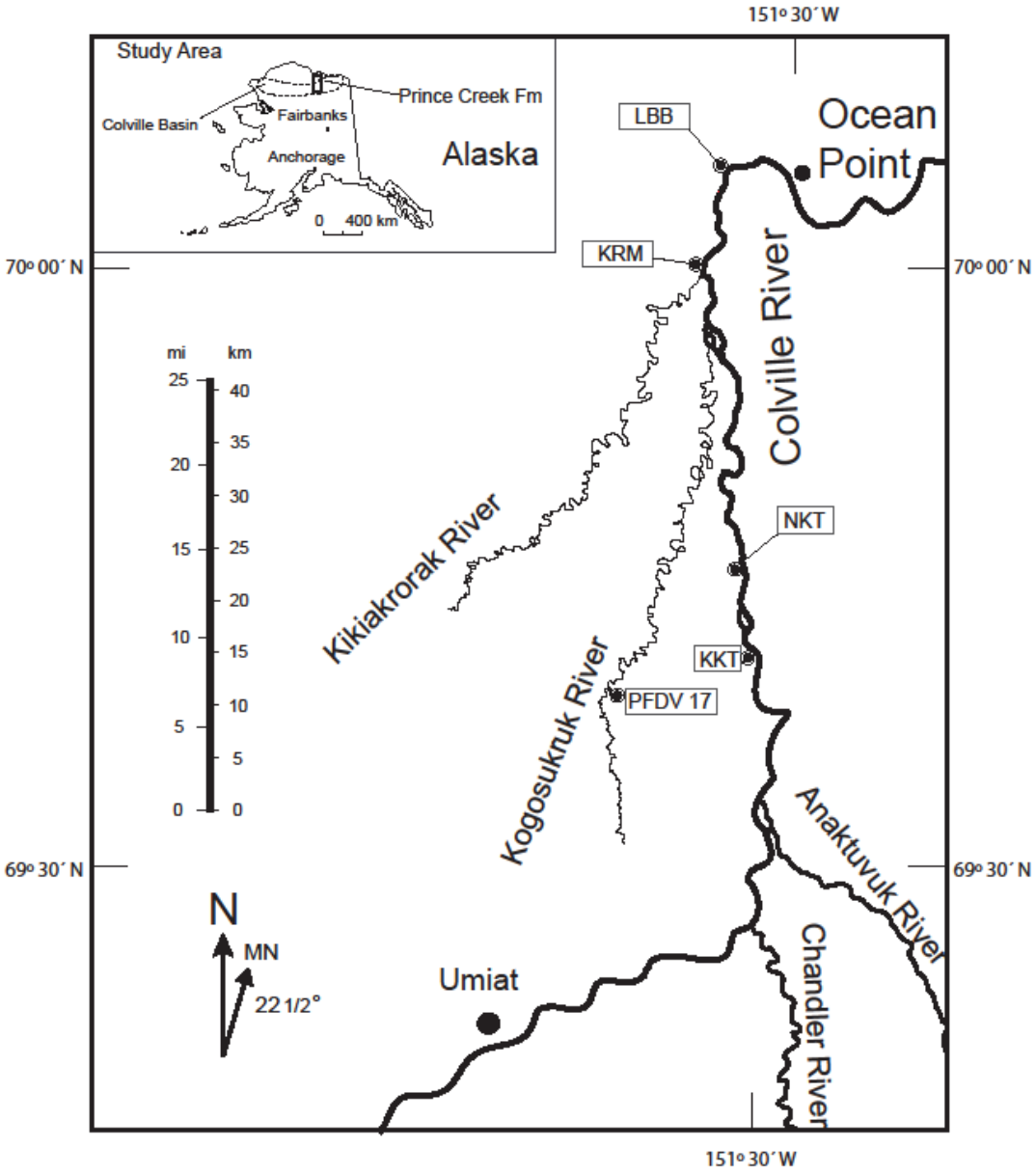

Fig. 3.9.1. Study area. Map with paleo-latitude data, illustrating the location of the stratigraphic sections and the paleosol profiles of the Prince Creek Formation at the Colville River, North Slope, Alaska. The labeled squares illustrate the name of the stratigraphic sections and the paleosol profiles North Kikak-Tegoseak Paleosol (NKT), Kikiakrorak River Mouth Paleosol (KRM), Liscomb Bonebed Paleosol (LBB) and two bentonite layers (KKT and PFDV-17). The small figure of Alaska at the top right shows the location of the Colville River and Coville Basin.

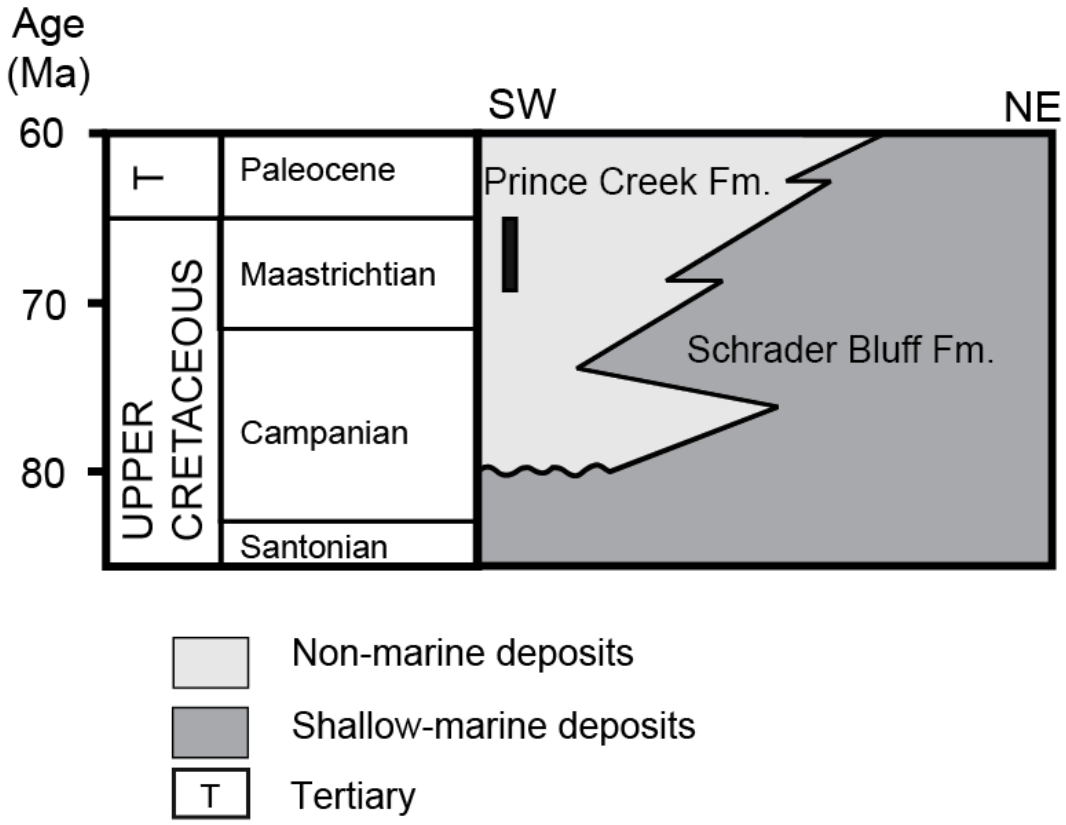

Fig. 3.9.2. Simplified sketch showing the age of the Prince Creek Formation and the stratigraphic relationship with the marine and marginal-marine sediments of the Schrader Bluff Formation. The black line is showing the Late Cretaceous interval of the Prince Creek Formation.

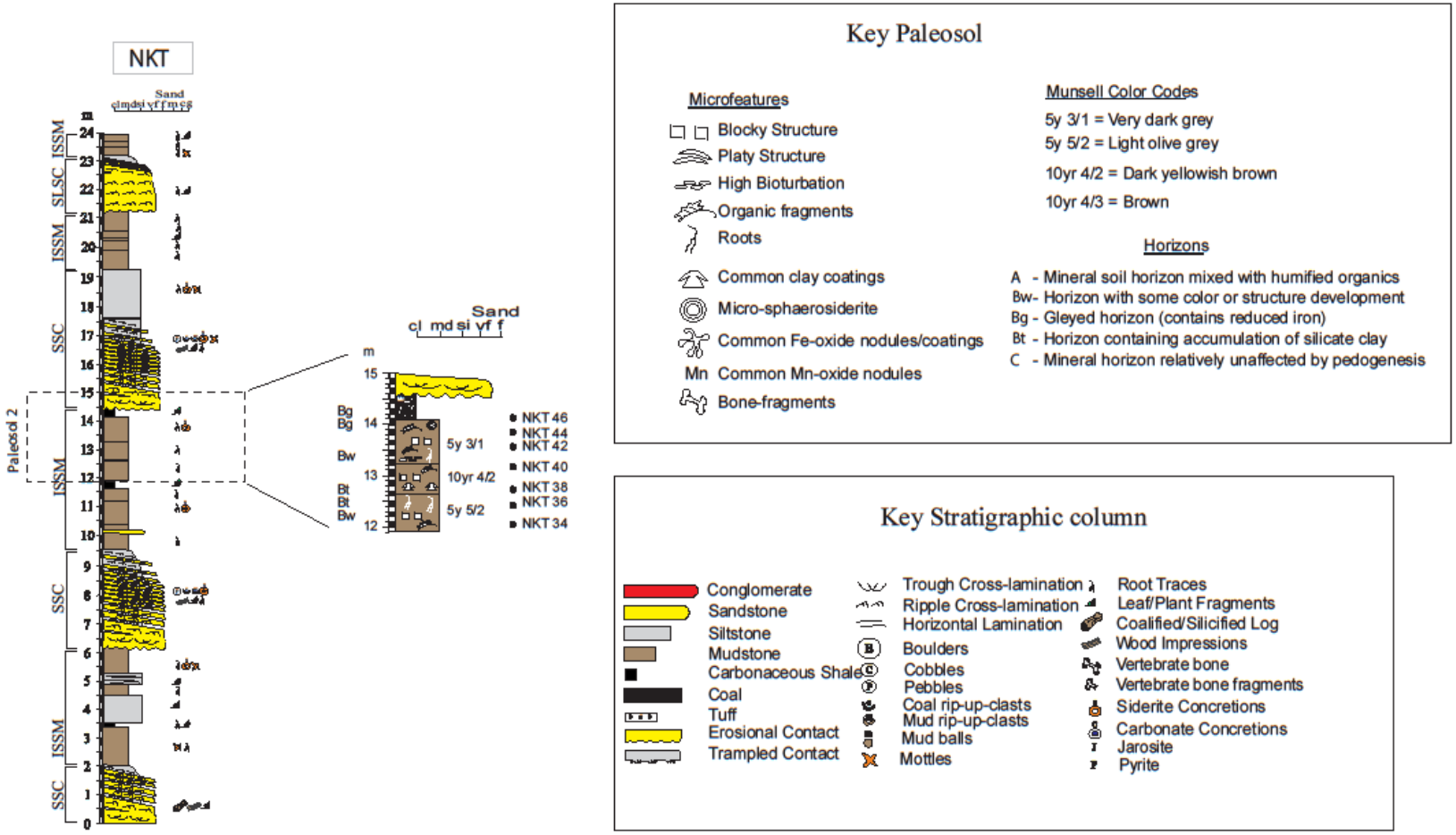

Fig. 3.9.3. NKT stratigraphic section and detailed NKT paleosol profile.

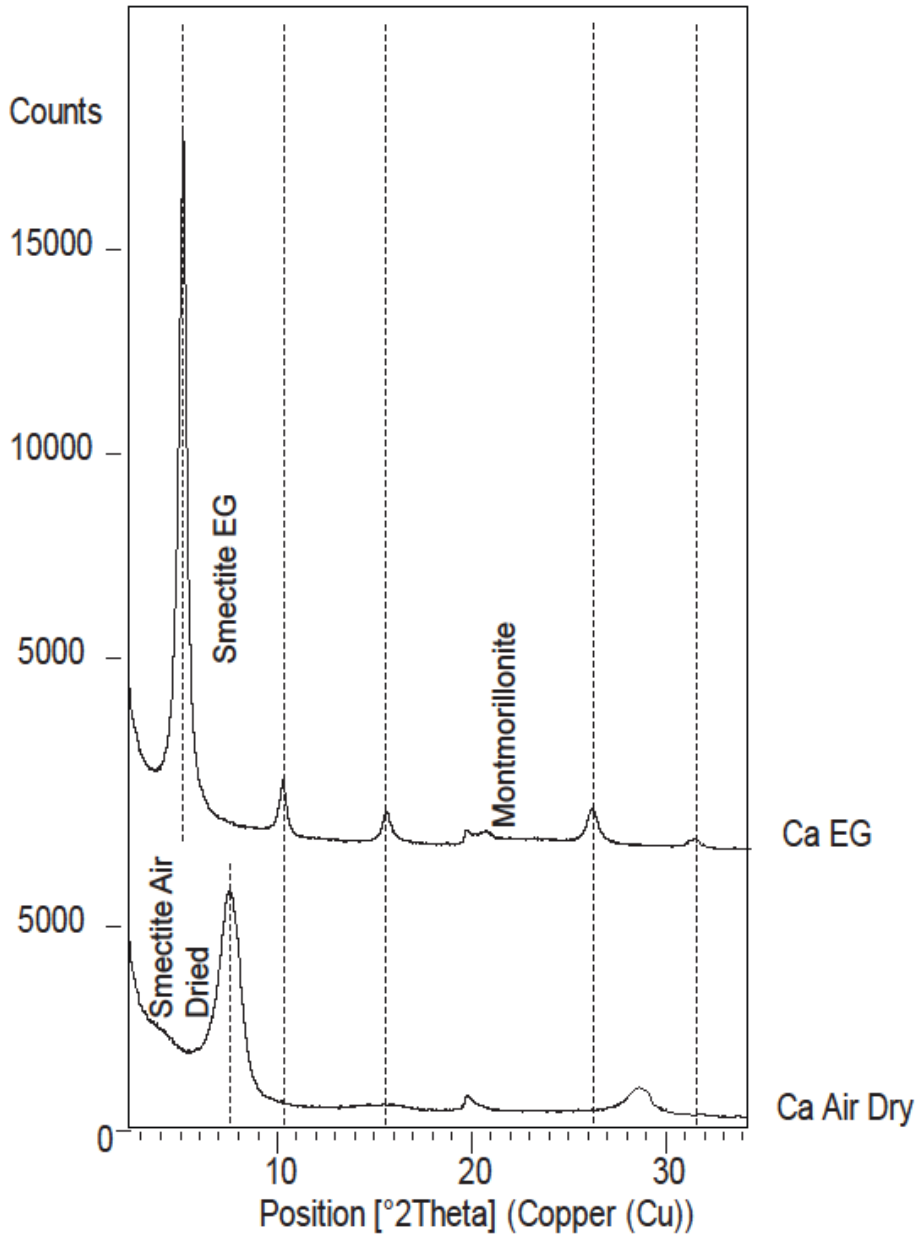

Fig. 3.9.4. Representative XRD pattern of oriented mount of KKT bentonite sample in the clay fraction. The spectrum shows a rational series of the diagnostic reflections of smectite, specifically montmorillonite.

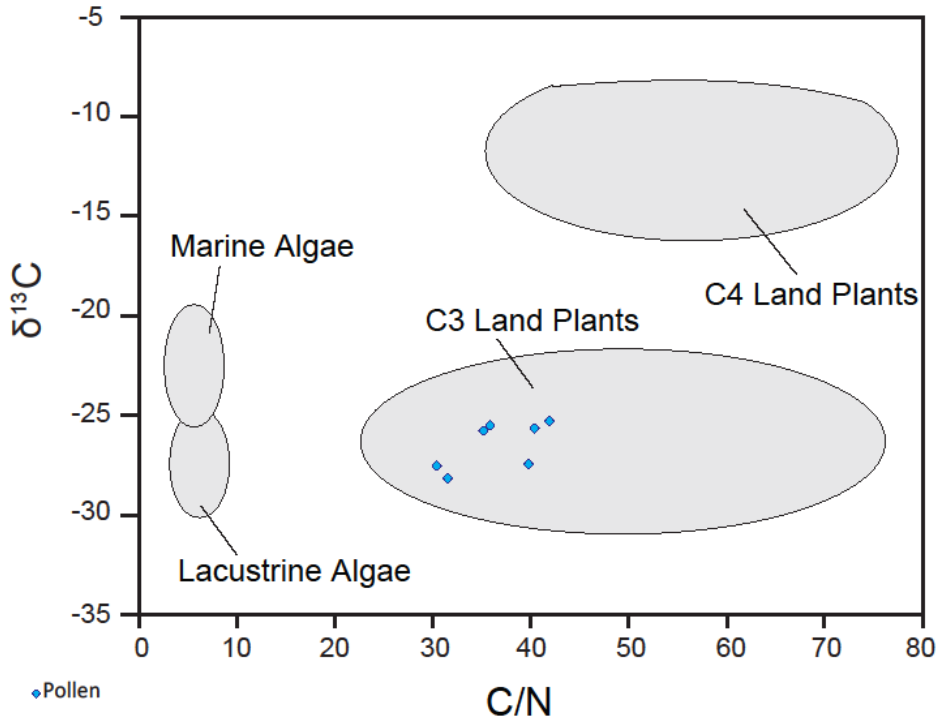

Fig. 3.9.5. C/N ratio and isotopic $\delta^{13}C$ value identifiers of organic matter produced by marine algae, lacustrine algae, C_3 land plants, and C_4 land plants (Meyers, 1997). The figure shows that the organic matter separated after pollen-extraction procedure (Traverse, 2007) is in the area of C_3 land plants.

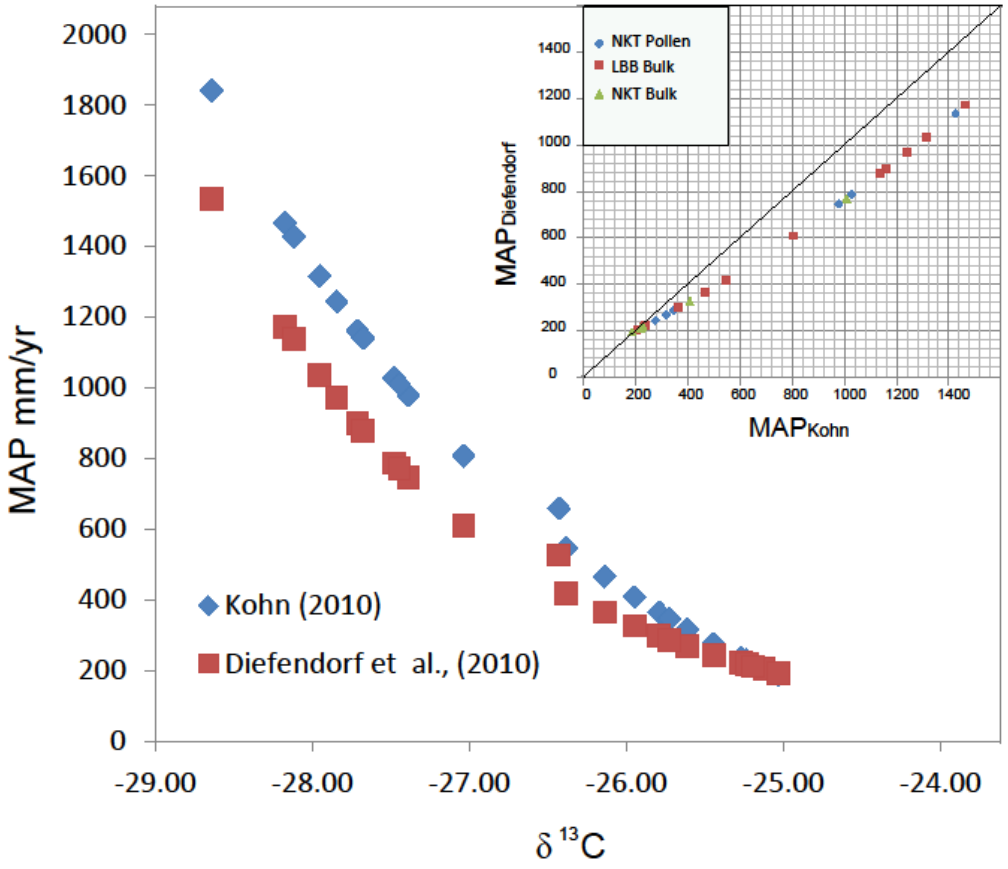

Fig. 3.9.6. $\delta^{13}C$ vs. MAP estimates from the Kohn (2010) and Diefendorf et al. (2010) models of carbon isotope compositions. Inner plot shows the correlation between MAP calculations based on both the Kohn (2010) and Diefendorf et al., (2010) equations.

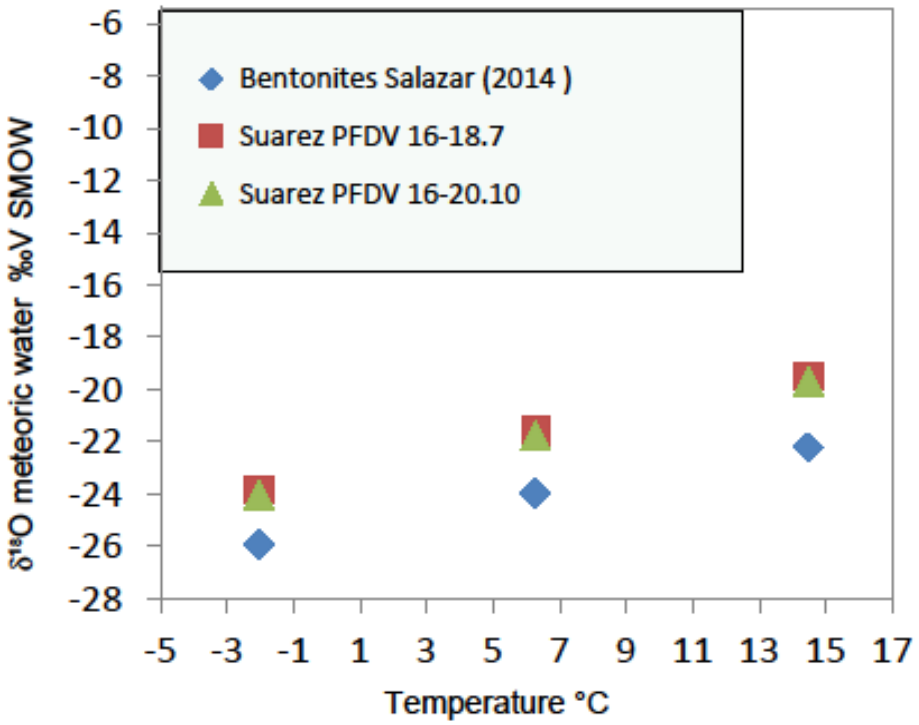

Fig. 3.9.7.Temperature (°C) vs. $\delta^{18}O$ of meteoric water calculated from siderite (Suarez et al., 2013) and smectite (this work) at -2, 6.3 and 14.5°C.

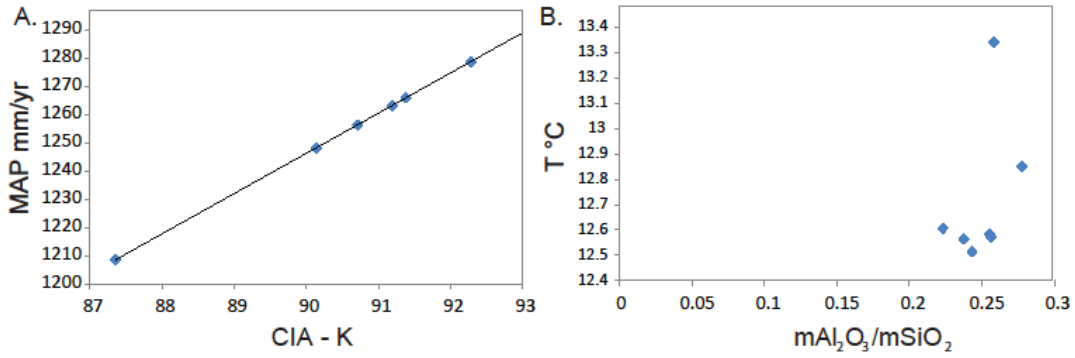

Fig. 3.9.8. Relationship between A) mean annual precipitation (MAP) and CIA–K and B) mean annual temperature (MAT) and the molecular weathering ratio of Al2O3 and SiO2 in the NKT paleosol of the Prince Creek Formation.

3.10 Tables

Table 3.10.1. N, C, $\delta^{15}N$, $\delta^{13}C$ and C/N ratio values of the bulk samples and the palynologyc separates.

Sample Name	Conc N (%)	Conc C (%)	$\delta^{15}N$ At-air (‰)	$\delta^{13}C$ PDB (‰)	C/N
NKT34	0.12	1.21	3.03	-27.45	9.80
NKT38	0.08	0.26	2.58	-25.23	3.28
NKT40	0.07	0.31	2.71	-25.19	4.17
NKT44	0.14	0.71	2.72	-25.95	4.98
NKT46	0.10	0.54	2.30	-25.03	5.53
Average		0.61	2.67	-25.77	5.55
Stand.dev.		0.38	0.26	1.00	2.52
NKT34-P	1.49	47.28	3.02	-28.12	31.63
NKT36-P	1.38	55.82	2.43	-25.61	40.41
NKT38-P	1.41	59.03	2.48	-25.24	41.95
NKT40-P	0.95	33.99	2.76	-25.44	35.88
NKT42-P	0.64	19.65	4.83	-27.48	30.48
NKT44-P	1.20	47.83	3.51	-27.39	39.80
NKT46-P	1.43	50.38	2.27	-25.73	35.18
Average		44.85	3.04	-26.43	36.48
Stand.dev.		13.66	0.89	1.19	4.43

Table 3.10.2. MAP calculations using Kohn (2010) Eq., Diefendorf et al., (2010) Eq. and using CIA-K (Maynard, 1992). MAT calculations using Sheldon et al., (2002) and Sheldon, (2006).

Sample Name	**d^{13}C PDB**	**MAP± 221.38 mm/yr Kohn (2010) Eq.**	**MAP ± 0.92 mm/yr Diefendorf et al., (2010) Eq.**	**MAP ± 18 mm/yr CIA-K**	**MAT ±4.4°C (Sheldon et al 2002)**	**MAT ±4.4°C (Sheldon, 2006)**
NKT34-P	-28.12	1426.88	1135.38			
NKT36-P	-25.61	315.85	268.06			
NKT38-P	-25.24	228.60	216.45			
NKT40-P	-25.44	275.12	243.58			
NKT42-P	-27.48	1027.53	785.66			
NKT44-P	-27.39	978.76	745.56			
NKT46-P	-25.73	346.09	286.67			
NKT34	-27.45	1008.55	769.99	1265.94	12.58	15.99
NKT38	-25.23	228.16	216.20	1256.40	12.56	15.15
NKT40	-25.19	218.95	210.94	1248.15	12.61	14.47
NKT44	-25.95	407.36	325.44	1278.82	12.85	17.04
NKT46	-25.03	186.45	192.68	1263.15	12.57	16.04

Table 3.10.3. Calculated $\delta^{18}O$ of meteoric water from smectite for NKT paleosol and the KKT and PFDV bentonites. Last two column s are Suarez et al., (2013) calculated $\delta^{18}O$ from siderite values.

		NKT-34	**NKT-36**	**NKT-38**	**NKT-40**	**NKT-42**	**NKT-44**	**NKT-46**	**D6KKT-20.5**	**PFDV-17-5.7**	**Suarez data PFDV 16-18.75**	**Suarez data PFDV 16-20.10**
T (° C)	$\delta^{18}O$	12.62	11.86	11.65	11.48	12.4	12.28	12.2	4.96	5.03		
-2	13.6	-18.46	-19.2	-19.4	-19.6	-18.7	-18.8	-19	-26.12	-26.1	-23.86	-24.07
0	13.4	-17.95	-18.7	-18.9	-19.1	-18.2	-18.3	-18	-25.61	-25.5		
2	13.21	-17.44	-18.2	-18.4	-18.6	-17.7	-17.8	-18	-25.1	-25		
4	13.02	-16.95	-17.7	-17.9	-18.1	-17.2	-17.3	-17	-24.61	-24.5		
6.3	12.81	-16.39	-17.2	-17.4	-17.5	-16.7	-16.7	-17	-24.05	-24	-21.43	-21.64
8	12.65	-15.99	-16.8	-17	-17.1	-16.3	-16.3	-16	-23.65	-23.6		
10	12.47	-15.53	-16.3	-16.5	-16.7	-15.8	-15.9	-16	-23.19	-23.1		
12	12.3	-15.08	-15.8	-16.1	-16.2	-15.3	-15.4	-16	-22.74	-22.7		
14.5	12.09	-14.52	-15.3	-15.5	-15.7	-14.8	-14.9	-15	-22.18	-22.1	-19.22	-19.43

3.11 References

ARENS CRYSTAL, N., JAHREN, A.H., and AMUNDSON, R., 2000, Can C_3 plants faithfully record the carbon isotopic composition of atmospheric carbon dioxide ? Can C_3 plants faithfully record the carbon isotopic composition of atmospheric carbon dioxide?: Paleobiology, v. 26, p. 137-164.

BARKER, C.E., and PAWLEWICZ, M.J., 1986, The correlation of vitrinite reflectance with maximum paleotemperature in humic organic matter, *in* Buntebarth, G., and Stegena, L., eds., Paleogeothermic: New York, USA, Springer-Verlag, p. 79-93.

BENNER, R., FOGEL, M.L., SPRAGUE, E.K., and HODSON, R.E., 1987, Depletion of 13C in lignin and its implications for d13C isotope studies: Nature, v. 329, p. 708-710.

BLAKE, G.R., and HARTGE, K.H., 1986, Bulk density, Methods of soil analysis. Part 1. Physical and mineralogical methods, p. 363-375.

BICE, K.L.J., ARTHUR, M.A., and MARINCOVICH, L.J., 1996, Late Paleocene Arctic Ocean shallow-marine temperatures from mollusc stable isotopes: Paleoceanography, v. 11, p. 241-249.

BIRD, K.J., and MOLENAAR, C.M., 1992, The North Slope foreland basin, Alaska, Foreland Basins and Foldbelts, American Association of Petroleum Geologists (AAPG.), p. 363-393.

BOCHERENS, H., FRIIS, E.M., MARIOTTI, A., and PEDERSEN, K.R., 1994, Carbon isotopic abundances in Mesozoic and Cenozoic fossil plants : Palaeoecological implications: Lethaia, v. 26, p. 347-358.

BRALOWER, T.J., SILVA, I.P., and MALONE, M.J., 2002, New evidence for abrupt climate change in the Cretaceous and Paleogene: An Ocean Drilling Program expedition to Shatsky Rise, northwest Pacific: GSA TODAY, p. 4-10.

BRIMHALL, G.H., and DIETRICH, W.E., 1987, Constitutive mass balance relations between chemical composition, volume, density, porosity, and strain in metasomatic hydrochemical systems: Results on weathering and pedogenesis, Geochimica et Cosmochimica Acta, p. 567-587.

BRIMHALL, G.H., CHRISTOPHER J., L., FORD, C., BRATT, J., TAYLOR, G., and WARIN, O., 1991a, Quantitative geochemical approach to pedogenesis: importance of parent material reduction, volumetric expansion, and eolian influx in lateritization, Geoderma, p. 51-91.

BRIMHALL, G.H., CHADWICK, O.A., LEWIS, C.J., COMPSTON, W., WILLIAMS, I.S., DANTI, K.J., DIETRICH, W.E., POWER, M.E., HENDRICKS, D., and BRATT, J., 1991b, Deformational mass transport and invasive processes in soil evolution.: Science (New York, N.Y.), v. 255, p. 695-702.

BURNS, W.M., HAYBA, D.O., ROWAN, E.L., and HOUSEKNECHT, D.W., 2005, Estimating the Amount of Eroded Section in a Partially Exhumed Basin from Geophysical Well Logs : An Example from the North Slope: North, v. 1732D, p. 18 p.

CADRIN, A.A.J., KYSER, T.K., CALDWELL, W.G.E., and LONGSTAFFE, F.J., 1995, Isotopic and chemical compositions of bentonites as paleoenvironmental indicators of the Cretaceous Western Interior Seaway: Palaeogeography, Palaeoclimatology, Palaeoecology, v. 119, p. 301-320.

CONRAD, J.E., MCKEE, E.H., and TURRIN, B.D., 1990, Age of tephra beds at the Ocean Point Dinosaur Locality, North Slope, Alaska, based on K–Ar and 40Ar/39Ar analysis, p. C1-C12.

COPLEN, T.B., 1994, Reporting of stable hydrogen, carbon, and oxygen isotopic abundances (Technical Report), Pure and Applied Chemistry, p. 273-276.

DELGADO, A., and REYES, E., 1996, Oxygen and hydrogen isotope compositions in clay minerals : A potential single-mineral geothermometer: Geochimica et Cosmochimica Acta, v. 60, p. 4285-4289.

DESCOLAS-GROS, C., and SCHÖLZEL, C., 2007, Stable isotope ratios of carbon and nitrogen in pollen grains in order to characterize plant functional groups and photosynthetic pathway types.: The New phytologist, v. 176, p. 390-401.

DIEFENDORF, A.F., MUELLER, K.E., WING, S.L., KOCH, P.L., and FREEMAN, K.H., 2010, Global patterns in leaf 13C discrimination and implications for studies of past and future climate: Proceedings of the National Academy of Sciences of the United States of America, v. 107, p. 5738-43.

DWORKIN, S.I., NORDT, L., and ATCHLEY, S., 2005, Determining terrestrial paleotemperatures using the oxygen isotopic composition of pedogenic carbonate: Earth and Planetary Science Letters, v. 237, p. 56-68.

FARQUHAR, G.D., EHLERINGER, J.R., and HUBICK, K.T., 1989, Carbon Isotope Discrimination and Photosynthesis: Annu. Rev. Plant Physiol. Plant Mol. Biol, v. 40, p. 503-537.

FIORILLO, A.R., MCCARTHY, P.J., and FLAIG, P.P., 2010a, Taphonomic and sedimentologic interpretations of the dinosaur-bearing Upper Cretaceous Strata of the Prince Creek Formation, Northern Alaska: Insights from an ancient high-latitude terrestrial ecosystem: Palaeogeography, Palaeoclimatology, Palaeoecology, v. 295, p. 376-388.

FIORILLO, A.R., MCCARTHY, P.J., FLAIG, P.P., BRANDLEN, E., NORTON, D.W., ZIPPI, P., JACOBS, L., GANGLOFF, R.A., and FARLOW, J.O., 2010b, Paleontology and paleoenvironmental interpretation of the Kikak-Tegoseak Quarry (Prince Creek Formation: Late Cretaceous), northern Alaska: a multi-disciplinary study of a high-latitude ceratopsian dinosaur bonebed, *in* Ryan, M.J., Chinnery-Allgeier, B.J., and Eberth, D.A., eds., New Perspectives On Horned Dinosaurs The Royal Tyrrell Museum Ceratopsian Symposium, Indiana University Press, p. 456-477.

FLAIG, P.P., 2010, Depositional environments of the Late Cretaceous (Maastrichtian) dinosaur-bearing Prince Creek Formation: Colville River region, North Slope, Alaska., p. 311.

FLAIG, P.P., RD, B., MCCARTHY, P.J., and FIORILLO, A.R., 2011, A tidally-influenced, high-latitude alluvial/coastal plain: the Late Cretaceous (Maastrichtian) Prince Creek Formation, North Slope, Alaska: SEPM Special Publication, v. 97, p. 233-264.

FLAIG, P.P., MCCARTHY, P.J., and FIORILLO, A.R., 2013, Anatomy, evolution and paleoenvironmental interpretation of an ancient arctic coastal plain: Integrated paleopedology and palynology from the Upper Cretaceous (Maastrichtian) Prince Creek Formation, North Slope, Alaska: SEPM Special Publication, v. 104, p. 179-230.

FRANK, T.D., THOMAS, D.J., LECKIE, R.M., ARTHUR, M.A., BOWN, P.R., JONES, K., and LEES, J.A., 2005, The Maastrichtian record from Shatsky Rise (northwest Pacific): A tropical perspective on global ecological and oceanographic changes: Paleoceanography, v. 20, p. 14.

FRASER, W.T., WATSON, J.S., SEPHTON, M.A., LOMAX, B.H., HARRINGTON, G., GOSLING, W.D., and SELF, S., 2014, Changes in spore chemistry and appearance with increasing maturity: Review of Palaeobotany and Palynology, v. 201, p. 41-46.

FREDERIKSEN, N.O., 2002, Palynology of Eocene Strata in the Sagavanirktok and Canning Formations on the North Slope of Alaska: Palynology, v. 26, p. 59-93.

GASTALDO, R.A., KNIGHT, C.L., NEVELING, J., and TABOR, N.J., 2014, Latest Permian paleosols from Wapadsberg Pass, South Africa: Implications for Changhsingian climate: Geological Society of America Bulletin, p. 1-15.

GHOSH, P., BHATTACHARYA, S.K., and GHOSH, P., 2005, Atmospheric CO 2 During the Late Paleozoic and Mesozoic : Estimates from Indian Soils: Ecological Studies, v. 177, p. 8-34.

GHOSH, P., GHOSH, P., and BHATTACHARYA, S.K., 2001, CO2 levels in the Late Palaeozoic and Mesozoic atmosphere from soil carbonate and organic matter, Satpura basin, Central India: Palaeogeography, Palaeoclimatology, Palaeoecology, v. 170, p. 219-236.

GRÖCKE, D.R., 1998, Carbon-isotope analyses of fossil plants as a chemostratigraphic and palaeoenvironmental tool: Lethaia, v. 31, p. 1-13.

GRÖCKE, D.R., 2002, The carbon isotope composition of ancient CO2 based on higher-plant organic matter.: Philosophical transactions. Series A, Mathematical, physical, and engineering sciences, v. 360, p. 633-58.

HAMER, J.M.M., SHELDON, N.D., and NICHOLS, G.J., 2007a, Global Aridity during the Early Miocene? A Terrestrial Paleoclimate Record from the Ebro Basin, Spain, The Journal of Geology, p. 601-608.

HAMER, J.M.M., SHELDON, N.D., NICHOLS, G.J., and COLLINSON, M.E., 2007b, Late Oligocene–Early Miocene paleosols of distal fluvial systems, Ebro Basin, Spain: Palaeogeography, Palaeoclimatology, Palaeoecology, v. 247, p. 220-235.

HASEGAWA, T., PRATT, L.M., MAEDA, H., SHIGETA, Y., OKAMOTO, T., KASE, T., and UEMURA, K., 2003, Upper Cretaceous stable carbon isotope stratigraphy of terrestrial organic matter from Sakhalin, Russian Far East: a proxy for the isotopic composition of paleoatmospheric CO2: Palaeogeography, Palaeoclimatology, Palaeoecology, v. 189, p. 97-115.

HERMAN, A.B., and SPICER, R.A., 1996, Palaeobotanical evidence for a warm Cretaceous Arctic Ocean, Nature, p. 330-333.

HILLHOUSE, J., and COE, R., 1994, Paleomagnetic data pom Alaska: The Geological Society of America, v. G-1, p. 797-812.

JAHREN, A.H., 2004, The carbon stable isotope composition of pollen: Review of Palaeobotany and Palynology, v. 132, p. 291-313.

JOHNSON, M.J., and HOWELL, D.G., 1996, Thermal maturity of sedimentary basins in Alaska-An overview: United States Geological Survey Bulletin, v. 2142, p. 131.

KELLER, G., 2001, The end-cretaceous mass extinction in the marine realm: year 2000 assessment: Planetary and Space Science, v. 49, p. 817-830.

KOHN, M.J., 2010, Carbon isotope compositions of terrestrial C_3 plants as indicators of (paleo)ecology and (paleo)climate.: Proceedings of the National Academy of Sciences of the United States of America, v. 107, p. 19691-5.

KOVÁCS, J., RAUCSIK, B., VARGA, A., ÚJVÁRI, G., VARGA, G., and OTTNER, F., 2013, Clay mineralogy of red clay deposits from the central Carpathian Basin (Hungary): implications for Plio-Pleistocene chemical weathering and palaeoclimate: Turkish Journal of Earth Sciences, v. 22, p. 414-426.

LAWVER, L.A., GRANTZ, A., and GAHAGAN, L.M., 2002, Plate kinematic evolution of the present Arctic region since the Ordovician". In: Tectonic evolution of the Bering Shelf-Chukchi Sea-Arctic margin and adjacent landmasses: Geol. Soc. Am. Special Paper, v. 360, p. 333-358.

LOADER, N.J., and HEMMING, D.L., 2000, Preparation of pollen for stable carbon isotope analyses: Chemical Geology, v. 165, p. 339-344.

LUDVIGSON, G.A., GONZÁLEZ, L.A., METZGER, R.A., WITZKE, B.J., BRENNER, R.L., MURILLO, A.P., and WHITE, T.S., 1998, Meteoric sphaerosiderite lines and their use for paleohydrology and paleoclimatology, Geology, p. 1039.

LUDVIGSON, G.A., FOWLE, D.A., ROBERTS, J.A., GONZA, L.A., DRIESE, S.G., PLACE, O.B., VILLARREAL, M.A., SMITH, J.O.N.J., and SUAREZ, M.B., 2013, Paleoclimatic applications and modern process studies of pedogenic siderite Department of Geological Sciences , University of Texas at San Antonio , 1 UTSA Circle , p. 79-87.

LYLE, W.M., PALMER JR., I.F., BOLM, J.G., and MAXEY, L.R., 1980, Post-Early Triassic formations of northeastern Alaska and their petroleum reservoir and source-rock potential by state of alaska, p. 21.

MARUOKA, T., KOEBERL, C., and BOHOR, B.F., 2007, Carbon isotopic compositions of organic matter across continental Cretaceous – Tertiary (K – T) boundary sections : Implications for paleoenvironment after the K – T impact event: Earth and Planetary Science Letters, v. 253, p. 226-238.

MAYNARD, J.B., 1992, Chemistry of Modern Soils as a Guide to Interpreting Precambrian Paleosols, The Journal of Geology, p. 279-289.

MEYERS, P.A., 1994, Preservation of elemental and isotopic source identification of sedimentary organic matter, Chemical Geology, p. 289-302.

MEYERS, P.A., 1997, Organic geochemical proxies of paleoceanographic, paleolimnologic, and paleoclimatic processes: Organic Geochemistry, v. 27, p. 213-250.

MONGRAIN, J., 2013, Depositional System, Paleoclimate, and Provenance of the Late Miocene to Pliocene Beluga and Sterling Formations, Cook Inlet Forearc Basin, Alaska., p. 181.

MOORE, T., WALLACE, W., BIRD, K., KARL, S., and MULL, C., 1994, Geology of northern Alaska, The geology of Alaska:, The Geologicla Society of America, p. 49-140.

MULL, C.G., HOUSEKNECHT, D.W., and BIRD, K.J., 2003, Revised Cretaceous and Tertiary stratigraphic nomenclature in the Colville Basin, Northern Alaska: U. S. Geological Survey Professional Paper 1673

NORDT, L., ATCHLEY, S., and DWORKIN, S., 2003, Terrestrial evidence for two greenhouse events in the latest Cretaceous: GSA TODAY.

PARRISH, J.T., and SPICER, R.A., 1988, Late Cretaceous terrestrial vegetation: A near-polar temperature curve, Geology, v. 16, p. 22-25

PHILLIPS, R.L., 2003, Depositional environments and processes in Upper Cretaceous nonmarine and marine sediments, Ocean Point dinosaur locality, North Slope, Alaska: Cretaceous Research, v. 24, p. 499-523.

ROBINSON, M.S., 1989, Kerogen microscopy of coal and shales from the North Slope of Alaska, Alaska Division of Geological and Geophysical Surveys Public Data File, p. 89-22.

SHELDON, N.D., 2006, Quaternary Glacial-Interglacial Climate Cycles in Hawaii, The Journal of Geology, v. 114, p. 367-376.

SHELDON, N.D., RETALLACK, G.J., and TANAKA, S., 2002, Geochemical Climofunctions from North American Soils and Application to Paleosols across the Eocene-Oligocene Boundary in Oregon: The Journal of Geology, v. 110, p. 687-696.

SHELDON, N.D., and TABOR, N.J., 2009, Quantitative paleoenvironmental and paleoclimatic reconstruction using paleosols: Earth-Science Reviews, v. 95, p. 1-52.

SLOAN, L.C., and REA, D.K., 1995, Atmospheric carbon dioxide and early Eocene climate : A general circulation modeling sensitivity study: Palaeogeography, Palaeoclimatology, Palaeoecology, v. 119, p. 275-292.

SMILEY, C.J., 1966, Cretaceous Floras from Kuk River Area, Alaska: Stratigraphic and Climatic Interpretations, Geological Society of America Bulletin, p. 1-14.

SMITH, D., 1993, Statistical treatment of data on environmental isotopes in precipitationTechnical report series no. 331, International Atomic Energy Agency (IAEA), Vienna, 1992, 781 pp., softback, 2100 Austrian Sch., ISBN 92-0-100892-9: Journal of Hydrology, v. 146, p. 454-455.

SOIL SURVEY STAFF, 1999, Soil taxonomy: A basic system of soil classification for making and interpreting soil surveys, p. 869.

SPICER, R.A., and CORFIELD, R.M., 1992, A review of terrestrial and marine climates in the Cretaceous with implications for modelling the 'Greenhouse Earth': Geological Magazine, v. 129, p. 169-180.

SPICER, R.A., and PARRISH, J.T., 1990a, Late Cretaceous-early Tertiary palaeoclimates of northern high latitudes: a quantitative view, Geological Society of London, p. 329-341.

SPICER, R.A., and PARRISH, J.T., 1990b, Latest Cretaceous woods of the central North Slope, Alaska: Palaeontology, v. 33, p. 225-242.

SPICER, R.A., PARRISH, J.T., and GRANT, P.R., 1992, Evolution of vegetation and coal-forming environments in the Late Cretaceous of the North Slope of Alaska: Geological Society of America Special Papers., v. 267, p. 177-192.

SPICER, R.A., and HERMAN, A.B., 2010, The Late Cretaceous environment of the Arctic: A quantitative reassessment based on plant fossils: Palaeogeography, Palaeoclimatology, Palaeoecology, v. 295, p. 423-442.

SUAREZ, C.A., LUDVIGSON, G.A., GONZALEZ, L.A., FIORILLO, A.R., FLAIG, P.P., and MCCARTHY, P.J., 2013, Use of multiple oxygen isotope proxies for elucidating Arctic Cretaceous palaeo-hydrology: Geological Society, London, Special Publications, v. 382.

TRAVERSE, A., 2007, Paleopalynology: Second Edition, Springer.

UFNAR, D.F., GONZA, L.A., BRENNER, R.L., and WITZKE, B.J., 2002, The mid-Cretaceous water bearer : isotope mass balance quantification of the Albian hydrologic cycle, v. 188, p. 51-71.

UFNAR, D.F., LUDVIGSON, G.A., GONZÁLEZ, L.A., BRENNER, R.L., and WITZKE, B.J., 2004a, High latitude meteoric δ18O compositions: Paleosol siderite in the Middle Cretaceous Nanushuk Formation, North Slope, Alaska, Geological Society of America Bulletin, p. 463-473.

UFNAR, D.F., GONZÁLEZ, L.A., LUDVIGSON, G.A., BRENNER, R.L., and WITZKE, B.J., 2004b, Evidence for increased latent heat transport during the Cretaceous (Albian) greenhouse warming, Geology, p. 1049-1052.

VAN BERGEN, P.F.., COLLINSON, M.E., and DE LEEUW, J.W., 1993, Chemical composition and ultrastructure of fossil and extant salvinialean microspore massulae and megaspores: Grana, v. 32, p. 18-30.

VITALI, F., LONGSTAFFE, F.J., MCCARTHY, P.J., PLINT, A.G., and CALDWELL, W.G.E., 2002, Stable isotopic investigation of clay minerals and pedogenesis in an interfluve paleosol from the Cenomanian Dunvegan Formation, N.E. British Columbia, Canada: Chemical Geology, v. 192, p. 269-287.

ZIEGLER, A.M., SCOTESE, C.R., and BARRETT, S.F., 1983, Mesozoic and Cenozoic paleogeographic maps, *in* Brosche, P., Sundermann, J., ed., Tidal friction and the earth's rotation II: Berlin, Springer-Verlag, p. 240-252.

General Conclusions

The pedogenic processes of the paleosols developed at the Prince Creek Formation and the depositional environment of the Lower Cantwell Formation at the East Fork of the Toklat River are studied and summarized to give context to the paleoclimate history.

1) Clay mineral origin in the Prince Creek Formation:

In the paleosols, smectite, discrete illite, kaolinite and chlorite are of detrital origin. I/S mixed-layered clay is of pedogenic origin. Smectite is the most abundant clay mineral. In the bentonites, smectite is developed *in situ* as the product of weathering. The smectite-rich bentonites can be considered the probable source for the epiclastic smectite in the paleosol profiles.

2) Pedogenic processes in the Prince Creek Formation:

The Illitization process of primary smectite to produce I/S has a pedogenic origin rather than a diagenetic one. Detrital illite is the most likely source of K^+ for transformation of smectite to I/S mixed layered clay.

Andosolization is evidenced by the presence of andic soil properties. Geochemical mass-balance, bulk density, acid ammonium oxalate and pyrophosphate extraction show that: i) hydrous oxides of Fe and Al are significant components of the NKT and KRM paleosols and are forming complexes with humus, ii) KRM has low bulk density and phosphorous gain of >100% that we interpret as evidence for andic soil properties, and iii) the NKT paleosol meets only one of the three criteria for andic soil properties (extractable Fe and Al > 2%) indicating that andic pedogenic processes were operating in NKT but that it is more weakly developed.

In summary, for the Prince creek Formation, the low pH, phosphorous accumulation, Fe- and Al-humus complexes, high organic matter and an abundance of 2:1 clay minerals indicate that the genesis of the paleosols was strongly influenced by volcanic ash in the parent material and that clay minerals from epiclastic sources contributed to the

development of non-allophanic properties. Therefore, the paleosols are considered to be Andept-like paleosols. The transformation of smectite to illite in the interlayered illlite-smectite clays, the main pedogenic process, occured *in situ* due to wet-dry cycles. These pedogenic processes are consistent with the paleoclimatic reconstructions of Late Cretaceous North Slope ecosystems. Redox-processes and illitization of smectite are known to occur in soils and paleosols subjected to alternating phases of wetting and drying which may be the result of fluctuations in water table levels or the results of seasonal saturation, perhaps due to spring flooding from snow melt in the ancestral Brooks Range, the result of a high water table.

3) Depositional environment of the East Fork of the Toklat River, Lower Cantwell Formation:

Based on the facies association analysis we interpret the depositional environment of the East Fork of the Toklat River as being part of the distal part of an alluvial fan. The depositional environment agrees with the characteristics of the distal alluvial fan and the lacustrine deposits described by Ridgway et al., (1997). The distal part of an alluvial fan is also a likely setting where anastomosis could have taken place, which could explain the continuous rise of the water table and significant organic matter accumulation processes.

4) Radiometric age of the Lower Cantwell Formation at the East Fork of the Toklat River Section:

The new U-Pb age of 69.5 ± 0.7 Ma from a bentonite constrains the age of the upper section of the Lower Cantwell Formation at the East Fork of the Toklat River. Together with the palynologic age of Late Campanian- Early Maastrichtian (Ridgway et al., 1997), the stratigraphic section can be bracketed between ~72 to ~ 69 Ma.

5) Positive excursions of $\delta^{13}C$ at the East Fork of the Toklat River, Lower Cantwell Formation:

The coupling between $\delta^{13}C_{Wood}$ and $\delta^{13}C_{bulk}$ indicates that the positive excursions are probably caused by $\delta^{13}C$ fluctuation in CO_2 in the global ocean-atmospheric reservoir.

Analyses of $\delta^{13}C$ of fossil wood, from the measured section, record fluctuations that correlate with other Late Cretaceous marine and terrestrial curves (West Texas, Tercis les Bains, Gubbio). The main features of the $\delta^{13}C$ wood record are: i) a major positive $\delta^{13}C_{Wood}$ excursion of -22.42‰ (located at 95.6m depth in the 69.5 ± 0.7 Ma bentonite layer) and ii) the most negative value -27.84‰ at ~52.5m overlain by four positive excursions located at depths between 53 and 60m.

In summary, the depositional environment of the lower Cantwell Formation indicates that deposition at the East Fork of the Toklat River was dominated by low-energy depositional processes. Overall, the facies associations indicate that the section is consistent with Ridgway et al.'s (1997) model and probably was deposited in the distal part of an alluvial fan. The age control and the terrestrial origin of the wood samples suggest that the main positive excursion is related to an intense greenhouse event that occured in the Mid-Maastrichtian called the Middle Maastrichtian Event. The most negative excursion and the 4 positive excursions above can be bracketed between 72.4 Ma and ~71.1 Ma based on the range of *Kurtzipites andersonii, which is* found in the lower Cantwell Formation (Ridgway et al., 1997). The timing and magnitude of the shifts are similar to those observed in $\delta^{13}C$ stable isotope curves of marine sediments (Thibault et al. 2012a and b; Jung et al., 2012; Voigt et al. 2012) and could be interpreted as short-term variations at the Campanian-Maastrichtian Boundary.

6) Mean annual precipitation (MAP) data and climatic interpretation of both formations:

Stable isotope analyses of palynological separates, wood and clays, together with geochemical analyses in bulk sediments and clays, provide additional approaches to reconstruct the paleoclimate of the Prince Creek and lower Cantwell Formations and the arctic during the Late Cretaceous.

For the lower Cantwell Formation, the average MAP value is 517.92± 134.44 mm/yr. These precipitation values are higher than the growing season MAP of 229.4±334.5mm obtained from CLAMP analysis (Tomsich et al., 2010). Both values, 517.92± 134.44

mm/yr (this study) and 229.4±334.5mm (Tomsich et al., 2010), indicate dry conditions in the late Cretaceous for the lower Cantwell Formation. On the other hand, MAP estimates based on both $\delta^{13}C$ values and the CIA-K approach indicate that precipitation in the Prince Creek Formation was between 745.56 and 1426.88 ± 221.38 mm/yr. $\delta^{18}O$ values of ~ -24‰ for meteoric water, calculated in smectite, are consistent with previous results (Suarez et al., 2013).

Overall Late Cretaceous paleoclimatic interpretation:

During the Late Cretaceous, the Prince Creek Formation, located between 83° and 85° N paleo-latitude (Ziegler et al., 1983; Lawver et al., 2002), and correlative rocks of the lower Cantwell Formation at a paleo-latitude of ~64ºN (Hillhouse and Coe, 1994), were likely affected by a greenhouse period called the Middle-Maastrichtian Event (MME).

This is the first time the Middle-Maastrichtian Event (MME) has been identified in the paleo-arctic, and it is probably responsible for increased latent heat transport that intensified the hydrological cycle in the Late Cretaceous paleo-arctic.

The new U-Pb age of 69.5± 0.7 Ma of the lower Cantwell Formation, combined with previous palynological data (Ridgway et al., 1997), constrains deposition of the East Fork Toklat River section between ~72 and ~ 69 Ma. The U-Pb age indicates that the East Fork Toklat River section is coeval with the 69.2 ± 0.5 Ma $^{40}Ar/^{39}Ar$ age (Flaig, 2010) of the Prince Creek Formation, and both formations were deposited during the MME (~69Ma).

In this greenhouse context, the mean annual precipitation (MAP) values obtained for the Prince Creek Formation vary between 745.56 and 1426.88 ± 221.38 mm/yr. In the lower Cantwell Formation at the East Fork Toklat River site, the estimated mean annual precipitation value is 530.47± 253.50 mm/yr. Tomsich et al. (2010) determined a growing season precipitation of 229.4 ±334.5 mm for the lower Cantwell Formation at Sable Mountain. In contrast, North Slope precipitation estimates from the Prince Creek Formation vary between 500 and 1500 mm/yr (Spicer and Parrish, 1990), suggesting that

the arctic coast received more precipitation than the interior of Alaska during the Late Cretaceous.

Previous studies in the paleo-arctic suggest a late Cretaceous near-polar mean annual temperature between 5° and 8°C for North Slope ecosystems, a warm month mean temperature of 10-12^{o}C and a cold month mean temperature of 2-4^{o}C (Parrish and Spicer, 1988; Spicer and Parrish, 1990; Fiorillo et al., 2010b). In contrast, and a mean annual temperature of 7.42 ºC has been determined for the lower Cantwell Formation with a warm month mean temperature of 17.1 ^{o}C and a cold month mean temperature of -2 ^{o}C (Tomsich et al., 2010).

The δ^{18}O values of smectite in the Prince Creek Formation indicate the depleted nature of the meteoric water. The low δ^{18}O could be explained as extremely δ^{18}O depleted precipitation at high latitudes during the Late Cretaceous (Suarez et al., 2013) that may have been the result of increased latent heat transport due to the MME greenhouse episode.

Precipitation and temperature values across 20° of paleolatitude during the Cretaceous greenhouse indicate that a latitudinal gradient may have existed across Alaska (from ~64° to 84°N), with areas along the arctic coast being generally wetter and more moderate in temperature and areas further inland being drier and more extreme in seasonal temperature contrasts. Additional data are required to better constrain to what extent these shifts in temperature and precipitation may be related to particular events such as the MME and to determine what effects these global changes had on life in the Late Cretaceous arctic. Both the Cantwell and Prince Creek formations serve as excellent analogs to understand changes that occur in high latitude environments subjected to greenhouse warming events.

References

BRALOWER, T.J., SILVA, I.P., and MALONE, M.J., 2002, New evidence for abrupt climate change in the Cretaceous and Paleogene: An Ocean Drilling Program expedition to Shatsky Rise, northwest Pacific: GSA TODAY, p. 4-10.

BROUWERS, E.M., CLEMENS, W.A., SPICER, R.A., AGER, T.A., CARTER, L.D., and SLITER, W.V., 1987, Dinosaurs on the north slope, alaska: high latitude, latest cretaceous environments.: Science (New York, N.Y.), v. 237, p. 1608-1610.

CLEMENS, W.A., and NELMS, L.G., 1993, Paleoecological implications of Alaskan terrestrial vertebrate fauna in latest Cretaceous time at high paleolatitudes, p. 503-506.

DWORKIN, S.I., NORDT, L., and ATCHLEY, S., 2005, Determining terrestrial paleotemperatures using the oxygen isotopic composition of pedogenic carbonate: Earth and Planetary Science Letters, v. 237, p. 56-68.

FIORILLO, A.R., HASIOTIS, S.T., KOBAYASHI, Y., and TOMSICH, C.S., 2009, A pterosaur manus track from Denali National Park, Alaska Range, Alaska, United States: Palaios, v. 24, p. 466-472.

FIORILLO, A.R., MCCARTHY, P.J., and FLAIG, P.P., 2010a, Taphonomic and sedimentologic interpretations of the dinosaur-bearing Upper Cretaceous Strata of the Prince Creek Formation, Northern Alaska: Insights from an ancient high-latitude terrestrial ecosystem: Palaeogeography, Palaeoclimatology, Palaeoecology, v. 295, p. 376-388.

FIORILLO, A.R., MCCARTHY, P.J., FLAIG, P.P., BRANDLEN, E., NORTON, D.W., ZIPPI, P., JACOBS, L., GANGLOFF, R.A., and FARLOW, J.O., 2010b, Paleontology and paleoenvironmental interpretation of the Kikak-Tegoseak Quarry (Prince Creek Formation: Late Cretaceous), northern Alaska: a multi-disciplinary study of a high-latitude ceratopsian dinosaur bonebed, *in* Ryan, M.J., Chinnery-Allgeier, B.J., and Eberth, D.A., eds., New Perspectives On Horned Dinosaurs The Royal Tyrrell Museum Ceratopsian Symposium, Indiana University Press, p. 456-477.

FIORILLO, A.R., and ADAMS, T.L., 2012, A Therizinosaur Track From the Lower Cantwell Formation (Upper Cretaceous) of Denali National Park, Alaska: Palaios, v. 27, p. 395-400.

FLAIG, P.P., 2010, Depositional environments of the Late Cretaceous (Maastrichtian) dinosaur-bearing Prince Creek Formation: Colville River region, North Slope, Alaska., p. 311.

FLAIG, P.P., RD, B., MCCARTHY, P.J., and FIORILLO, A.R., 2011, A tidally-influenced, high-latitude alluvial/coastal plain: the Late Cretaceous (Maastrichtian) Prince Creek Formation, North Slope, Alaska: SEPM Special Publication, v. 97, p. 233-264.

FLAIG, P.P., MCCARTHY, P.J., and FIORILLO, A.R., 2013, Anatomy, evolution and paleoenvironmental interpretation of an ancient arctic coastal plain: Integrated paleopedology and palynology from the Upper Cretaceous (Maastrichtian) Prince Creek Formation, North Slope, Alaska: SEPM Special Publication, v. 104, p. 179-230.

FRANK, T.D., THOMAS, D.J., LECKIE, R.M., ARTHUR, M.A., BOWN, P.R., JONES, K., and LEES, J.A., 2005, The Maastrichtian record from Shatsky Rise (northwest Pacific): A tropical perspective on global ecological and oceanographic changes: Paleoceanography, v. 20, p. 14.

GRÖCKE, D.R., 2002, The carbon isotope composition of ancient CO2 based on higher-plant organic matter.: Philosophical transactions. Series A, Mathematical, physical, and engineering sciences, v. 360, p. 633-58.

HILLHOUSE, J., and COE, R., 1994, Paleomagnetic data pom Alaska: The Geological Society of America, v. G-1, p. 797-812.

JUNG, C., VOIGT, S., and FRIEDRICH, O., 2012, High-resolution carbon-isotope stratigraphy across the Campanian–Maastrichtian boundary at Shatsky Rise (tropical Pacific): Cretaceous Research, v. 37, p. 177-185.

KELLER, G., 2001, The end-cretaceous mass extinction in the marine realm: year 2000 assessment: Planetary and Space Science, v. 49, p. 817-830.

LAWVER, L.A., GRANTZ, A., and GAHAGAN, L.M., 2002, Plate kinematic evolution of the present Arctic region since the Ordovician". In: Tectonic evolution of the Bering Shelf-Chukchi Sea-Arctic margin and adjacent landmasses: Geol. Soc. Am. Special Paper, v. 360, p. 333-358.

NORDT, L., ATCHLEY, S., and DWORKIN, S., 2003, Terrestrial evidence for two greenhouse events in the latest Cretaceous: GSA TODAY.

PARRISH, J.M., PARRISH, J.T., HUTCHISON, J.H., and SPICER, R.A., 1987, Late Cretaceous Vertebrate Fossils from the North Slope of Alaska and Implications for Dinosaur Ecology: PALAIOS, v. 2, p. 377-389.

PARRISH, J.T., and SPICER, R.A., 1988, Late Cretaceous terrestrial vegetation: A near-polar temperature curve, Geology, v. 16, p. 22-25

RETALLACK, G.J., 2004, Late Miocene climate and life on land in Oregon within a context of Neogene global change: Palaeogeography, Palaeoclimatology, Palaeoecology, v. 214, p. 97-123.

RIDGWAY, K.D., TROP, J.M., and SWEET, A.R., 1997, Thrust-top basin formation along a suture zone, Cantwell basin, Alaska Range: Implications for development of the Denali fault system: Geological Society of America Bulletin, v. 109, p. 505-523.

SPICER, R.A., and PARRISH, J.T., 1990, Late Cretaceous-early Tertiary palaeoclimates of northern high latitudes: a quantitative view, Geological Society of London, p. 329-341.

SUAREZ, C.A., LUDVIGSON, G.A., GONZALEZ, L.A., FIORILLO, A.R., FLAIG, P.P., and MCCARTHY, P.J., 2013, Use of multiple oxygen isotope proxies for elucidating Arctic Cretaceous palaeo-hydrology: Geological Society, London, Special Publications, v. 382.

TOMSICH, C.S., MCCARTHY, P.J., FOWELL, S.J., and SUNDERLIN, D., 2010, Paleofloristic and paleoenvironmental information from a Late Cretaceous (Maastrichtian) flora of the lower Cantwell Formation near Sable Mountain, Denali National Park, Alaska: Palaeogeography, Palaeoclimatology, Palaeoecology, v. 295, p. 389-408.

THIBAULT, N., HUSSON, D., HARLOU, R., GARDIN, S., GALBRUN, B., HURET, E., and MINOLETTI, F., 2012, Astronomical calibration of upper Campanian–Maastrichtian carbon isotope events and calcareous plankton biostratigraphy in the Indian Ocean (ODP Hole 762C): Implication for the age of the Campanian–Maastrichtian boundary: Palaeogeography, Palaeoclimatology, Palaeoecology, v. 337-338, p. 52-71.

VOIGT, S., GALE, A.S., JUNG, C., and JENKYNS, H.C., 2012, Global correlation of Upper Campanian – Maastrichtian successions using carbon-isotope stratigraphy: development of a new Maastrichtian timescale: Newsletters on Stratigraphy, v. 45, p. 25-53.

ZIEGLER, A.M., SCOTESE, C.R., and BARRETT, S.F., 1983, Mesozoic and Cenozoic paleogeographic maps, *in* Brosche, P., Sundermann, J., ed., Tidal friction and the earth's rotation II: Berlin, Springer-Verlag, p. 240-252.